Nuno Miguel Passarinho Trindade

Licenciado em Ciências da Engenharia Química e Bioquímica

Stochastic modeling of the thermal and catalytic degradation of polyethylene using simultaneous DSC/TG analysis

Dissertação para obtenção do Grau de Mestre em Engenharia Química e Bioquímica

Orientador: Francisco Manuel da Silva Lemos, professor catedrático, Instituto Superior Técnico – Universidade Técnica de Lisboa

Co-orientador: Isabel Maria de Figueiredo de Ligeiro da Fonseca, professora auxiliar, Faculdade de Ciências e Tecnologia – Universidade Nova de Lisboa

Júri:

Presidente: Prof. Doutora Maria Ascensão C. F. Miranda Reis
Arguente: Doutora Inês Alexandra Morgado N. Matos
Vogais: Prof. Doutor Francisco Manuel da Silva Lemos
Prof. Doutora Isabel Maria F. Ligeiro Fonseca

FACULDADE DE CIÊNCIAS E TECNOLOGIA
UNIVERSIDADE NOVA DE LISBOA

Outubro de 2012

UNIVERSIDADE NOVA DE LISBOA

FACULDADE DE CIÊNCIAS E TECNOLOGIA

DEPARTAMENTO DE QUÍMICA

STOCHASTIC MODELING OF THE THERMAL AND CATALYTIC DEGRADATION OF POLYETHYLENE USING SIMULTANEOUS DSC/TG ANALYSIS

NUNO MIGUEL PASSARINHO TRINDADE

Dissertação apresentada para obtenção do grau de Mestre em Engenharia Química e Bioquímica

Orientador: Francisco Manuel da Silva Lemos, professor catedrático, IST/UTL

Co-orientadora: Isabel Maria de Figueiredo L. da Fonseca, professora auxiliar, FCT/UNL

Júri:

Presidente: Maria Ascensão C. F. Miranda Reis, FCT/UNL

Arguente: Inês Alexandra Morgado N. Matos, FCT/UNL

Vogais: Francisco Manuel da Silva Lemos, IST/UTL

Isabel Maria de Figueiredo L. da Fonseca, FCT/UNL

OUTUBRO

2012

STOCHASTIC MODELING OF THERMAL AND CATALYTIC CRACKING OF POLYETHYLENE USING SIMULTANEOUS DSC/TG ANALYSIS.

“Plastic is too valuable to throw away!”

in Plastics 2010 – the facts (Association of Plastics Manufacturers in Europe)

“If you have knowledge, let others light their candles at it”.

Margaret Fuller

ACKNOWLEDGEMENTS

To all of those who have contributed to the development of the present work, in a way or another, in a scientific/academic perspective or not, I would like to express my sincere appreciation.

First of all, I would like to address a special acknowledgment to my co-supervisor, Professor Isabel Fonseca, for her prompt answer when I was looking for a theme I could work on to produce a thesis. I really appreciate that you provide me the opportunity of working in the group I was in, at Instituto Superior Técnico. Thank you very much for your permanent concern during this period, always making sure that everything was doing fine. I really appreciated it, professor!

To Prof Francisco and Prof. Amélia Lemos, my supervisors, I would like to express my fully gratitude for what they have done for me during the last months. Thanks for the guidance and knowledge transmission. I really appreciate that you have been always there for me when I was in troubles or when my mind start to that there was a situation but everything was, in fact, OK. A last word of gratitude: I am very grateful by the way I have been received in your lab and in your group: ENVERG (Environmental and Eco-Processes Engineering Research Group). Thank you very much!

To Anabela Coelho and Jorge Santamaría, my lab partners, I would also like to show my appreciation by the way they treated me and for the support they gave me, demonstrated either in laboratory practices or in their fellowship attitudes. Thank you for the good atmosphere you provided me in the lab and for all the advices and tips!

To my course colleagues, I would like to say I am very grateful and happy for the time we spent together during this graduation. We have definitely grown up as individuals, professionals and we have learnt just as much as we had fun… a lot! Lucky we are!

Now, I want to acknowledge to the ones who have been very important for me during this period, even though not in a scientific/academic perspective. To all of my friends, I would like to demonstrate my gratitude for supporting and encouraging me all this time and for showing me that there is “life beyond the thesis”! Thanks to each one of you for your friendship!

To my family, especially to my mother, my father and my sister, for their permanent support, encourage and patience. I am very grateful for your support and for always believing in me! Thank you for all you have been through during this graduation!

To all, thank you very much!

ABSTRACT

In the present work a stochastic model to be used for analyzing and predicting experimental data from simultaneous thermogravimetric (TG) and differential scanning calorimetry (DSC) experiments on the thermal and catalytic degradation of high-density polyethylene (HDPE) was developed. Unlike the deterministic models, already developed, with this one it's possible to compute the mass and energy curves measured by simultaneous TG/DSC assays, as well as to predict the product distribution resulting from primary cracking of the polymer, without using any experimental information.

For the stochastic model to predict the mass change as well as the energy involved in the whole process of HDPE pyrolysis, a reliable model for the cracking reaction and a set of vaporization laws suitable to compute the vaporization rates are needed.

In order to understand the vaporization process, this was investigated separately from cracking. For that, a set of results from TG/DSC experiments using species that vaporize well before they crack was used to obtain a global correlation between the kinetic parameters for vaporization and the number of C-C bonds in the hydrocarbon chain. The best fitting curves were chosen based on the model ability to superimpose the experimental rates and produce consistent results for heavier hydrocarbons. The model correlations were implemented in the program's code and allowed the prediction of the vaporization rates.

For the determination of the global kinetic parameters of the degradation reaction to use in the stochastic model, a study on how these parameters influence the TG/DSC curves progress was performed varying those parameters in several simulations, comparing them with experimental data from thermal and catalytic (ZSM-5 zeolite) degradation of HDPE and choosing the best fitting. For additional improvements in the DSC stochastic model simulated curves, the thermodynamic parameters were also fitted.

Additional molecular simulation studies based on quantum models were performed for a deeper understanding on the reaction mechanism and progress.

The prediction of the products distribution was not the main object of the investigation in this work although preliminary results have been obtained which reveal some discrepancies in relation to the experimental data. Therefore, in future investigations, an improvement of this aspect is necessary to have a stochastic model which predicts the whole information needed to characterize HDPE degradation reaction.

Keywords: high-density polyethylene (HDPE); kinetic modeling; stochastic modeling; thermal and catalytic degradation; differential scanning calorimetry (DSC); thermogravimetry (TG).

RESUMO

Neste trabalho foi desenvolvido um modelo estocástico com o intuito de analisar e prever os resultados experimentais, provenientes da análise simultânea por termogravimetria (TG) e calorimetria diferencial de varrimento (CDV), da degradação térmica e catalíca do polietileno de alta densidade (PEAD). Ao contrário dos modelos determinísticos já existentes, com o presente modelo é possível calcular as curvas de degradação de massa e energia medidas pelas técnicas TG/CDV, bem como prever a distribuição de produtos obtidos do *cracking* do polímero, sem recorrer a qualquer informação experimental.

Para se obter um modelo estocástico que preveja a variação da massa e a energia envolvidas no processo de pirólise do PEAD, é necessário ter um modelo cinético que descreva o processo de *cracking* e as leis de vaporização que descrevam adequadamente as velocidades de vaporização.

Com o objectivo de perceber o processo de vaporização, este foi estudado separadamente do *cracking*. Assim, utilizou-se um conjunto de resultados experimentais (análise TG/CDV) de compostos que vaporizam muito antes de sofrerem *cracking* para obter uma correlação global entre os parâmetros cinéticos de vaporização e o número de ligações C-C na cadeia do hidrocarboneto. Utilizou-se o modelo desenvolvido para fazer várias simulações com diferentes expressões matemáticas para descrever a vaporização e o melhor ajuste foi escolhido com base na sobreposição das curvas aos resultados experimentais e na capacidade de produzir resultados consistentes para hidrocarbonetos mais pesados. As correlações escolhidas foram, então, implementadas no código do programa, permitindo descrever as velocidades de vaporização.

Para determinar os parâmetros cinéticos globais da reacção de degradação, com posterior utilização no modelo, foi efectuado um estudo sobre a influência dos mesmos no andamento das curvas de TG e CDV. O estudo consistiu na execução de várias simulações com diferentes valores dos parâmetros cinéticos, na comparação destes com os resultados experimentais da degradação térmica e catalítica (com o zeólito ZSM-5) do PEAD e na escolha do melhor ajuste. Posteriormente ajustaram-se os valores dos parâmetros termodinâmicos para se obterem ajustes ainda melhores nas curvas de CDV simuladas pelo modelo estocástico.

Foi ainda efectuado um estudo de simulação molecular, com base em modelos quânticos, de forma a obter um conhecimento mais profundo sobre o mecanismo e o progresso da reacção.

A previsão da distribuição de produtos não foi o objecto principal de estudo deste trabalho ainda que tenham sido obtidos resultados preliminares que apresentam algumas discrepâncias em relação aos resultados experimentais. Assim, em trabalhos futuros, sugere-se o desenvolvimento deste tópico para se obter um modelo estocástico que consiga prever toda a informação relativa à degradação do PEAD.

Termos-chave: polietileno de alta densidade (PEAD); modelação cinética; modelo estocástico; degradação térmica e catalítica; calorimetria diferencial de varrimento (CDV); termogravimetria (TG).

TABLE OF CONTENTS

LIST OF FIGURES

LIST OF TABLES

NOMENCLATURE

APME	Association of Plastics Manufacturers in Europe
% (w/w)	Mass percentage
$\Delta H_{(C-C)}$	Average C-C bond enthalpy
ΔH_{vap}	Average vaporization enthalpy
C_p	Average Heat Capacity
DSC	Differential Scanning Calorimetry
DSC/TG	simultaneous Differential Scanning Calorimetry and Thermogravimetry
dt	Time step of integration
E_a	Activation energy of the cracking process
E_{av}	Activation energy of vaporization
FCC	Fluid Catalytic Cracking
GC	Gas Chromatography
GC-MS	Gas Chromatography – Mass Spectrometry
h	Plank's constant
HDPE	High-density Polyethylene
k(T)	Temperature-dependent cracking kinetic constant rate
k_{ref}	Cracking kinetic constant rate at reference temperature
k_{refv}	Vaporization kinetic constant rate at reference temperature
k_v **(T)**	Temperature-dependent kinetic constant rate of vaporization
LDPE	Low-density Polyethylene
LLDE	Linear Low-density Polyethylene
m	Experimental weight of the sample
$m_{\text{mod mixt}}$ **(t)**	Total weight of the sample given by the model (vaporization of hydrocarbon's mixtures)
$m_{\text{total sample}}$	Total weight of the sample
$m_{0\ \text{mixt}}$	Initial sample of the hydrocarbon's mixture sample
m_e	Electron mass
m_h	Weight of the heavier hydrocarbon in the mixture
m_{heat}	Mass of bonds heated per time unit
m_l	Weight of the lighter hydrocarbon in the mixture
MSW	Municipal solid wastes
m_v	Mass of bonds evaporated per time unit
n_b	Number of bonds broken per time unit
n-C6	n-hexane
n-C7	n-heptane
n-C9	n –nonane
n-C10	n-dodecane
n-C12	n-dodecane
n-C20	n-icosane
n_l	Number of C-C bonds in an hydrocarbon chain
Nr. Bonds	Number of bonds per molecule

Nr. Molecules	Number of molecules
PE	Polyethylene
PET	Polyethylene therephtalate
PP	Polypropylene
PVC	Polyvinyl chloride
p_x	Probability of the occurrence of the first-order processes of vaporization and cracking
r	Distance between the nuclear and the electron charges
T	Temperature
t	Time
TCDPE	Thermal and Catalytic Degradation of Polyethylene
T_f	Final temperature used in the simulation process
TG	Thermogravimetry
TGA	Thermogravimetric Analysis
T_i	Initial temperature used in the simulation process
T_{ref}	Reference Temperature
$T_{vaporization}$	Approximated vaporization temperature
VMHK	Vaporization of Mixtures of Hydrocarbons Kinetics
VPHK	Vaporization of Pure Hydrocarbon Kinetics
X	Mass fraction
X_{mod}	Mass fraction obtained from $m_{mod\ mixt\ (t)}$ and $m_{0\ mixt}$
X_{exp}	Mass fraction associated to experimental data
X_{glob}	Mass fraction by means of the global fitting
X_{ind}	Mass fraction obtained by means of the individual fittings
Z	Atomic charge
α	Number of bonds lost to the gas phase
β	Heating rate
Ψ (x,y,z)	Wavefunction in Schrödinger equation

MOTIVATION AND MAIN OBJECTIVES

In the last years, a huge amount of plastics has been produced as result of their versatility of applications and low cost production. Among the various types of plastics produced, polyethylene is the one which is majorly consumed. This massive plastic production leads to a social and environmental issue related to waste management, since the residues have low biodegradability and high chemical inertness. Therefore, an increasingly amount of municipal solid waste in landfills has been observed.

Thus it is urgent to develop techniques that allow, at the same time, the proper disposal of the wastes and to harness of the plastic residues potential.

In the case of polyethylene, its catalytic degradation emerges as an efficient alternative to achieve that goal. With this process, it is possible to eliminate PE waste and convert it into added value hydrocarbons that can be used as chemicals or fuels. This latter aspect makes the process even more advantageous due to petroleum resources scarcity.

For such an important technique in terms of energetic, social and environmental issues, it is crucial to have a deeper knowledge for a possible further industrial implementation. For this purpose, the modeling of the process emerges as a powerful tool since it allows predicting the reaction process.

Starting from this background, the main goal of this work is to contribute to the development of a reliable model that can predict the thermal and catalytic degradation of polyethylene.

The most used technique to evaluate this reaction is the simultaneous DSC/TG analysis. The models that are already developed to predict the latter process are deterministic ones and present a major limitation since they do not work in an autonomous way, i.e., they can predict thermal and catalytic of PE but only partially or using experimental information.

The objective of this work is to develop a stochastic model that allows the prediction of the process in a reliable *ab initio* way, only by inserting the operation conditions, thermodynamic and kinetic data, as well as the type and number of molecules whose degradation is tested. Therefore, the drawbacks of the deterministic models can be solved.

1. INTRODUCTION

1.1. Plastic materials demand and production

If we take a look to our day-to-day lives, it is easy to identify a countless number of objects made of plastic and it is also easy to understand our huge dependence on this type of materials. In fact, due to an enormous growth of welfare in the second half of the twentieth century and simultaneously due to plastic's excellent properties and low cost, we have witnessed a huge increase in their demand and, consequently, in their production in the last decades, unparalleled in other materials (Gobin, Manos 2004, Contreras, Garcia et al. 2012)

According to a 2010 report from Association of Plastics Manufacturers in Europe (Association of Plastics Manufacturers in Europe (APME) 2010), the world plastics industry has grown continuously in the last fifty years, being verified an increase in the production from 1,5 million tons in 1950 to 230 million tons in 2009, which corresponds to an increment of 9% per year, on average (see Figure 1.1).

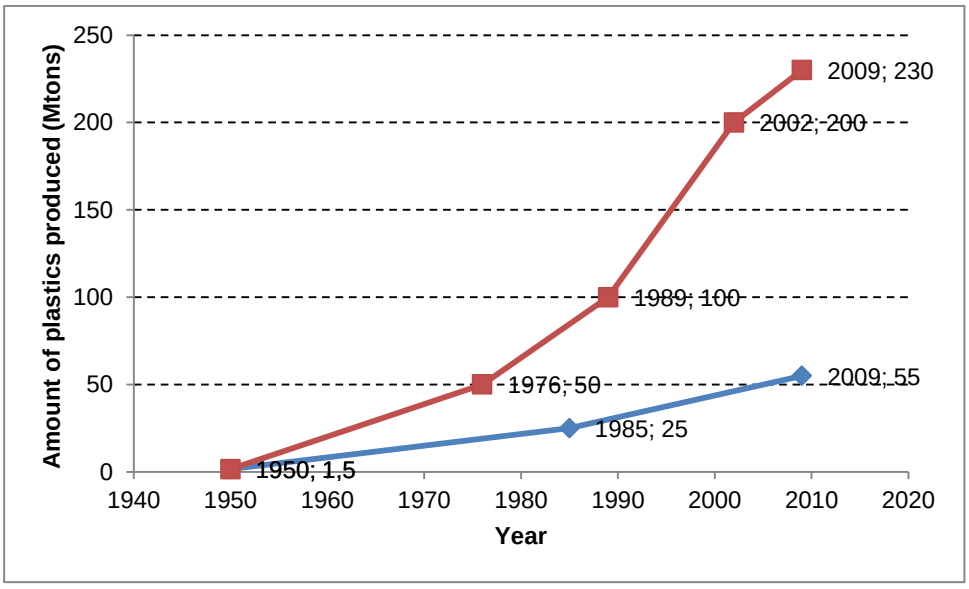

Figure 1.1 - World (red line and symbols) and Europe (blue line and symbols) plastics production between 1950 and 2009 [source: Plastics Europe Market Research Group (PEMR), from (Association of Plastics Manufacturers in Europe (APME) 2010)].

In the same study (Association of Plastics Manufacturers in Europe (APME) 2010) it is also noticeable that in 2009, from the 230 million tons of the plastics produced in the world, around 24% were manufactured in the European continent (comprises EU27, Norway and Switzerland) in a total of 55 million tons.

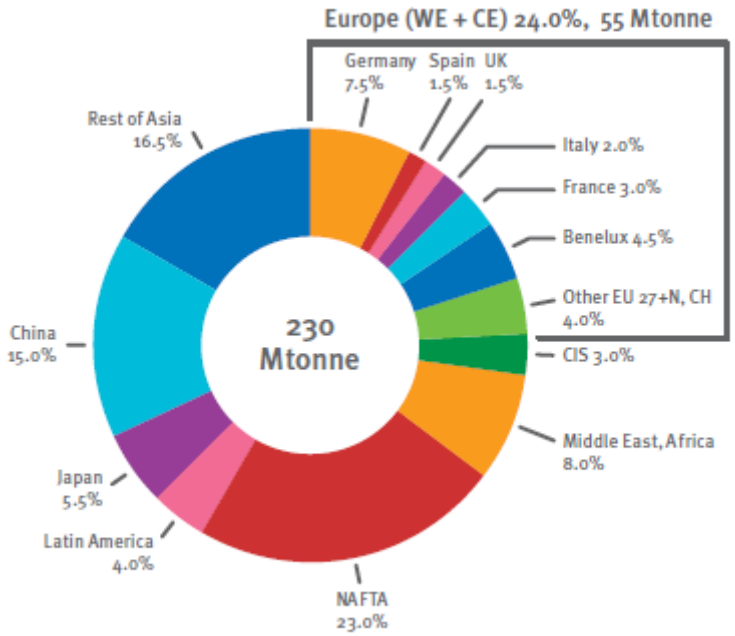

Figure 1.2 - World plastics production in 2009 [source: PlasticsEurope Market Research Group (PEMR), from (Association of Plastics Manufacturers in Europe (APME) 2010)].

Among the amount of polymers produced in Europe, in 2009, there are five high-volume plastics families: polyethylene (PE), polypropylene (PP), polyvinyl chloride (PVC), polystyrene (solid PS and expandable PS) and polyethylene terephtalate (PET). In fact, these five types of polymers account for around 75% of all European plastics demand (see Figure 1.3).

Due to their growing range of applications and due to their versatility, polymer demand in Europe is led by polyolefins, such as PE and PP (Association of Plastics Manufacturers in Europe (APME) 2010, Contreras, Garcia et al. 2012). Thus, polyethylene (low density, LDPE; high density, HDPE and linear low density, LLDPE) and polypropylene (PP) are the most used polymers, accounting for around 50% of all plastics demand, in the 2009 in Europe (EU27, Norway and Switzerland) (Association of Plastics Manufacturers in Europe (APME) 2010).

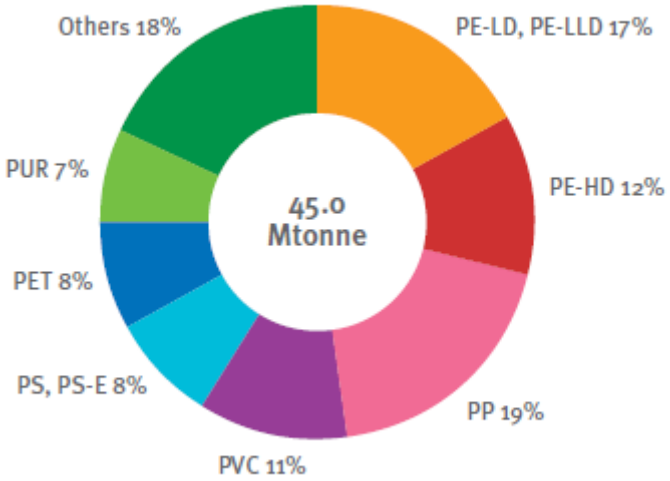

Figure 1.3 - Europe (EU27, Norway and Switzerland) plastics demand by polymer types in 2009 [source: PlasticsEurope Market Research Group (PEMRG), from (Association of Plastics Manufacturers in Europe (APME) 2010)].

1.2. Plastic wastes: is it possible to have a life after consumption?

As it is shown in Figure 1.2 and Figure 1.3, millions of tons of plastics are produced every year. This massive consumption leads to a proportional emergence in the amount of plastic residues since a lot of the applications correspond to low lifetime products. To get an idea of this huge phenomenon, in the last decade the consumption of plastics has led to a consequent 3% increment in post-consumer end-of-life plastic waste (Association of Plastics Manufacturers in Europe (APME) 2010) Moreover, in Europe, in 2004, the 40 millions of plastic material consumed have been transformed into 30 million tons of waste. As it is known, the low biodegradability and chemical inertness of such materials make their wastes' disposal a serious environmental problem (Contreras, Garcia et al. 2012).

The most current methods to manage municipal solid wastes (MSW), where plastic residues are included, are landfill and incineration (Coelho 2008).

In the first disposal method, there's a problem relating with the fact that plastics take a considerable time to break down at landfills (Coelho 2008). Thus, they occupy a large volume of landfills sites or rubbish tips, which is exacerbated by the fact that this waste type is more voluminous than others, leading to scarcity of disposal areas (Association of Plastics Manufacturers in Europe (APME) 2010, Gobin, Manos 2004, Contreras, Garcia et al. 2012, Coelho 2008) Additional drawbacks are associated to this disposal technique: the process generates explosive and toxic gases and its costs are become higher and higher (Association of Plastics Manufacturers in Europe (APME) 2010, Contreras, Garcia et al. 2012, Coelho 2008)

In alternative to landfilling and to decrease the volume occupied by plastic waste appears the direct incineration. In this technique plastic residues are burnt to produce energy (Contreras, Garcia et

al. 2012). Nonetheless, because of the generation of toxic gases, it can be said that this process shifts a solid waste issue to an air pollution one (Gobin, Manos 2004). Moreover, the high operating temperatures, the fact that the energy released is often not properly harnessed and due to the production of compounds with a very low economic value, this method is criticized by several environmentalists and researchers.(Contreras, Garcia et al. 2012).

By means of the previous methods it is not possible to take advantage of the whole plastic waste potential and there are also environmental issues associated, which make them unreliable treatments. Therefore, to take full advantage of these residues, part of the solution has to be the acceptance by society to use resources efficiently and that these valuable materials should not go to landfill or direct incineration. In this way, restrictions on landfilling are being implemented through countries legislation (Association of Plastics Manufacturers in Europe (APME) 2010). These restrictions create strong drivers to increase both recycling and energy recovery which has taken rates above 80% in 2009, according to (Association of Plastics Manufacturers in Europe (APME) 2010). In fact, plastic wastes' re-use, due to their high content of carbon and calorific value, allows their using as a raw material or as fuel source, making them an available supply of chemicals and energy (Coelho, Costa et al. 2010). As it can be observed in Figure 1.4, this process of capture value from plastic (from recycling and energy recovery) waste is underway, even though it is slow: there's an increase of only 2% per year (Association of Plastics Manufacturers in Europe (APME) 2010).

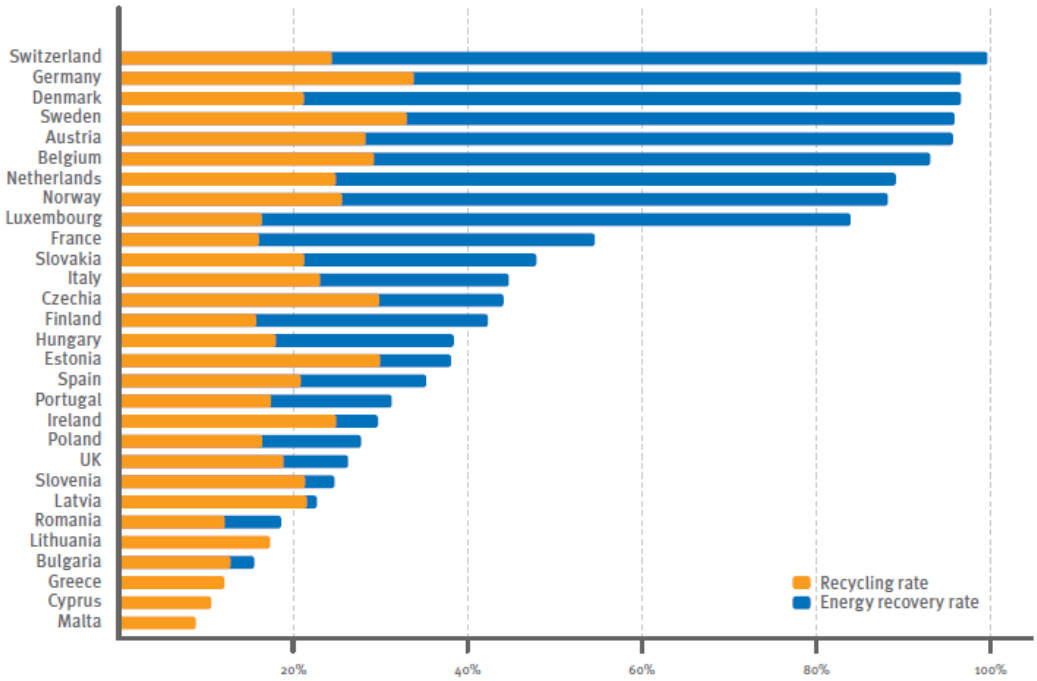

Figure 1.4 - Total recovery ratio by country (referred to post-consumer plastic waste), in 2009 [source: (Association of Plastics Manufacturers in Europe (APME) 2010)].

Thus it can be concluded that plastic materials can have a “life” after their consumption but only if recycling methods are used to treat them. Indeed, one can say: “plastics are too valuable to throw away!” (Association of Plastics Manufacturers in Europe (APME) 2010).

A recycling method is now presented. Even though it has still handicaps, mechanical recycling presents some features that provide taking advantage of plastic waste value.

According to (Association of Plastics Manufacturers in Europe (APME) 2010), the EU members plus Norway and Switzerland, in 2009, from the 24,3 million of tons of post-consumer waste produced, have treated 22,2% through mechanical recycling. It comprises a way to reprocess the end-of-plastics into re-usable materials through a physical treatment that doesn’t break the original polymer chains and molecules, leaving material’s original structure and properties intact (Association of Plastics Manufacturers in Europe (APME) 2010).

This technique include the steps of sorting the polymeric residues by type, shredding the waste into particles of smaller dimensions, melting them down and remolding the thermoplastic to transform it into new-machine ready granules (Association of Plastics Manufacturers in Europe (APME) 2010, Contreras, Garcia et al. 2012).

Unlike landfilling and incineration, the recycled materials obtained with the current method are welcomed by society. Nevertheless, there are some drawbacks associated with it: the products have a very poor quality since the residues are subjected to high temperatures melting and also due to the varying quality of the original waste and the eventual presence of impurities and additives (Contreras, Garcia et al. 2012). Besides the recycled products are often more expensive than the virgin material (Garforth, Ali et al. 2005).

1.3. Plastic waste pyrolysis or degradation

As a way to harness the whole potential of plastic waste a different technology based on polymer pyrolysis has appeared; this allows the transformation of these residues into high added value hydrocarbons (liquid or gaseous) to be used as chemicals and/or fuel (Contreras, Garcia et al. 2012, Coelho, Costa et al. 2012) . For these reasons, the present technique becomes a good alternative to the methods already outlined (Gobin, Manos 2004, Contreras, Garcia et al. 2012, Coelho, Costa et al. 2012) since it solves the disposal problems and spares the petroleum resources (Coelho, Costa et al. 2012)

Pyrolysis methods are defined as the chemical changes that occur when heat is applied to a material, in the absence of oxygen (Overend 1986). Focusing in PE, its transformation into hydrocarbons can be performed either by thermal or catalytic degradation (Coelho, Costa et al. 2012, Association of Plastics Manufacturers in Europe (APME) 2010, Gobin, Manos 2004, Coelho 2008).

1.3.1. **Thermal degradation of polyethylene**

a. General considerations

The thermal degradation of polyethylene presents some advantages when compared to the other methods of polymeric waste management that have already been showed.

Nevertheless, pure thermal degradation requires high operation temperatures, ranging from 500^{o}C to 800^{o}C (Contreras, Garcia et al. 2012). In fact, according to (Coelho, Costa et al. 2012), the degradation temperature of HDPE in a purely thermal assay under dynamic conditions in an inert atmosphere is around 483^{o}C. These operation conditions and the fact that the cracking reactions are endothermic require, consequently, a high energetic input (Contreras, Garcia et al. 2012, Gobin, Manos 2004). Due to the factors enunciated before, together with the production of poor quality compounds, the current recycling method became economically unattractive (Gobin, Manos 2004, Coelho, Fonseca et al. 2010, Coelho, Costa et al. 2012, Contreras, Garcia et al. 2012).

b. Reaction mechanism

There are four types of reaction mechanisms associated with the thermal cracking of plastics: end-up chain scission; random-chain scission; chain-stripping or cross-linking (Buekens, Huang 1998). The different mechanisms and, consequently, the product distributions are related with bond dissociation energies, chain defects in the polymers, the aromaticity degree, as well as the presence of hetero-atoms in the polymer-chain (Buekens, Huang 1998). PE pyrolysis, in turn, occurs through a random-chain scission mechanism (Scoethers, Buekens 1979) that will be outlined in the following paragraphs.

When a certain amount of heat supplied to a long chain of ethylene monomers, the scission of the polymer bonds occurs and smaller fragments are produced (Coelho 2008). Since all C-C bonds in the polymer chain have, in principle, the same strength, bond scission is expected to occur randomly (Coelho 2008).

According to (Bockhorn, Hornung et al. 1999), the general mechanism for thermal degradation of polyethylene can be described as follows:

- Due to the heat applied, the degradation reaction is initiated by an homolytic random scission of the polymer chain into primary radicals (species with an unpaired electron). This step is called initiation (see Figure 1.5);

Figure 1.5 - Ilustration of the initiation step according to a free radical chain mechanism for PE thermal degradation [adapted from (Bockhorn, Hornung et al. 1999)].

- Following initiation, a propagation step takes place. It can occur by means of two different ways[1]: intramolecular hydrogen transfer or intermolecular hydrogen transfer;

- Intramolecular hydrogen transfer is favored by lower temperatures and it consists in two stages: first there is a hydrogen transfer within the primary radical molecule. Thus is obtained a more stable radical (e.g. secondary, tertiary, etc.) (see Figure 1.6). This new stable radical undergoes a new reaction stage and, by means of β-scission, origins a primary radical and an olefin, according to two different paths. The primary radicals will continue the depolymerization;

Figure 1.6 – Possible paths that allows the β-scission of the more radicals, resulting a primary radical and an olefin [adapted from (Bockhorn, Hornung et al. 1999)].

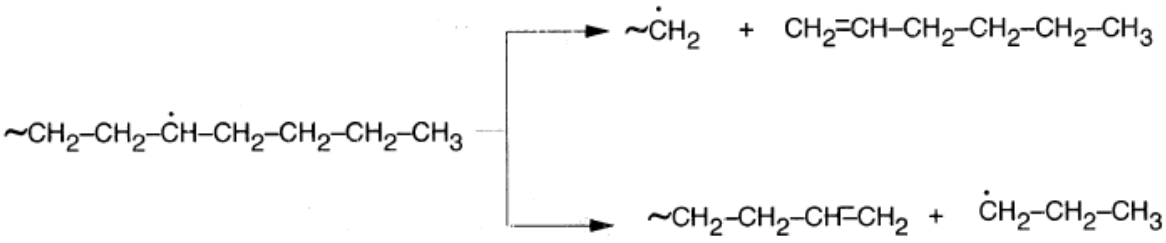

Figure 1.7 - Intramolecular –hydrogen- transfer- formation of a more stable radical from a primary one [adapted from (Bockhorn, Hornung et al. 1999)]

- At higher temperatures, the abstraction of a hydrogen atom by means of intermolecular hydrogen transfer between a primary radical and a paraffin fragment, to form a paraffin and a more stable radical occurs (see Figure 1.8);

Figure 1.8 - Formation of more stable radicals, via intermolecular hydrogen transfer [adapted from (Bockhorn, Hornung et al. 1999)].

[1] Note that these two paths of the depolymerization occur simultaneously, even though their extension is controlled thermodynamically, namely by the influence of temperature.

- Finally, termination steps occur by combination of two primary radicals to form an inert molecule (see Figure 1.9).

Figure 1.9 – Termination step according to a free radical chain mechanism (adapted from (Bockhorn, Hornung et al. 1999)).

c. Promising improvements

As it was seen previously, although this process presents some advantages in relation to mechanical recycling and, in turn, to landfill and incineration (Association of Plastics Manufacturers in Europe (APME) 2010), there are still some drawbacks associated to its operation conditions and product's quality.

More recently, it has been proved that the use of solid catalysts presents as a promising technique (Association of Plastics Manufacturers in Europe (APME) 2010, Contreras, Garcia et al. 2012, Gobin, Manos 2004, Coelho, Fonseca et al. 2010, Coelho, Costa et al. 2012, Marcilla, Gómez-Siurana et al. 2007, Marcilla, Gómez-Siurana et al. 2007).

In the following subchapter this alternative process, the catalytic degradation of polyethylene, will be more minutely outlined.

1.3.2. Catalytic degradation of polyethylene

a. General considerations

In order to improve the thermal degradation of polyethylene and solve some of the problems associated with its valorization, the use of solid catalysts seems to be a promising alternative. In a general way, the use of catalysts allows the reduction of process temperature, resulting in a reduction of the energetic input, as well as it makes possible to control hydrocarbons product distribution. In this way, hydrocarbons products in the motor fuel boiling point range are formed, which means that materials of high added value are obtained and their upgrade is no longer necessary (Association of Plastics Manufacturers in Europe (APME) 2010, Contreras, Garcia et al. 2012, Gobin, Manos 2004, Coelho, Fonseca et al. 2010, Coelho, Costa et al. 2012). These products are those which are suitable for liquid fuel usage. In fact, when compared to thermal cracking, this process produces more volatile hydrocarbons[2] such as those in the range of C_5-C_9 and compounds with a greater octane index[3], such as aromatics, naphtenes and iso-alkanes (in the previous mentioned range) (Buekens, Huang 1998).

[2] Hydrocarbons have to be volatile enough to start the engine when it is cold (Buekens, Huang 1998).

These improvements make the process economically viable (Marcilla, Gómez-Siurana et al. 2007, Gobin, Manos 2004, Contreras, Garcia et al. 2012, Coelho, Fonseca et al. 2010, Coelho, Costa et al. 2012).

In a general way, this process can be schematized as follows (Figure 1.10):

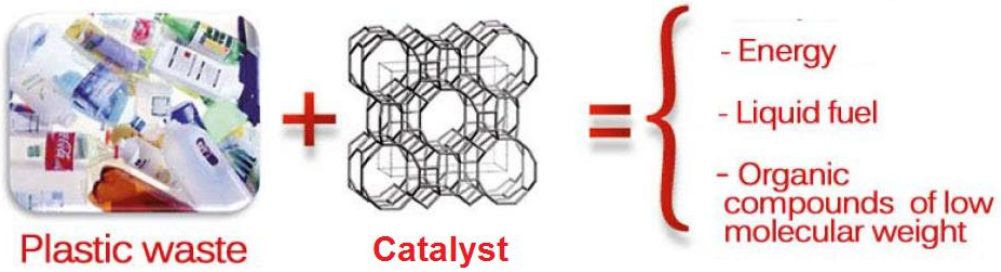

Figure 1.10 - Illustration of the general process of plastics catalytic degradation [adapted from (Contreras, Garcia et al. 2012)].

b. Most used catalysts

The most commonly used catalysts are porous solid catalysts such as mesoporous and microporous materials like MCM-41, pillared clays and different zeolites (HY, H-ZSM-5, H-Beta), being the last ones the most studied catalysts (Coelho 2008, Contreras, Garcia et al. 2012, Gobin, Manos 2004, Marcilla, Gómez-Siurana et al. 2007).

According to (García, Serrano et al. 2005), there's a direct correlation between catalysts' acidity and pore size with the compounds produced by cracking. In one hand, the cracking of polyethylene using mesoporous catalysts like MCM-41, due to its large pore size and medium acidity, produces hydrocarbons within the range of gasoline, which may be explained from the occurrence of a random scission mechanism. On the other hand, ZSM-5 catalyzed degradation of PE results in the formation of lighter and gaseous hydrocarbons and some aromatic compounds. This product distribution is achieved due, for example, to and an end-chain cracking mechanism which is consequence of its small pore size and strong acidity (García, Serrano et al. 2005).

Like catalysts' acidity and pore size, the particle size also plays an important role on the production of the degradation products type. Both for H-ZSM-5 and H-Beta zeolites, showed a high cracking activity due to their large external surface area and low diffusional problems. On contrary, amorphous silica-alumina MCM-41 showed lower values of activity (García, Serrano et al. 2005).

H-ZSM-5 and HY zeolite catalysts are used in the fluid catalytic cracker (FCC) and can in fact degrade PE with a higher yield on hydrocarbons and obtain a relatively low coke content (<1% (w/w) and 8% (w/w), respectively), confirming, thus, the possibility of co-fed a refinery cracking unity with plastic waste.

3 It is a measure to evaluate the gasoline quality for prevention of early ignition which leads to cylinder knock (Buekens, Huang 1998).

c. Zeolite catalysts fundamentals[4]

Zeolite catalysts are crystalline materials and are part of a family of materials denominated aluminosilicates. Their structure is based on a tridimensional framework of tetrahedrical sites TO_4 (SiO_4 or AlO_4^-) linked by the oxygen atoms. The repetition of these unities leads to a microporous structure that can consist of channels and/or cavities.

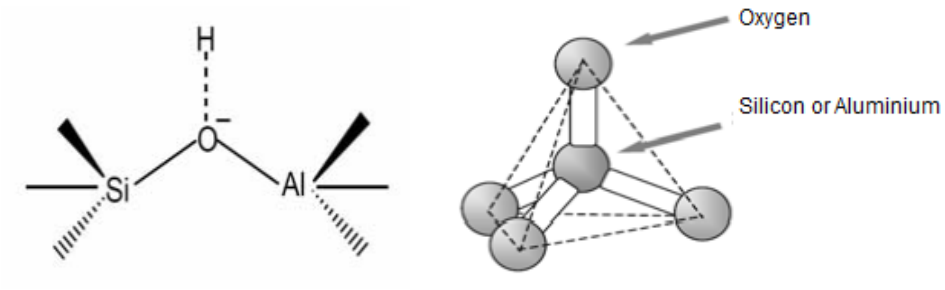

Figure 1.11 – Chemical structure of a zeolite [adapted from (Haag, Lago et al. 1984)] (on reader's left side); primary building unit of zeolite structure [adapted from (Georgiev, Bogdanov et al. 2009)] (on reader's right side).

Due to the existence of trivalent aluminium atoms, the overall zeolite framework has a negative charge which is compensated by the existing cations (usually metals or protons) in the lattice, ensuring, in this way, the electrical neutrality.

The ability to modify, in an easy way, the composition, structure and porosity of these compounds, either by direct synthesis or by post-synthesis treatments (dealumination, ion exchange, etc) have led researchers to produce more than 130 different types of zeolites. Therefore, zeolites can be used in acid, basic, acid-base, redox or bifunctional catalysis, even though they are mostly used in acid and bifunctional catalysis. In catalytic degradation of polyethylene by using zeolites, acid catalysis is used.

In zeolites there are two types of acid sites: Brønsetd acid sites and Lewis acid sites.

Brønsetd acid sites are related with the presence of hydroxyl (OH) groups. These in turn can be classified in: structural or bridging groups [SiO(H)Al], terminal silanol groups [SiOH] and aluminium hydroxyl groups [AlOH]. The first type of OH groups represents Brønsetd acid sites which are the strongest and are located mainly in the zeolites microporous. On the other, terminal silanol groups are usually generated in the external surface of zeolite's structure or by the presence of structural defects. Finally, the last type of acid sites result from the existence of an aluminium extra-framework phase.

Lewis acid sites are electron acceptors sites and, thus, are not related to the presence of hydroxyl group. Instead, they are associated with the tri-coordinate aluminium and another cationic species present.

An important information on zeolite's acidity is the silicon to aluminium ratio (or silica to alumina – SiO_2/Al_2O_3 ratio), which is related to the number of acid Brønsetd sites. In fact, the total number of

[4] This subchapter is based on the following reference: (Guisnet, Ramôa 2004)

such acid sites corresponds to the number of tetrahedral aluminium atoms in the framework, which are balanced by the presence of protons to ensure the electrical neutrality. An increasing in Si/Al value means that the number of Brønsetd sites decreases since the fraction of Al atoms also decreases. On the other hand, decreasing the Si/Al ratio also causes an increment in Brønsetd acid sites strength.

A way to increase Lewis acidity is the presence of multivalent cations in the zeolite lattice.

d. Reaction mechanism

The cracking occurred in FCC unities in refinery can be explained with basis in a carbocation reaction mechanism due to the acidity of the catalysts' Lewis or Brønsted sites (Buekens, Huang 1998). For catalytic cracking of polyethylene, similar mechanisms have been postulated (Buekens, Huang 1998). It is now accepted that catalytic cracking occurs through the formation of carbocations and two mechanisms are possible: by formation of carbenium ions (paraffin with a carbon atom tri-coordinated and positively charged) or by formation of carbonium ions (paraffins with a carbon atom penta-coordinated, positively charged) (Rebelo 2009).

Carbenium-ion mechanism

I. Initiation step

There are two possible ways of initiation step to occur: by protonation of an olefinic bond by a Brönsted acid site or by the hydride abstraction in Lewis acid sites.

The initiation possibility concerning the protonation of a double bond may be related to the existence of defect sites in polymer's chain (e.g. an olefinic bond). On these olefinic defects, the Brønsted acid sites from the acid catalyst, HX, attack, by proton addition, being produced a carbenium ion and the deprotonated acid site, X^- (Buekens, Huang 1998).

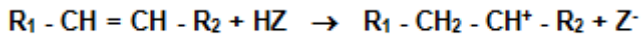

Figure 1.12 – Initiation step of PE catalytic cracking by means of an olefin protonation by a Brönsted acid site.

On the other hand, the reaction initiates by means of a Lewis acid site hydride-ion abstraction, being originated a carbenium ion and the protonated Lewis acid site.

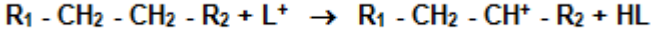

Figure 1.13 - Initiation step of PE catalytic cracking by means of Lewis acid site hydride-ion abstraction.

II. Propagation step

The depolymerization proceeds by successive attacks from acidic sites or by other carbonium ions (R^+) with subsequent chain scission, which leads to the production of an oligomeric fraction (in the average range of C_{30}-C_{80}) (Buekens, Huang 1998). The oligomeric fraction is further cleaved by means of β-scission of chain-end carbenium ion, leading to gas formation (lighter fragments) and to liquid formation (in the average range of C_{10}-C_{25}) (Buekens, Huang 1998). Even though this is the most important step in the catalytic cracking of PE, propagation may proceed in two other ways from the carbenium ions produced in the initiation step. It can occur the loss of a proton, being originated a new olefin or an intermolecular hydrogen transfer from the carbenium ion to another paraffin may take plac (Rebelo 2009).

III. Isomerization step

Intermolecular hydrogen transfer or carbon-atom shift can make possible a double-bond isomerization of an olefin, having as intermediate an carbenium ion (see Figure 1.14). Other isomerizations can also occur, namely by methyl groups shift or saturated hydrocarbons isomerization (Buekens, Huang 1998).

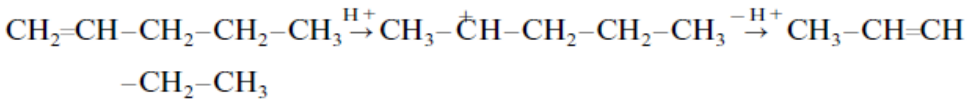

Figure 1.14 - Isomerization step according to carbocation mechanism of PE's catalytic cracking [adapted from (Buekens, Huang 1998)].

IV. Aromatization step

Some unstable carbenium ions can undergo cyclization reactions. One example of such reactions is the hydride ion abstraction on an olefin, resulting in a olefinic carbonium ion (see Figure 1.15). The so formed carbenium ion suffers subsequently an intramolecular attack on the double bound leading to the production of aromatics (see **Erro! A origem da referência não foi encontrada.**).

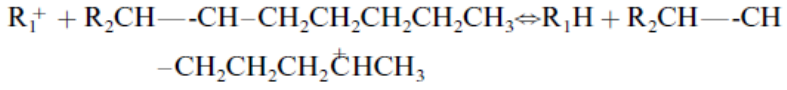

Figure 1.15 - Formation of an olefinic carbenium ion that undergoes further cyclization, according to carbocation mechanism of PE's catalytic cracking [adapted from (Buekens, Huang 1998)].

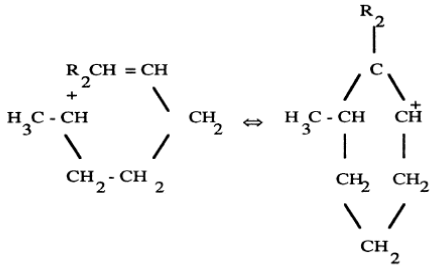

Figure 1.16 - Formation of aromatics by means of an intramolecular attack on the double bond in a olefinic carbenium ion that undergoes further cyclization, according to carbocation mechanism of PE's catalytic cracking [adapted from (Buekens, Huang 1998)].

According to the literature (Buekens, Huang 1998), the decrease in pyrolysis temperature and enhancing in the production of iso-alkanes and aromatics, when comparing with thermal pyrolysis, is well explained by the carbocation mechanism here exposed.

Carbonium ion mechanism

Even though the latter mechanism is well accepted, for some cracking catalysts, the acidic sites have enough strength to induce C-C bond protolytic scission (Coelho 2008).

This mechanism has emerged due to the product distribution data of catalytic cracking processes, where light specie lie methane, ethane and even dihydrogen which, in turn, are unlikely to be produced in the previous classical mechanism exposed (Kotrel, Knözinger et al. 2000). This type of catalytic cracking is more favorable to occur at higher temperatures and low concentrations of olefins (Kotrel, Knözinger et al. 2000).

In fact, this latter mechanism based on the protonation of an alkane leading to the production of a carbonium-ion, a highly-unstable intermediate, that will end up to collapse (see Figure 1.17) and to form to give the cracking products – Haag-Dessau mechanism (Kotrel, Knözinger et al. 2000). A generic scheme of the mechanism is presented below (Figure 1.17) and an example of the cracking of an alkane is also presented (Figure 1.18):

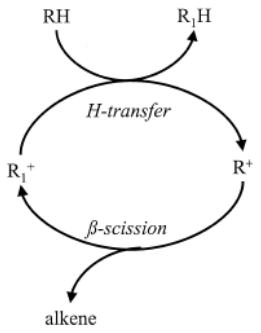

Figure 1.17 - Haag-Dessau cracking mechanism for an alkane molecule (RH) proceeding by means of carbonium ion [adapted from (Kotrel, Knözinger et al. 2000)]

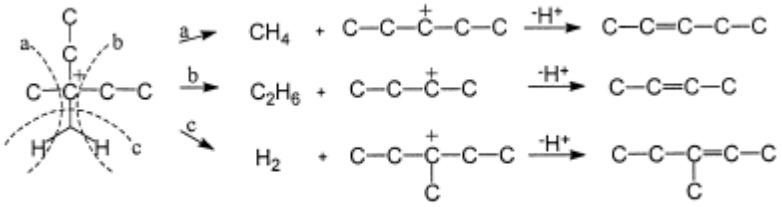

Figure 1.18 - Preferential protonation and collapse of a 3-methylpentane molecule [adapted from (Kotrel, Knözinger et al. 2000)]

1.4. Evaluation of thermal and catalytic cracking of polyethylene

1.4.1. Experimental techniques

Thermal and catalytic degradation of polyethylene (as well as other polymers) have been widely studied by several authors and have been performed in various types of reactors such as batch (Marcilla, Beltrán et al. 2009), semi-batch (Gobin, Manos 2004), fixed bed (Marcilla, Gómez-Siurana et al. 2007) and fluidized bed reactors (Mastral, Esperanza et al. 2002). Among the several studies performed, GC (gas chromatography) and GC-MS (gas chromatography – mass spectrometry) were firstly used as analytical tools and provided only the recognition of the products distribution and the calculation of products yield (Marcilla, Beltrán et al. 2009, Mastral, Esperanza et al. 2002, Gobin, Manos 2004). Therefore, one couldn't take a picture of the whole thermal or catalytic cracking process since it was not possible to monitor the reaction over the time/temperature increase.

On the contrary, TGA (thermogravimetric analysis) is said to be one of the best ways to follow the reaction extent and also to study its kinetics (Marcilla, Gómez-Siurana et al. 2007, Marcilla, Gómez-Siurana et al. 2007, Gobin, Manos 2004, Garforth, Fiddy et al. 1997, García, Serrano et al. 2005).

Although of TG analysis is useful to monitor the degradation reaction of PE, there are still some limitations associated with it that can be overcame by coupling a DSC (differential scanning calorimetry) analysis (Coelho, Fonseca et al. 2010, Coelho, Costa et al. 2010, Coelho, Costa et al. 2012, Coelho 2008). If the reaction can be followed since its beginning (by a fully monitoring experimental method), one can have a deeper knowledge of the process that makes possible the understanding of the mechanism in order to establish its kinetics (Coelho 2008, Coelho, Costa et al. 2010). As it is known, the degradation occurs by bond breaking of the main polymer chain, generating smaller molecules. However, since the initial size is extremely large, the first bond breakages are likely to produce molecules that are still very large (Coelho, Costa et al. 2010). The techniques that don´t have a simultaneous DSC/TG analysis system will only detect the reaction when the products became sufficiently small to evaporate into the gas phase. Nevertheless, with the technique used in this work, it is possible to follow the reaction since the beginning since each bond broken consumes a certain amount of energy and, by measuring the heat flow into the sample during the reaction, by means of

DSC analysis, it allows the measurement of the whole degradation process rate (Coelho, Costa et al. 2010).

1.4.2. **Kinetic modeling**

The kinetic modeling of the PE degradation reaction, either thermal or catalytic, is a very important tool in terms of the knowledge of the process. It makes possible not only a better understanding of the reaction progress and mechanism but also because, when the kinetic parameters (e.g. kinetic constant rate, activation energy and order of the reaction) are obtained, one can easily compute the experimental data and perform interpolations (Marcilla, Gómez-Siurana et al. 2007). These latter reasons are very advantageous for engineering purposes (Marcilla, Gómez-Siurana et al. 2007), namely to develop this process to an industrial scale.

An "ideal" or "perfect" kinetic model would be the one that provide a good fitting to experimental data and that involves the minimum number of parameters, among other factors. Thus, a compromise between the number of parameters, the physical reliability of the model, the reasonable simplifications to be introduced as well as the use intended for the data and the equations obtained must be found (Marcilla, Reyes-Labarta et al. 2001).

Several models have been developed for purposes of kinetic modeling of PE degradation, majorly based in thermogravimetric studies (Marcilla, Gómez-Siurana et al. 2007, Ceamanos, Mastral et al. 2002, Fernandes Jr, Araujo et al. 1997) and a few others based on DSC analysis such as the one presented by (Marcilla, Reyes-Labarta et al. 2001). However, due to the complexity of the reaction mechanism, the values of the kinetics parameters encountered in literature are very different (Coelho 2008). This discrepancy occurs because of the existing diversity of mathematical expressions used, the various kinetic analysis applied (sometimes the complexity of the mechanistic issues makes possible only the development of pseudo-kinetic models) and due to the different operating conditions associated to parameter's determination (e.g. heating rate, temperature, pressure) (Coelho 2008). Therefore, some of these kinetic models cannot be used as a reliable tool neither to predict the experimental data nor to provide correct kinetic parameters values. Another drawback associated with the previously mentioned kinetic models is the fact that they use only partial information, like the one supplied by TG curves (see sub-chapter 1.4.1), cannot provide a clear view of the whole process since the beginning of the degradation reaction occurs without any mass loss (Coelho, Costa et al. 2010).

In this way, (Coelho, Costa et al. 2010) have developed a novel kinetic model based on information from simultaneous DSC/TG analysis. This model consists in the combination of an energetic and a material balance applied to the sample in the thermo-balance's pan. Regarding the modeling of the heat flow, the authors assume that it is composed by three components: the heat required to heat the sample, the heat associated with the vaporization of the species which are small enough to go into the gas phase and the heat required to break polymer bonds (Coelho, Costa et al. 2010). On the other, the material balance applied to the sample has only two components: the number of bonds associated with polymer breakage and the average number of bonds which lost to the gas

phase (per unit mass of evaporated material, at a given moment)(Coelho, Costa et al. 2010). The equations used are as follows:

$$Heat\ flow = -m.C_p.\frac{dT}{dt} + \Delta H_{vap}.\frac{dm}{dt} - k(T).N.\Delta H_{C-C}$$

Eq. 1.1

where m is the experimental weight of the sample at any given time, C_p is the average heat capacity of the sample, ΔH_{vap} is the average enthalpy of vaporization and ΔH_{C-C} represents the average C-C bond breakage enthalpy.

$$\frac{dN}{dt} = -k(T).N + \frac{dm}{dt}.\alpha = -k_{ref}.e^{\left(-\frac{E_a}{R}\left(\frac{1}{T}-\frac{1}{T_{ref}}\right)\right)}.N + \frac{dm}{dt}.\alpha$$

Eq. 1.2

where $\frac{dm}{dt}$ is the experimental rate of mass loss, α means the average number of bonds lost to the gas phase (per unit of mass evaporated and at a given time instant), N represents the number of bonds, $k(T)$ is the first-order kinetic rate law, described by an Arrhenius law and T_{ref} = 573 K.

Eq. 1.1 was solved numerically and Eq. 1.2 was used to compute the simulated heat flow. The model parameters (see (Coelho, Costa et al. 2010) for a better understanding) were estimated by a least-square procedure using the sum of the squares of the residues on the heat flow as the objective function. In spite of the simplifying assumptions the model produces quite good fittings (Coelho, Costa et al. 2010).

1.5. Stochastic models applied to polymer degradation reactions

The models previously described in sub-chapter 1.4.2 - deterministic models - are those in which outcomes are precisely determined through known relationships (usually ordinary differential equations) without room for random variation. Instead, every set of variables are determined by parameters in the model and by sets of previous states of these variables, i.e. a given input will always produce the same output. These methods are commonly expressed by a set of coupled ordinary differential equations (Wells 2009). Unlike the latter methods, stochastic models are those in which one or more variables are random, using ranges of values for variables in the form of probability distributions.

Stochastic simulations have already been used to model different complex systems like biochemical ones (Alfonsi, Cancès et al. 2005, Lachor, Krzystof et al. 2011). According to the literature (Gillespie 2007), this type of models would be more accurate for chemical reactions simulation since there are some properties of the chemical systems where randomness is inherent (e.g. the fact that chemical systems are not fully isolated from external disturbances, the population of each chemical species do not evolve deterministically). Moreover, (Wells 2009) refers that the stochastic approach

has a clear physical basis than the deterministic approach and reinforces the importance of using stochastic simulations in chemical reactions because the stochastic nature of the reactions causes fluctuations, causing an effect on the system that cannot be evaluated by classical deterministic models. Regarding the polymer degradation reactions, it is known that they undergo through pretty complex mechanisms and can occur through a variety of mechanisms that are, in most of the times, a sequence of parallel-consecutive reactions, which makes the modeling even more complex for deterministic approaches (Galina, Lechowicz 1998, Ziff, McGrady 1986).

In addition to all the reasons pointed out before, in the specific case of PE degradation investigated in this work, the development of a stochastic model would be able to predict the TG and DSC curves based on a model without the need to use any experimental data and just having as inputs the number of molecules involved and the experimental conditions, unlike the deterministic kinetic modeling reported in (Coelho, Fonseca et al. 2010). In addition, using a stochastic model makes possible to generate a product distribution.

In general there are two types of stochastic approaches that can be used in polymerization/depolymerization reactions: the Markov chain approach and the Monte Carlo method (Pandit, Juvekar et al. 1993). Let's focus our attention on Monte Carlo approach since a variation of this method has been used in the model developed in this work (see Chapter 3 for further information).

In a general way, Monte Carlo simulation is a type of simulation that relies on repeated random sampling and statistical analysis to compute the results (Raychaudhuri 2008). Typically, the following steps are performed in a Monte Carlo simulation of a physical or chemical process (Raychaudhuri 2008):

- **Static model simulation:** each simulation starts off with developing of a deterministic model, which, by means of mathematical relationships' application, transforms the input values into the desired output;

- **Input distribution identification:** this is the step where randomness is added to input variables. Here numerical methods are used to fit the data to the theoretical discrete or continuous distributions, contained in historical distributions data base. Essentially this fitting is the same as finding the parameters of a distribution that would generate the given data.

- **Random variable generation:** after the input variables distribution is found, a set of random numbers (from the latter distribution) is generated. These set of random numbers will be used in the deterministic model to produce one set of output values. A very common way of generating the random numbers is to make it between 0 and 1 and it's called generating uniform random numbers.

- **Analysis and decision making:** a statistical analysis on the possible output values is performed. This step provides, with statistical confidence, the decisions that one might make after running the simulation.

Stochastic models have been shown to be an important and accurate tool for predicting the polymerization/depolymerization of macromolecular substrates (Train, Klein 1987). The simulations obtained for the case of ligning hydrodeoxygenation (Train, Klein 1987) and PET hydrolysis (Pandit, Juvekar et al. 1993) are in agree with experimental data. In this way, we believed that a stochastic model to predict the HDPE thermal and catalytic is urgent and can be a reality.

2. EXPERIMENTAL PROCEDURES AND APPARATUS

This chapter contains the description of all the materials used in the experiments performed in this work as well as in previous works whose experimental data are used here. In the same way, the methods and techniques used to study the vaporization and cracking and thus obtain further information in the computational model developed are also reviewed. These assays can be divided in: vaporization of pure hydrocarbons kinetics (VPHK), vaporization of hydrocarbons mixtures kinetics (VHMK) and thermal and catalytic degradation of polyethylene (TCDPE).

2.1. Materials and Reagents

In order to analyse the vaporization kinetics and the cracking phenomenon several simultaneous thermogravimetric and differential scanning calorimetry experiments have been performed. The materials used in such experiments are listed in Table 2.1.

Table 2.1 - List of the materials used in this work experiments as well as in the assays performed in previous works whose data are used (VKPH- vaporization of pure hydrocarbons kinetics; VKHM – vaporization of hydrocarbons mixtures' kinetics; TCDPE – thermal and catalytic degradation of HDPE; n.a. – not applicable).

Compound	Supplier	Physic State	Purity	Assays
n-hexane	Aldrich	liquid	≥ 99%	VPHK
n-heptane	Aldrich	liquid	99%	VPHK; VHMK
n-nonane	Aldrich	liquid	99%	VKPH
n-decane	Aldrich	liquid	≥ 99%	VPHK; VHMK
n-dodecane	Aldrich	liquid	≥ 99%	VPHK; VHMK
n-icosane	Alfa-Aesar	solid	99%	VPHK; VHMK
high-density polyethylene[5]	Repsol	solid (powder)	n.a.	TCDPE
ZSM-5 catalyst[6] (Si/Al molar ratio of 15)	Zeolyst	solid (powder)	n.a.	TCDPE

2.2. Thermogravimetric (TG) and Differential Scanning Calorimetry (DSC) analysis

All TG/DSC experiments were performed using a TA Instruments SDT 2960 simultaneous DSC-TGA apparatus. Prior to the runs, the instrument was calibrated according to the manufacturer's

5 The polymer employed was a pure, unadditivated high-density polyethylene in powder form, with an average molar mass of 300 kDa and a density of 0,96 $g.cm^{-3}$, kindly supplied by Repsol.

6 The catalyst was calcinated at 500^{o}C for 8 hours under a flow of dry air of 0,5 $L.g_{zeo}^{-1}.h^{-1}$. After calcination, the catalyst was cooled and kept in a constant high-humidity container so as to keep the catalyst's surface protected from undesired adsorption.

specification, in relation to weight, temperature and DSC calibrations. Before each experiment performed, the system has been maintained under a nitrogen flow which was kept for 30 min. in order to remove all the air from it.

2.2.1. **Sample Preparation**

For all type of assays, the samples were placed directly in a TG pan at room temperature.

In the study of the vaporization kinetics of pure hydrocarbons (VKPH) and for the vaporization kinetics of hydrocarbons mixtures' (VKHM) assays, alumina pans were used, whereas in the experiments of thermal and catalytic degradation of HDPE, the samples were placed in quartz pans.

In the VKPH assays, a fixed amount (around 10 mg) of each hydrocarbon was placed in the pan. Both the mixtures of hydrocarbon/hydrocarbon and HDPE/catalyst were prepared at room temperature. For VKHM samples, the heavier compound was weighted in first place followed by the lighter one in order to obtain a sample between the range of 25-30 mg. It can be seen a more detailed description of the sample composition of these assays in Table 2.2.

In the TCDP experiments, the HDPE/catalyst mixtures were prepared using an amount of 1 mg of catalyst to obtain around 11-12 mg of total sample. Pure HDPE samples were directly placed in the pan weighting around 10-11 mg.

Table 2.2 – Composition of the hydrocarbons mixtures used.

	Heavier Hydrocarbon		Lighter Hydrocarbon		
Hydrocarbons Mixture	**m (mg)**	**% (w/w)**	**m (mg)**	**% (w/w)**	**$m_{total\ sample}$ (mg)**
n-C10 + n-C12	9,53	37,74	15,73	62,26	25,26
n-C10 + n-C20	15,26	50,94	14,69	49,06	29,95

2.2.2. **Temperature profile**

a. Vaporization of pure hydrocarbons' kinetics measurements

After the 30 min nitrogen-purge, the runs were performed under nitrogen, with a continuous flow of 80 mL/min and using a 10^{o}C/min temperature increase rate from room temperature up to 500^{o}C in the apparatus mentioned previously. At the end of the heating, the temperature was kept for an additional 10 min time. When the run is finished, the oven was cooled down to the ambient temperature and a second run was performed with the same pan arrangement to obtain baselines, particularly for the DSC signal, which is very sensitive to the layout of the pans inside the oven. This profile is depicted in Figure 2.1.

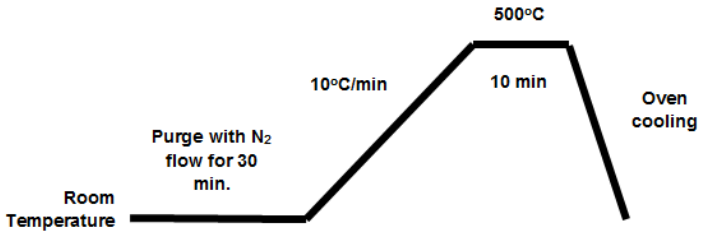

Figure 2.1 – Temperature profile for vaporization of pure hydrocarbons kinetics experiments.

b. Vaporization of hydrocarbons mixtures kinetics measurements

The temperature profile for this type of experiments is alike to the one outlined previously, with exception to the maximum temperature reached in the TG/DSC apparatus that is, in this case, of 300^{o}C. All the remainder procedures are the same (see Figure 2.2).

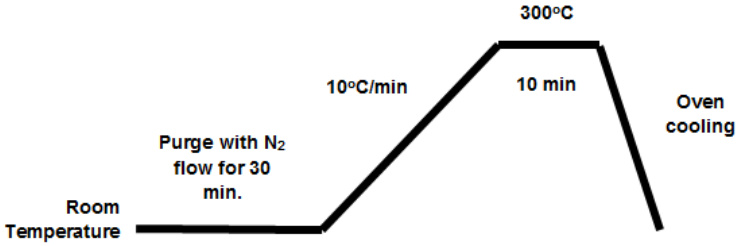

Figure 2.2 - Temperature profile for vaporization of hydrocarbons mixtures kinetics experiments.

c. Thermal and catalytic degradation of HDPE

Concerning the temperature profile of the first assays, these one has the only difference that the maximum temperature reached is 600^{o}C (see Figure 2.3**Erro! A origem da referência não foi encontrada.**).

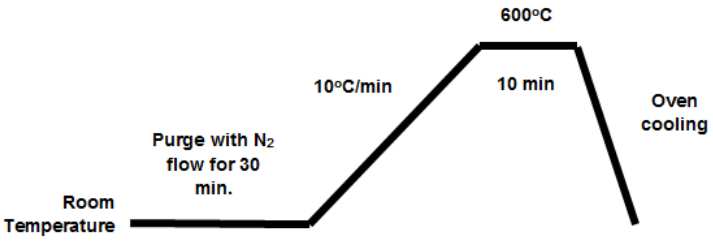

Figure 2.3 - Temperature profile for thermal and catalytic degradation of polyethylene experiments.

2.2.3. Equipment

The TG/DSC installation is composed by three main components: a sensitive recording balance, a furnace with an associated controller/ atmosphere management and a computer using data

recorder and plotter software. The installation is equipped with gas flow lines and a gas flow measurer and also has a gas outlet.

Figure 2.4 shows the components of this installation. Figure 2.5, Figure 2.6, and Figure 2.7 depict some details of the apparatus.

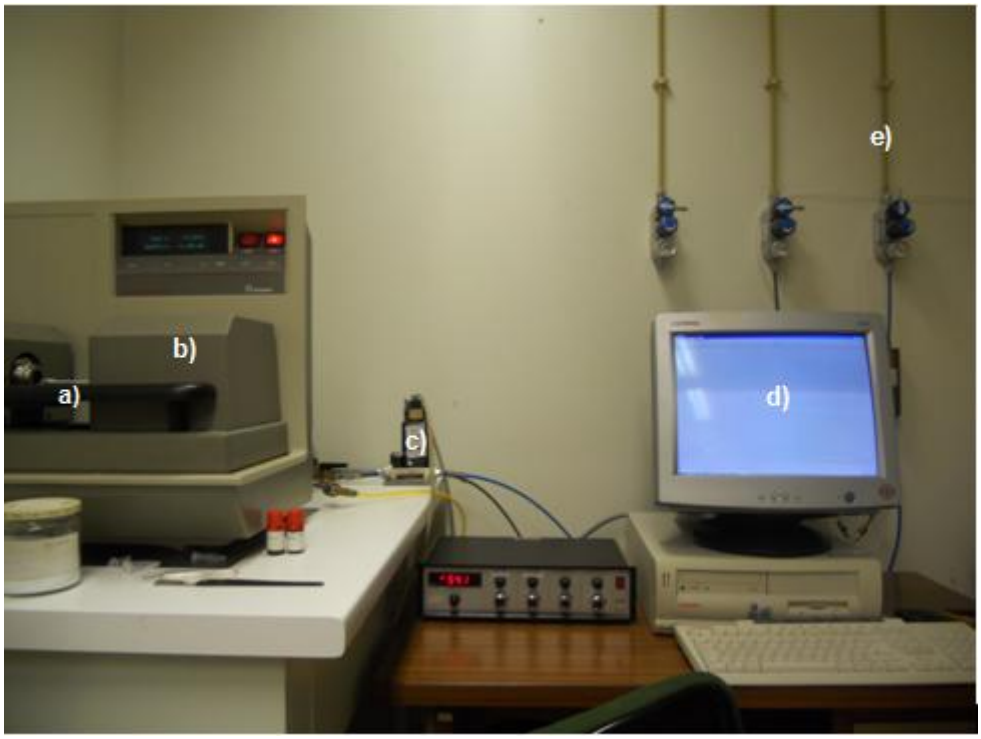

Figure 2.4 – DSC/TG installation used in the experiments performed: a) balance; b) furnace; c) gas (N_2) flow controller; d) computer; e) gas (N_2) line).

Figure 2.5 – TG/DSC instrument (TA Instruments ® SDT 2960).

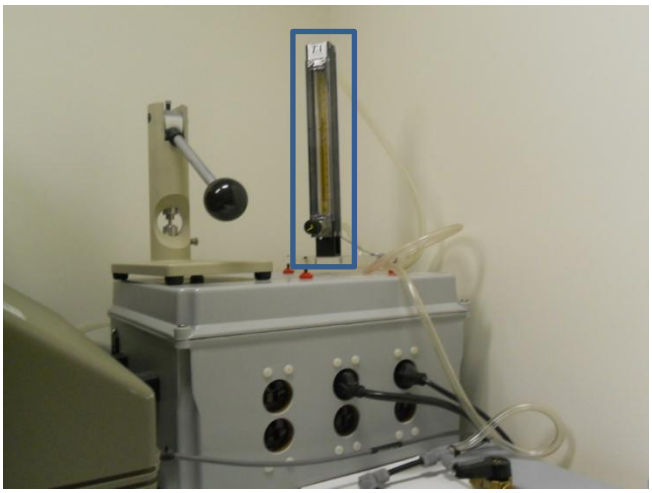

Figure 2.6 – Gas (N_2) flow measurer.

Figure 2.7 – Two pans suspended in the balance's arms with the oven open.

2.2.4. Data evaluation software and data collection

To access the data obtained from the TG/DSC experiments the data software TA Universal Analysis 2000 was used.

The data collected during the experiments was stored in the computer that communicates with and controls the apparatus. A data processing tool is also available.

2.3. Product analysis using Gas chromatography (GC)

The product distribution of the developed stochastic model was not the main object of investigation in the present work. Even though in some of the works whose results have been used here this technique has been performed, it will not be detailed. For more information about the procedures of gas collection, the temperature profile used for the runs and the equipment itself, see (Coelho, Costa et al. 2012) and (Coelho 2008).

3. COMPUTATIONAL MODEL

For the deterministic models already existing, the main shortcoming is the inability to predict the DSC curves related to PE thermal and catalytic degradation in simultaneous TG/DSC experiments without using TG experimental data. On the contrary, in this work the main goal is to develop a stochastic model that can be self-contained. In fact, the model developed is able to determine and compute the TG and DSC curves as well as the product distribution (both overall and in the gas phase) starting only from basic inputs such as the molecule in study and the experimental conditions.

Thus, this third chapter is dedicated to all aspects concerning such model. Here the interface where the model is implemented, the assumptions considered as well as the model's construction and operating themselves will be outlined.

3.1. Model's interface

The computational model was developed in an Excel 2007 worksheet using Visual Basic for Applications (see Appendix). Despite the fact that the Excel worksheet constrains the running speed of the model, it does provide an extremely easy platform for data input and graphic generation. The program reads the information supplied by the user on the type of molecules to process and the experimental conditions and computes the TG and DSC curves as well as the product distribution both overall and in the gas-phase, as already mentioned.

3.2. Model's assumptions

The model was constructed with the following assumptions:

- the bond breaking kinetics is first order in relation to breakable bonds and the probability of a given bond breaking is always the same, regardless of the bond's position in the molecule with the exception of the terminal bonds that cannot be broken (since they would generated either methyl carbocations or methyl radicals);

- the evaporation kinetics is also first order (see exposition and equations in sub-chapters 4.2 and 4.3)

- thus, both the vaporization and the bond breaking process are described as follows:

$$\frac{dm}{dt} = k_x . m$$

Eq. 3.1

- the probability, p_x, of each of these first order processes occurring in the time interval, dt, can be computed as:

$$p_x = \frac{dm}{m}$$

Eq. 3.2

Combining Eq. 3.1 and Eq. 3.2, the probability of occurrence for vaporization or cracking is given then by Eq. 3.3:

$$p_x = k_x . dt$$

Eq. 3.3

The value of p_x is saturated to 1 for large enough values of k_x. Thus, the probability of a bond being broken is computed as the rate constant for bond breaking, computed at the current temperature multiplied by the time interval. Simulations are carried-out with different time interval step so as to ensure that a precise solution is obtained.

3.3. Model's construction and operating

The procedure is implemented by starting with a bond vector that is initialised so as to describe a certain molecular arrangement. Each element in the bond vector corresponds to a certain bond and the value stored indicates if the bond is intact (value ≥ 1) or broken (value = 0) and, in the case of the bond being intact if it is in the sample in the pan (value = 1) or if it has moved into the gas phase (value = 2).

In Figure 3.1, two schemes represent the initial states for two different simulations, one with a very large molecule, like a polyethylene molecule (all bonds are intact) or when simulation a set of hexane molecules (for each five intact bonds, a broken one is inserted to separate the different molecules).

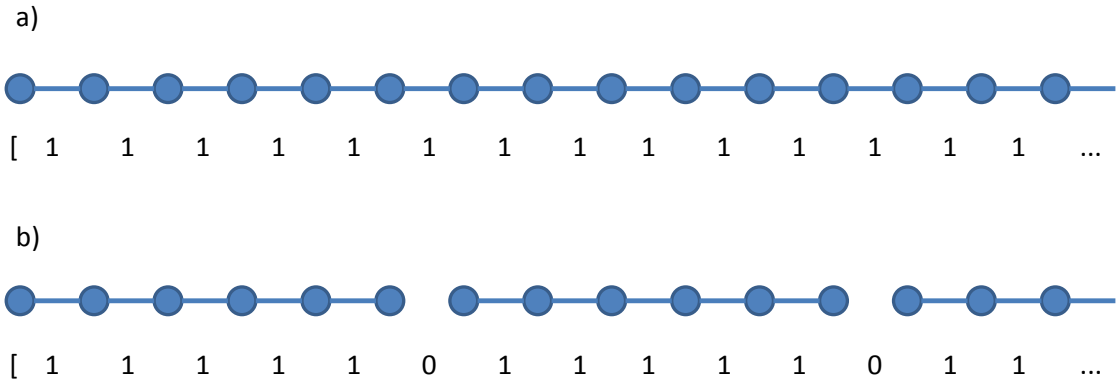

Figure 3.1 – Bond vector to describe two different initial situations: a) large molecule (all bonds intact) and b) hexane molecules (one broken bond for each five intact ones).

The sequence of activities in the computational model can be visualised in the flowchart depicted in Figure 3.2.

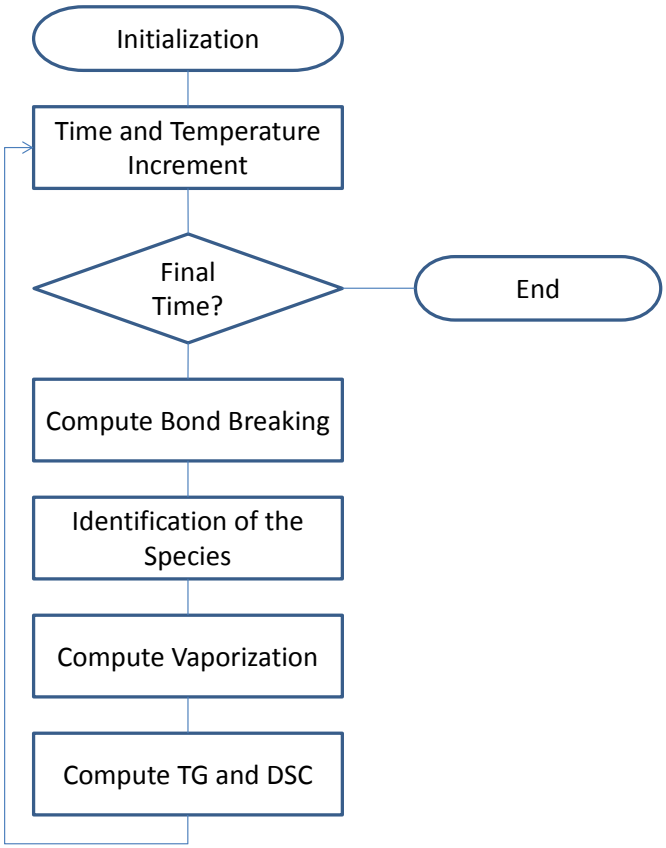

Figure 3.2 - Simplified flowchart for the computational model.

The sequence of steps is repeated as the temperature is increased according to the experimental temperature program. For each temperature the whole bond array is run through and, should an unbroken bond be found, a random number with a uniform distribution between 0 and 1 is generated and compared with the probability for a bond to be broken (given by Eq. 3.3). If the random number generated is lower or equal to the probability calculated, the model decides that that specific bond is broken. Otherwise, it is maintained intact. We should note that bonds can only be broken if there are not at the “edge” of a molecule, *i.e.*, they are not the first or last bonds in a molecule.

After the whole bond array is processed, it is scanned again, this time to identify the chemical species that have been produced by the bond breaking sequence. When a particular molecule is found, a decision is made on whether or not this molecule evaporates. Based on the evaporation rate laws the evaporation probability for the molecule in question is computed and a random number with a uniform distribution between 0 and 1 is generated and compared with this value. Once more, if the random number is lower or equal than the evaporation probability value, the model decides it is moved into the gas phase. When the molecule is to evaporate, the set of bonds corresponding to this

molecule are marked as being in the gas-phase (value = 2) and the process proceeds to the next molecule, until the end of the bond array is reached. This process is exemplified in Figure 3.3.

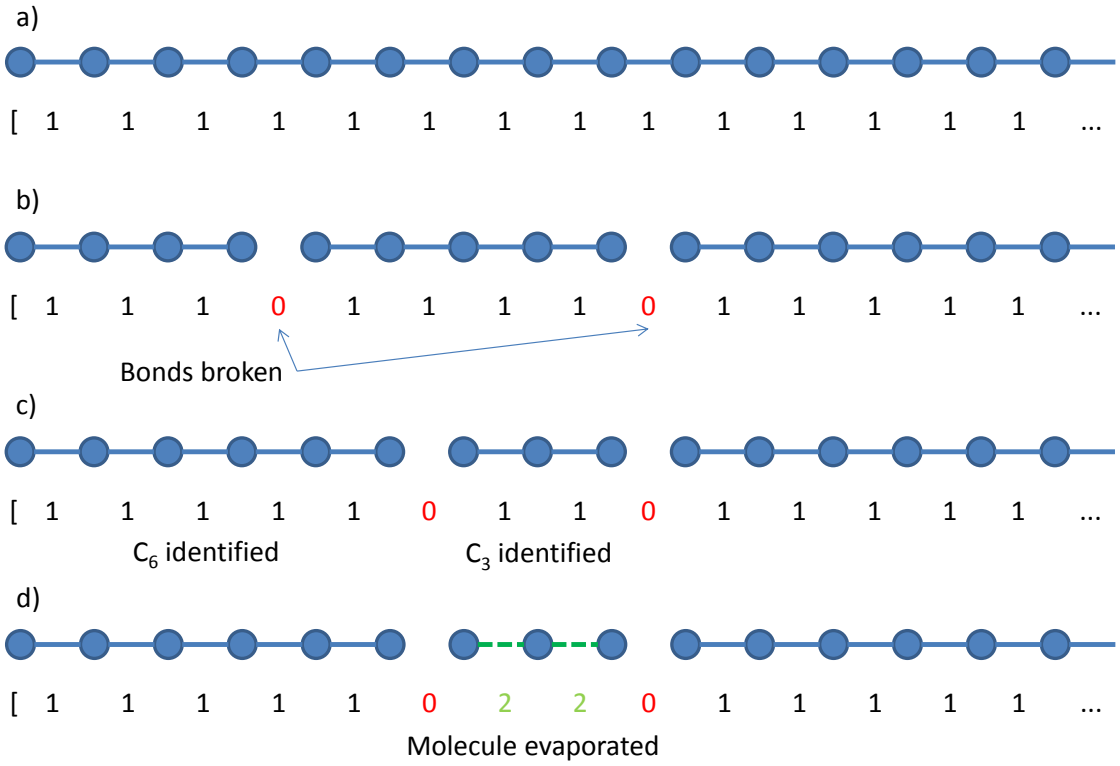

Figure 3.3 – Sequence of computations in a cycle: a) initial state b) all bonds are scanned and decision on which are broken is made; c) bond array is scanned again to identify molecules that were formed and d) decision on evaporation is made.

4. VAPORIZATION IN PARAFFINS PYROLYSIS

As mentioned before, there are two main phenomena involved in the polyethylene, as well as paraffins, thermal and catalytic degradation. There is a first step of bond breaking that generates smaller molecules which, with temperature increase, evaporate into the gas phase. The first phenomenon corresponds to cracking and the latter is vaporization.

To have a stochastic model that can predict the mass change as well as the heat flow for the whole process of polyethylene's pyrolysis, one needs to have a reliable model for the cracking reaction, as well as a set of vaporization laws suitable to compute the vaporization rates, so that this phenomenon may be adequately described. In order to have a clear picture of the vaporization process it has to be possible to separate it from cracking processes so one has to look at species that vaporize well before they crack.

The present chapter is fully devoted to the study of the vaporization process of short-chain paraffins. The mathematical laws encountered to describe this phenomenon will be used for further computational stochastic model simulations.

4.1. Experimental data

In the current study, TG/DSC experimental data corresponding to the temperature programmed evaporation of six hydrocarbons (n-hexane, n-heptane, n-nonane, n-decane, n-dodecane and n-icosane) of previous works were used. These compounds are relatively small, not undergoing cracking in the temperature range before total evaporation and, thus, allowing the investigation of the vaporization process separated from the first one.

The data obtained from TG/DSC equipment (mentioned in Chapter 2-Experimental Procedures and Apparatus) were exported using the TA Universal Analysis 2000 software. The data files contain the values of time (min), temperature (^{o}C), weight (mg), heat flow (mW) and the temporal derived of the weight (mg/min).

The data was processed as mass fraction, X_{exp}, defined according to Eq. 4.1:

$$\boldsymbol{X_{exp} = \frac{m}{m_0}}$$

Eq. 4.1

where m is the mass of the compound remaining in the TG/DSC instrument's pan and m_0 is the initial mass of the sample.

The evaporation curves for the different hydrocarbons studied are plotted versus temperature in Figure 4.1.

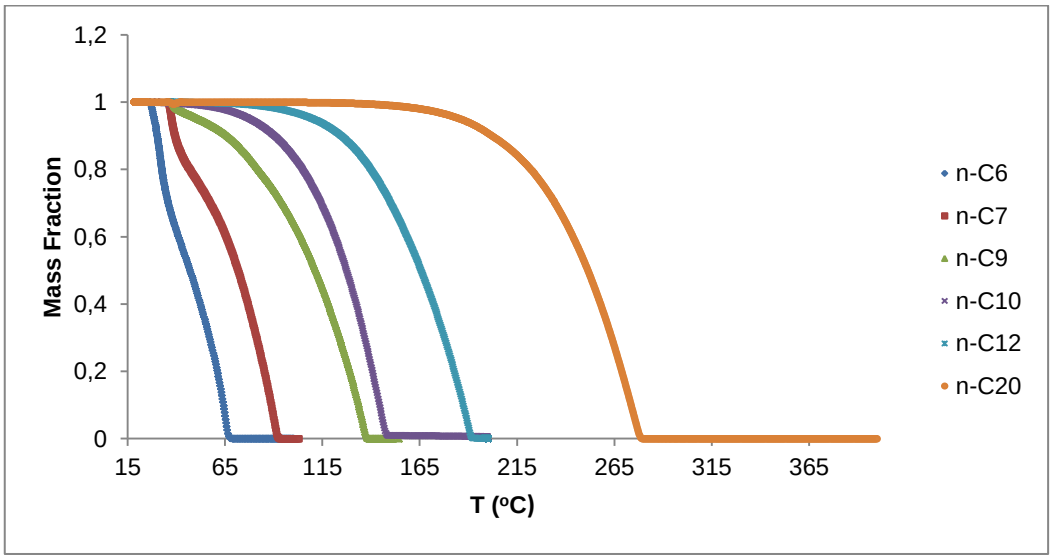

Figure 4.1 –Vaporization curves for the hydrocarbons studied, obtained from TG/DSC results.

Observing the curves in Figure 4.1, it can be seen that the results are consistent since it is clear that as the number of carbon atoms in the paraffin-chain increases, there's also an increase in the vaporization temperature, as it would be expected.

For more detail, see Table 4.1, where the approximate vaporization temperatures for each compound are listed. In this table, the tabled boiling points for the present hydrocarbons are also listed.

Table 4.1 – Approximated temperatures[7] of vaporization for the paraffins in study.

Compound	$T_{vaporization}$ (ºC)	Boiling point[8] (ºC)
n-hexane	22,63	68,75
n-heptane	31,19	98,35
n-nonane	34,41	150,65
n-decane	49,79	174,05
n-dodecane	80,46	215,85
n-icosane	148,17	343,05

As can be seen in Table 4.1, it is noticeable, as well as in the vaporization rate curves, an increase either in the approximate vaporization temperatures or in the boiling points' values, as the number of the C-C bonds in the hydrocarbon chain increases. The discrepancy between the values of the vaporization temperatures and the boiling points values is obviously related with the physical phenomenon involved. While the vaporization is a surface phenomenon, a transition state from liquid

7 It is important to note that these values were measured directly from the graphical representation of the vaporization rates. Therefore they are not exact values but are used only to elucidate at which temperature vaporization occurs

8 Values from NIST (National Institute of Standards and Technology) WebBook, accessed on 4th September 2012.

to gas phase and occurs at any temperature. The boiling process that takes place only at the temperature when the liquid pressure equals the atmosphere pressure, involves the transition of the whole bulk of the liquid, requiring higher amounts of energy.

4.2. Determining a kinetic law for each paraffin degradation: individual fitting

The main goal of the chapter is to obtain a global rate law expression that enable the calculation of the vaporization rate (based on k_{refv} and E_{av}) for a generic paraffin with n_l number of bonds (corresponding to $n_l + 1$ number of carbon atoms in the chain) and assuming a first-order reaction[9] in order to parraffins for both parameters to use in the stochastic computational model.

For this purpose, one has started by obtaining first a kinetic law for the vaporization of each paraffin from experimental data. Assuming that the vaporization process can be described by a simple first order rate law (Eq. 4.2), an ***individual fitting*** to each of the compound's data, using a least-squares methodology, was performed, providing the values of the kinetic parameters desired. The description of such fitting is outlined below.

In Eq. 4.2, the temperature-dependent rate constant for the vaporization is described according to an Arrhenius law (Eq. 4.3):

$$\frac{dX}{dt} = -k_v(T).X$$

Eq. 4.2

$$k_v(T) = k_{refv}.e^{-\left(\frac{E_{av}}{R}\left(\frac{1}{T}-\frac{1}{T_{ref}}\right)\right)}$$

Eq. 4.3

In Eq. 4.2, $k(T)$ is the temperature-dependent rate constant of vaporization. In Eq. 4.3, T_{ref} is a reference temperature chosen within the range where significance degradation takes place (for this work, we used T_{ref} = 300 K), k_{refv} is the vaporization rate constant at the reference temperature and E_{av} is the corresponding activation energy of vaporization.

Combining Eq. 4.2 and Eq. 4.3, it is obtained an expression that enables the calculation of the mass fraction variation with time, $\frac{dX}{dt}$, as a function of the assay's temperature[10] (Eq. 4.4):

9 Even though it is usually referred in literature that paraffins' vaporization follows a zero-order kinetics (Font, Gómez-Rico et al. 2011), we have performed an individual fitting (with the present data) and the order of the reaction, n, was left as a parameter. The average optimization result was n= 0,73 (results not shown) and, then, we assumed a first-order kinetics for paraffins' vaporization.

10 In the experimental data, there's a correspondence between time and temperature. Thus, calculating the $\frac{dX}{dt}$ values for each temperature enables us to know the same values for any given time instant.

$$\frac{dX}{dt} = k_{refv}.e^{-\frac{E_{av}}{R}\left(\frac{1}{T}-\frac{1}{T_{ref}}\right)}.X$$

Eq. 4.4

Using Euler's method, it's possible to compute the mass fraction as function of time, applying Eq. 4.5[11]:

$$X\,(t+\Delta t) = X(t) + \left(\frac{dX}{dt}\right)_{t+\Delta t}.\Delta t$$

Eq. 4.5

where $X\,(t+\Delta t)$ is the remaining mass fraction for given a time instant t, $X(t)$is the remaining mass fraction for the time instant immediately before, Δt is the discrete difference between two immediately consecutive time instants and $\left(\frac{dX}{dt}\right)_{t+\Delta t}$ is the mass fraction variation related to the that time interval.

The kinetic parameters for the individual degradation of each paraffin studied (constant rate of vaporization at the reference temperature, k_{refv}, and activation energy of vaporization, E_{av}) were estimated by fitting this model using a least-squares procedure applied to the sum of the residues on mass fraction as the objective function (O.F.) to be minimized (Eq. 4.6).

$$O.F. = \sum\left[(X)_{exp} - (X)_{ind}\right]^2$$

Eq. 4.6

where X_{ind} represents the values of the mass fraction calculated by means of the previous procedure.

This optimization was performed using the "Solver" tool in an Excel (© Windows) spreadsheet. The results of the individual fittings are depicted in Figure 4.2 Erro! A origem da referência não foi encontrada. and the kinetic parameters obtained as well as the approximated temperature of the end of vaporization and the sum of the residues values are presented in Table 4.2.

[11] for the first time instant, it was considered, logically, $X = 1$.

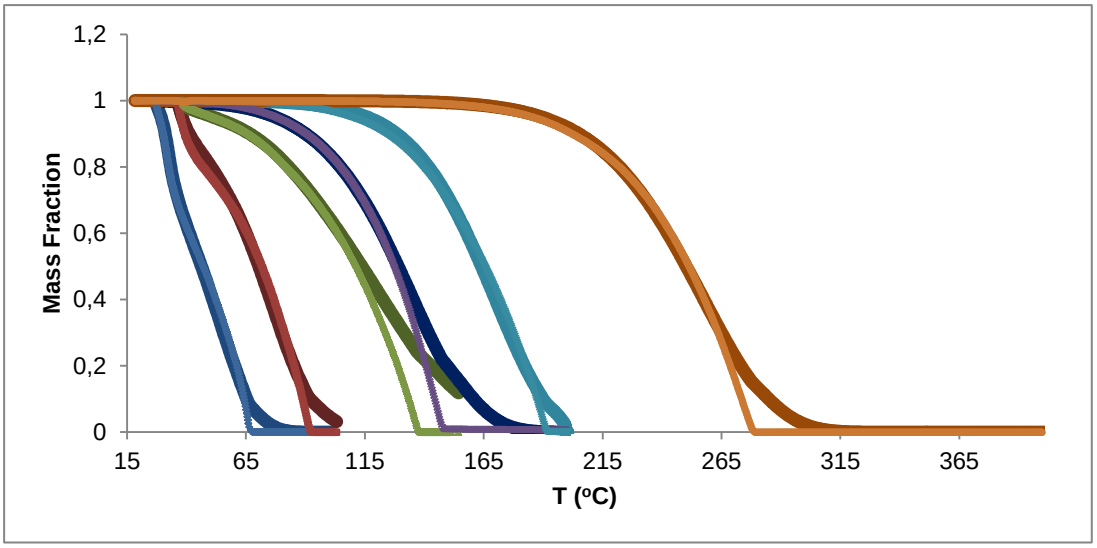

Figure 4.2 – Experimental (symbols) and individual fitting vaporization curves (lines): n-hexane (blue), n-heptane (red), n-nonane (green), n-decane (violet), n-dodecane (light blue) and n-icosane (orange).

Table 4.2 - Kinetic parameters obtained by the individual fitting, approximate temperatures of vaporization estimated from fitted curves and sum of the residues minimized by the "Solver" tool.

Compound	k_{refv} (min^{-1})	E_{av} ($cal.mol^{-1}$)	$T_{vaporization}$ (^oC)	Sum of the resisdues
n-hexane	1,08E-01	13411,87	24,28	1,44E-01
n-heptane	3,42E-02	11377,33	39,09	2,46E-01
n-nonane	1,06E-02	8054,74	44,29	1,61E-03
n-decane	1,35E-03	12702,01	65,27	1,85E-05
n-dodecane	4,92E-05	16815,72	90,42	2,56E-01
n-icosane	4,06E-07	18802,20	140,77	7,29E-02

Observing and comparing graphically the experimental and the fitted curves, it can be seen that there's not a perfect overlapping between them. However, the fitting results can be considered quite good since, for all the paraffins, the curves are superimposable almost in all their extension, except for the evaporation in the final fractions. These satisfactory results are supported by the low values of the residues (see Table 4.2). Still in a graphical approach, it is noted that, for all the fitted curves, the model predicts that the vaporization takes place at slightly higher temperatures comparing with the experimental ones (see Table 4.2).

In terms of physical meaning, the longer the hydrocarbon chain is, the harder it is (energetic and kinetically) for the vaporization to occur, i.e., the rate of vaporization is slower and the energetic barrier needed for the reaction to start is higher. So, it is expected that, as the length of the paraffin chain increases, the constant rate decreases and the activation energy increases.

Considering the values of the fitting-parameters, it's noteworthy that there's no regular trend of the activation energy with the number of carbon atoms of the compound. There is an inversion for n-nonane that, surprisingly, presents a lower value of k_{refv} but also a lower value of $E_a v$ when compared with n-heptane. Probably this behavior might be explained based in the order of the reaction assumed. Perhaps the real order of the reaction is slightly different from one (n ≈ 0,55).

4.3. Obtaining a generic kinetic law for paraffins vaporization: global fitting

At this point, the main goal is to find the equations that allow us to automatically compute estimates of the kinetic constant and the activation energy of vaporization for any given linear-chain paraffin (global correlations for the kinetic constant and for the activation energy, respectively). These correlations will be expressed as mathematical expressions where the kinetic parameters are function of the number of bonds in the hydrocarbon chain.

Once the individual fittings for the different paraffins studied are concluded and a general trend is observed, in the present sub-chapter, there will be detailed the description of the different attempts to obtain these correlations.

The objective is, thus, to choose a suitable mathematical function, determine the values of its coefficients and evaluate if the vaporization rates computed fit within a reasonable degree of accuracy the experimental evaporation curves. Two different approaches to obtain the function's coefficient values and, thus, the global laws themselves were tested.

In both cases the fitting parameters are the coefficients that are require to describe the rate constant at the reference temperature and the activation energy for the vaporization as a function of the number of C-C bonds in the molecule, n_l:

$$k_{refv} = f_k(n_l, parameters)$$

$$E_{av} = f_E(n_l, parameters)$$

In the first methodology the values for k_{refv} and E_{av} are computed using the equations and then each of the vaporization experiments is simulated and the residuals between these simulated values and the original experimental data are computed. The coefficients are obtained by minimization of the sum of the residuals. In this way, it can be said that the modeled values of the mass fractions are fitted in a one-step fitting.

In the second methodology the values for k_{refv} and E_{av} are obtained, by least-squares regression, for each individual experiment and then the parameters are estimated by fitting the equations to these values. In this case, once the values whose residues were minimized were the kinetic parameters used for further calculation of the modeled mass fraction and so a two-steps fitting was done.

Following two charts illustrating the two methodologies explained previously are presented (see Figure 4.3 and Figure 4.4).

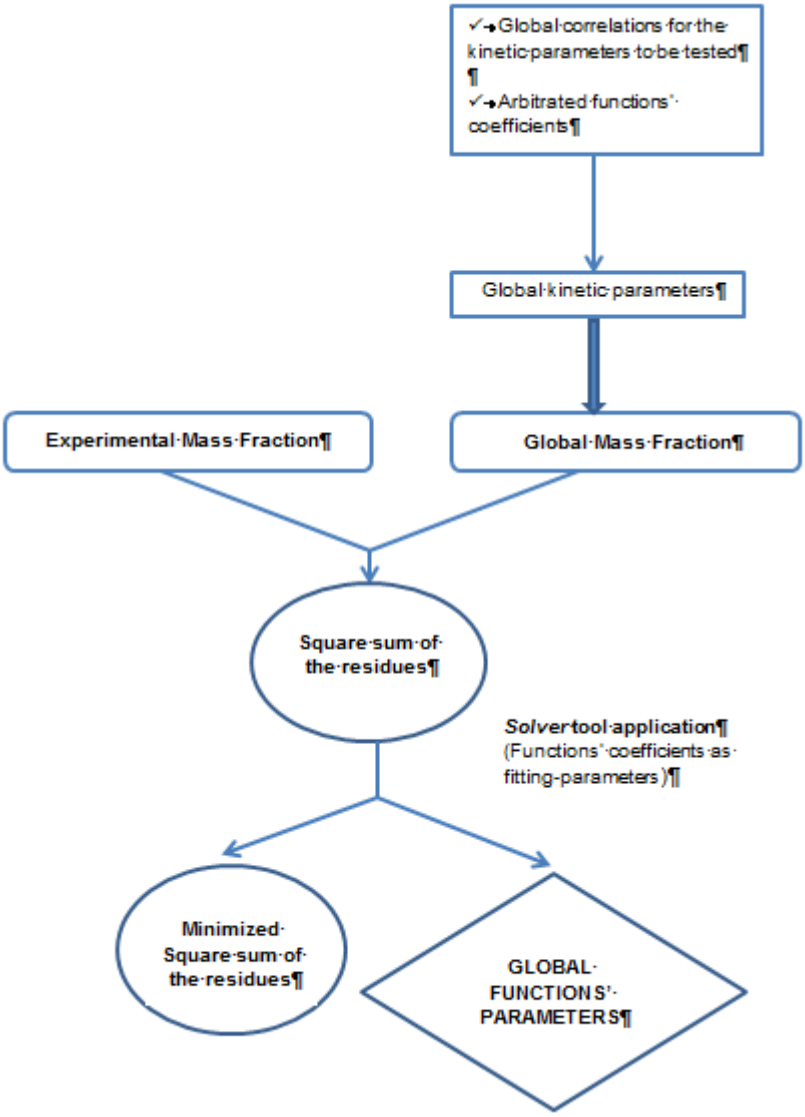

Figure 4.3 – Flowchart that illustrates the method I for obtaining the global correlations' coefficients.

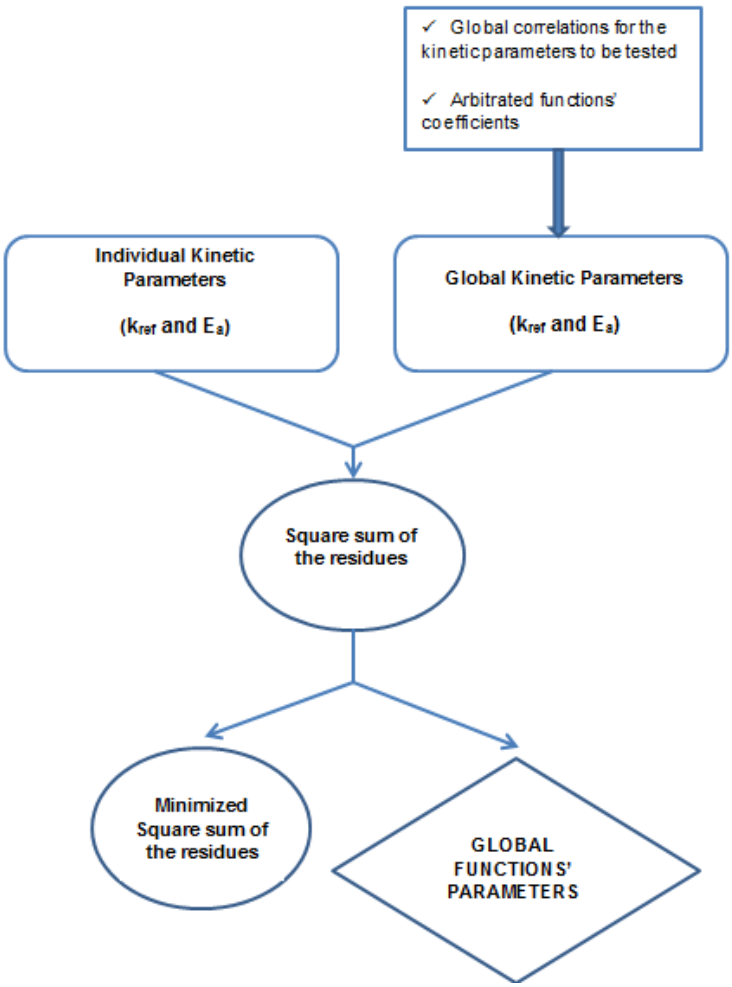

Figure 4.4 - Flowchart that illustrates the method II for obtaining the global correlations' coefficients

4.4. Different mathematical expressions to use as the global kinetic laws

To find the global laws that provide a good fitting of the simulated curves to the experimental data, many attempts have been performed. In the following sections those attempts are presented. In each one of them the global fittings obtained by the two methods mentioned before are also shown.

All the simulations were performed under the same conditions (see Table 4.3) and using the computational model already presented.

Table 4.3 – Simulation conditions used for all simulations performed in vaporization kinetic of pure hydroacarbon studies (T_i – initial simulation temperature; T_f – final simulation temperature; β – heating rate; dt – integration step; C_p – average heat capacity; $\Delta H_{(C-C)}$ – average C-C bond enthalpy; k_{ref} – cracking kinetic constant rate at reference constant; ΔH_{vap} – average vaporization enthalpy; nr. Molecules – number of molecules used in the simulation).

Simulation conditions	
T_i (^oC)	25
T_f (^oC)	700
β ($^oC.min^{-1}$)	10
dt (min)	0,025
C_p ($cal.g^{-1}.^oC^{-1}$)	1,5
$\Delta H_{(C-C)}$ ($cal.mol^{-1}$)	20000
k_{ref} (min^{-1})	0[12]
E_a ($cal.mol^{-1}$)	30000
ΔHvap ($cal.mol^{-1}$)	277,876
Nr. Molecules	20000

4.4.1. **Exponential function for the rate constant at the reference temperature and quadratic function for the activation energy**

As a first attempt to find the global laws for both k_{refv} and E_{av}, it has been tried to use an exponential function to describe the first kinetic parameter with the number of bonds in the hydrocarbons chain and a quadratic function for the second parameter. So the correlations in test are generically written as:

$$E_{av} = a_{\_E_a} + b_{\_E_a}.n_l + c_{\_E_a}.n_l^2$$

Eq. 4.7

$$k_{refv} = a_{\_kref}.e^{(b_{\_kref.}\, n_l)}$$

Eq. 4.8

a. Method I.

After application of the procedure described earlier, the several coefficients and the total sum of the residues were obtained and are presented in Table 4.4

12 Since it's being investigated only vaporization, the cracking constant rate value is zero.

Table 4.4 - Global fitting results (exponential function for k_{refv}; quadratic function for E_{av}; method I).

Global fitting results	
a_E_a (cal.mol^{-1})	7138,35
b_E_a (cal.mol^{-2})	466,03
c_E_a (cal.mol^{-3})	23,51
a_k_{ref} (min^{-1})	46,29
b_$_{kref}$ (mol^{-1})	-1,18
Total sum of residues	1,63

Thus, the global laws encountered are:

$$E_{av}(cal/mol) = 7138{,}35 + 466{,}03.n_l + 23{,}51.n_l^2$$

$$k_{refv}\ (min^{-1}) = 46{,}29.e^{(-1{,}18.n_l)}$$

After the determination of the previous equations, they've been inserted in stochastic model program's code and simulations for each of the paraffins have been performed. The experimental rates of vaporization and the so simulated curves are presented in Figure 4.5.

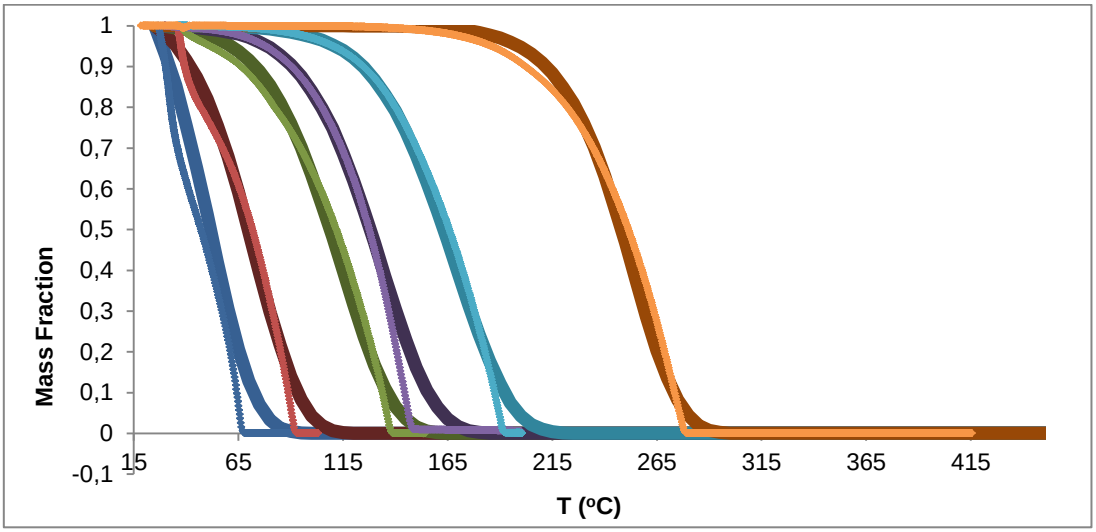

Figure 4.5 – Experimental and simulated [k_{ref} exponential; E_a quadratic; method I) vaporization curves, respectively, for: n-hexane (blue dots and line); n-heptane (red dots and line); n-nonane (green dots and line); n-decane (violet dots and line); n-dodecane (light blue dots and line) and n –icosane (orange dots and line)].

In a first observation of Figure 4.5, it can be noted that there is a quite good fitting of the simulated curves to the experimental data using the present equations since there's an overlapping of both experimental and simulated curves in almost all their extension. However, using these set of correlations, it has been verified that, for heavier hydrocarbons, the vaporization starts to occur at lower temperatures than for some of the lighter compounds fitted here. See the example of the

vaporization rate curve for n-C40 simulated by means of the computational model using this set of global rules (Figure 4.6).

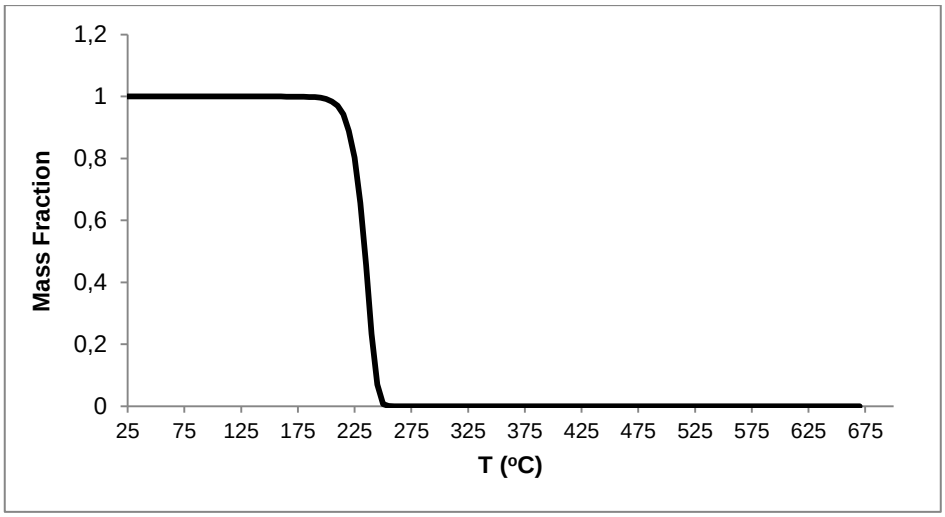

Figure 4.6 – Rate of vaporization for n-C40, simulated by the computational model (quadratic function for E_a, exponential function for k_{ref}; method I)

From Figure 4.6, it is clear that the curve for n-tetracontane presents a low temperature of vaporization when compared with the vaporization temperature for lighter compounds (e.g. n-icosane), according to this attempt ($T_{vaporization}$ (n-C20) = 185ºC and $T_{vaporization}$ (n-C40) = 180ºC).

b. Method II

Using now the second method described to find the global laws functions' coefficients, the main results attained are those listed in Table 4.5 and the kinetic parameters both obtained from individual and global fittings are presented in Figure 4.7.

Table 4.5 - global fitting results (exponential function for k_{refv}; quadratic function for E_{av}; method II).

Global fitting results	
a_E_a (cal.mol^{-1})	10890,77
b_E_a (cal.mol^{-2})	0,51
c_E_a (cal.mol^{-3})	22,95
a_k_{ref} (min^{-1})	23,64
b_{kref} (mol^{-1})	1,08
Total sum of residues (for k_{refv})	4,59E-05
Total sum of residues (for E_{av})	3,25E+07

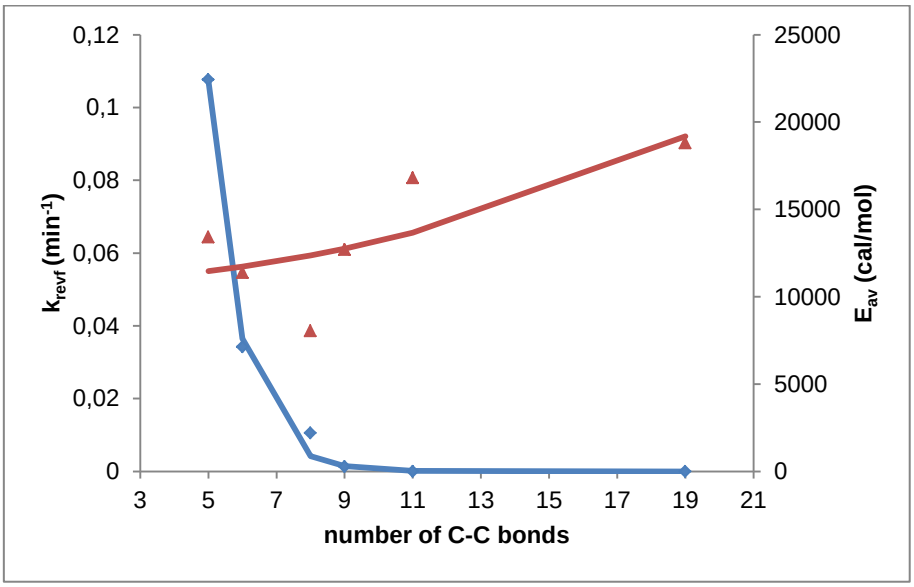

Figure 4.7 – kinetic parameters' values for the different paraffins: k_{refv} from individual fitting (blue symbols) and from global fitting (blue line) and E_{av} from individual fitting (red symbols) and from global fitting (red line); global laws: quadratic for E_a and exponential for k_{ref}, method II.

According to Table 4.5, the mathematical laws encountered from this fitting are:

$$E_a(cal/mol) = 10890{,}77 + 0{,}51.n_l + 22{,}95.n_l^2$$

$$k_{ref}\ (min^{-1}) = 23{,}64.e^{(-1{,}08.n_l)}$$

Inserting the previous expressions in the program's code, it was possible to perform the simulations, through the stochastic model, which are depicted in Figure 4.7.

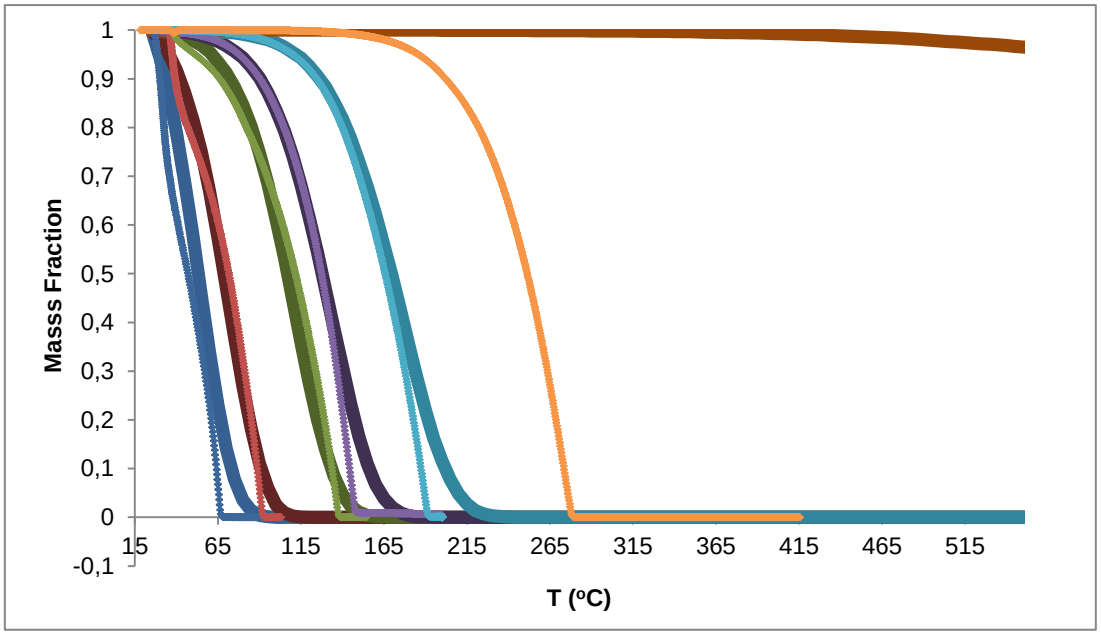

Figure 4.8 - Experimental and simulated [k_{refv} exponential; E_{av} quadratic; method II) vaporization curves, respectively, for: n-hexane (blue dots and line); n-heptane (red dots and line); n-nonane (green dots and line); n-decane (violet dots and line); n-dodecane (light blue dots and line) and n –icosane (orange dots and line)].

From Figure 4.8 it's clear that using this set of global laws, good fittings of simulated to experimental evaporation curves are obtained, with exception to the case of n-icosane vaporization. In the same way as for the results from method I, for those compounds, it is noticeable that the approximated temperatures for end of vaporization are only slightly higher than those verified in the experimental data, which is not a serious issue. It is also perceptible that there is a good overlapping between the modeled and experimental curves in almost their whole extension. However the computed rate of vaporization from n-C20 cannot be adjusted to the correspondent data.

For the latter reason, the global laws here determined don't allow a reasonable prediction of the vaporization process in short-chain paraffins pyrolysis.

4.4.2. **Exponential function for the rate constant at the reference temperature and third-degree polynomial function for the activation energy**

In this second attempt it has been maintained the exponential function to describe the relation between the values of k_{refv} and the number of bonds in the chain due to the satisfactory coincidence between the individual and global fitting values for this parameter (see Figure 4.7). On the other hand, the opposite situation happened with the E_{av} values.

For this reason and because of the shortcomings found in the previous attempt, it has been tried to implement a third-degree polynomial as the global law for the activation energy. The set of laws tested has the generic form:

$$E_{av} = a_{\_E_a} + b_{\_E_a}.n_l + c_{\_E_a}.n_l^2 + d_{\_E_a}.n_l^3$$

Eq. 4.9

$$k_{refv} = a_{\_kref}.e^{(b_{\_kref}.n_l)}$$

Eq. 4.10

a. Method I

Chosen the type of functions to test, the current method has been applied and its main results are shown in Table 4.6.

Table 4.6 - Global fitting results (exponential function for k_{ref}; 3rd degree polynomial function for E_a; method I).

Global fitting results	
a_E_a (cal.mol^{-1})	7171,95
b_E_a (cal.mol^{-2})	491,52
c_E_a (cal.mol^{-3})	19,38
d_E_a (cal.mol^{-4})	0,14
a_k_{ref} (min^{-1})	45,81
b_$_{kref}$ (mol^{-1})	-1,18
Total sum of residues	1,63

Considering the values obtained above and the type of functions to implement, the global laws can be written as:

$$E_{av}(cal/mol) = 7171{,}95 + 491{,}52.n_l + 19{,}38.n_l^2 + 0{,}14.n_l^3$$

$$k_{refv}\ (min^{-1}) = 45{,}81.e^{(-1{,}18.n_l)}$$

Once the global laws are determined, they've been inserted in the stochastic model description and the various simulations have been performed. These results are represented in Figure 4.9.

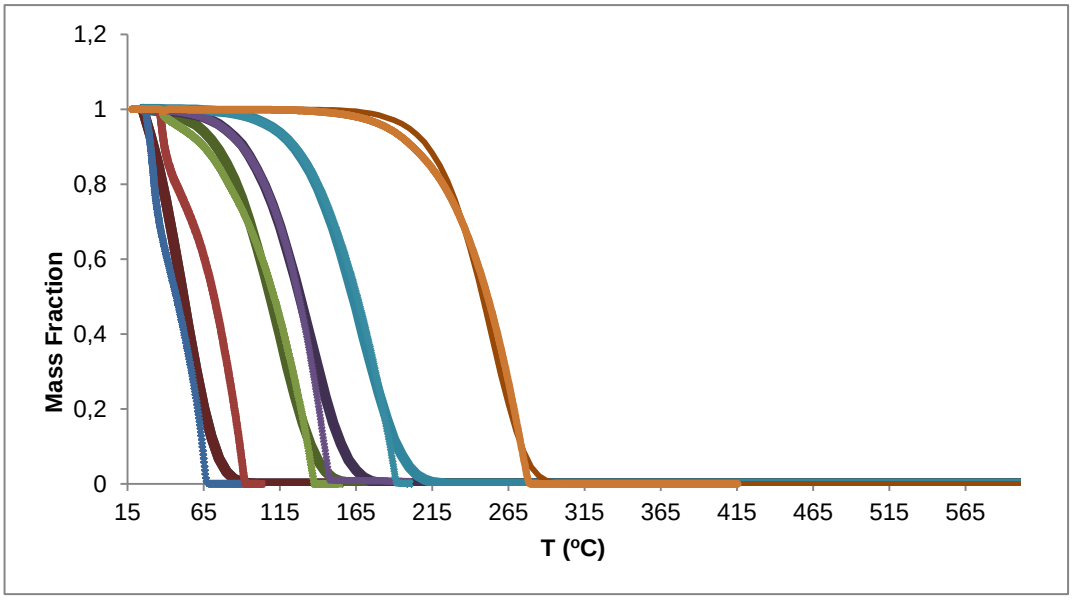

Figure 4.9- Experimental and simulated [k_{refv} exponential; E_{av} 3rd degree polynomial; method I) vaporization curves, respectively, for: n-hexane (blue dots and line); n-heptane (red dots and line); n-nonane (green dots and line); n-decane (violet dots and line); n-dodecane (light blue dots and line) and n –icosane (orange dots and line)].

The quality of the results produced by the present correlations is very good since there is a very satisfactory overlapping between the experimental and simulated vaporization curves. Even if the coincidence in the vaporization segment of the different curves is not perfect, the simulated vaporization temperatures are only marginally higher than the ones from data. Though the positive characteristics already mentioned, once more the present model cannot predict the vaporization curves for molecules heavier than n-C20. Again it has been verified, for n-C40, that the vaporization temperature predicted is 165^{o}C, whereas for n-C20 it is 173,32^{o}C. This occurrence is depicted in Figure 4.10.

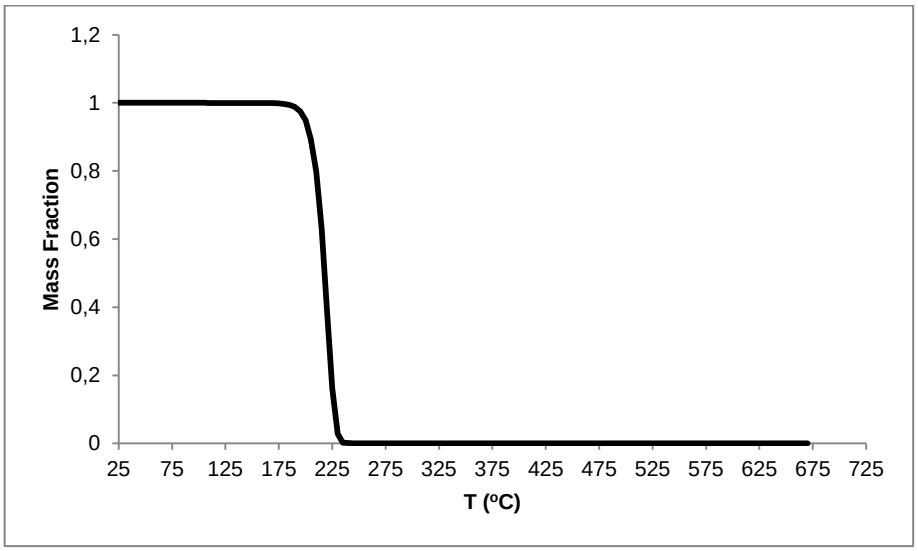

Figure 4.10- Rate of vaporization for n-C40, simulated by the computational model (3rd degree polynomial function for E_{av}, exponential function for k_{refv}; method I)

b. Method II

The main results obtained with the application of method II for the case of the previous functions are listed as follows (Table 4.7).

Table 4.7 - Global fitting results (exponential function for k_{refv} 3rd degree polynomial function for E_{av}; method II).

Global fitting results	
a_E_a (cal.mol^{-1})	10769,29
b_E_a (cal.mol^{-2})	24,78
c_E_a (cal.mo^{-3})	21,96
d_E_a (cal.mol^{-4})	0,00
a_k_{ref} (min^{-1})	23,71
b_$_{kref}$ (mol^{-1})	-1,08
Total sum of residues (for E_{av})	3,25E+07
Total sum of residues (for k_{refv})	4,59E-05

From Table 4.7, it can be seen that using this methodology and starting from the present data, it is impossible to obtain a 3rd degree polynomial function for the activation energy since the value of d_E_a is zero and a quadratic function is obtained instead.

4.4.3. **Exponential function for the rate constant at the reference temperature and linear function for the activation energy**

Taking into account that through the exponential function can be obtained values of the rate constant of vaporization similar to those obtained from the individual fittings, this function was once more kept the same. Still it have been found some shortcomings in the simulation of the vaporization rates using polynomial functions with a degree greater than, namely in the prediction of heavier hydrocarbons rate of vaporization (see Figure 4.6 and Figure 4.10). Perhaps these problems emerged due to the irregular behavior of such functions for a larger number of bonds. Therefore, in the present attempt, a linear function for the description of the E_{av} with the number of bonds in the paraffins chain will be tested. Thus, the generic form of the correlations to be tested in the present sub-chapter is:

$$E_{av} = a_{\_E_a} + b_{\_E_a}.n_l$$

Eq. 4.11

$$k_{refv} = a_{\_kref}.e^{(b_{\_kref.}\, n_l)}$$

Eq. 4.12

a. Method I

Starting from the set of functions to use as global laws of vaporizations and applying the procedure mentioned before as method I, the following results were obtained (see Table 4.8).

Table 4.8 - Global fitting results (exponential function for k_{ref}; linear function for E_a; method I).

Global fitting results	
a_E_a (cal.mol^{-1})	8280,77
b_E_a (cal.mol^{-2})	1512,05
a_k_{ref} (min^{-1})	440,14
b_$_{kref}$ (mol^{-1})	-1,76
Total sum of residues	13,95

Determined the values of the coefficients' functions, the global laws are, then, the following ones:

$$E_{av}(cal/mol) = 8280{,}77 + 1512{,}05.n_l$$
$$k_{refv}\ (min^{-1}) = 440{,}14.e^{(-1{,}76.n_l)}$$

In this way, the previous expressions were inserted in the program's code for stochastic simulations which are depicted in Figure 4.11.

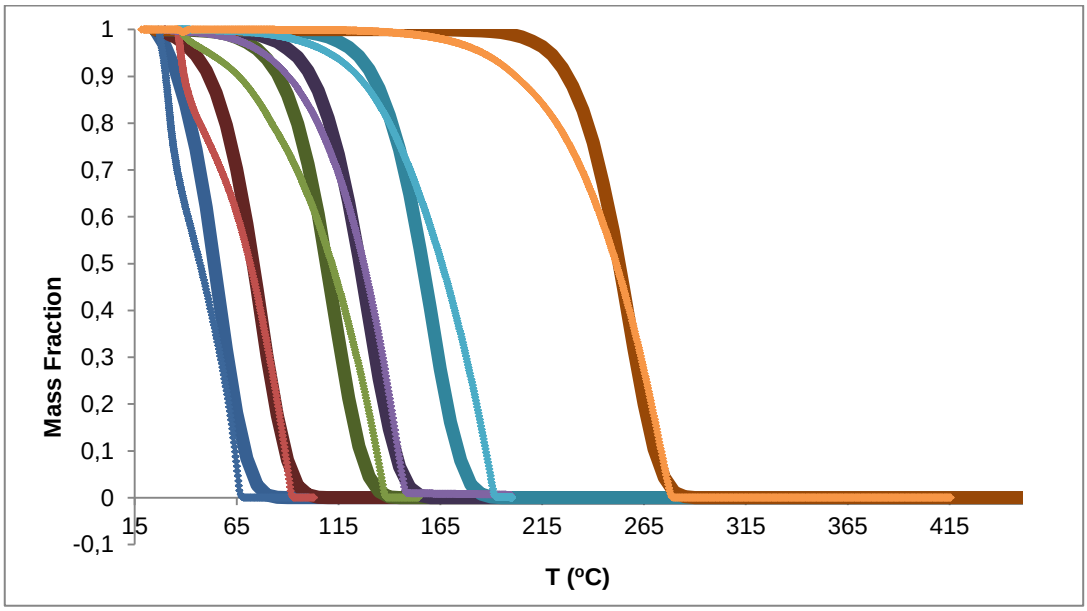

Figure 4.11 - Experimental rates of vaporization and simulated [k_{refv} exponential; E_{av} linear; method I) vaporization curves, respectively, for: n-hexane (blue dots and line); n-heptane (red dots and line); n-nonane (green dots and line); n-decane (violet dots and line); n-dodecane (light blue dots and line) and n –icosane (orange dots and line)].

The simulated and experimental evaporation rate curves are not superimposable in all their extension. Still the fittings can be considered very good since in the portion of the curves in which the vaporization takes place the curves do overlap for practically all paraffins studied. In fact, this is the attempt that provides the simulated vaporization temperatures closer to the experimental ones.

With these vaporization rules, one can obtain consistent results for the rate of vaporization in hydrocarbons heavier than n-C20 (data not shown).

b. Method II

The values of the functions' coefficients for the global laws as well as the value of the sum of the residues related to the present fitting are listed in Table 4.9. In addition, the values of the kinetic parameters obtained from the individual and the global fittings are shown in Figure 4.12.

Table 4.9 - Global fitting results (exponential function for k_{ref}; linear function for E_a; method II).

Global fitting results	
a_E_a (cal.mol^{-1})	8280,77
b_E_a (cal.mol^{-2})	563,17
a_k_{ref} (min^{-1})	23,64
b_{kref} (mol^{-1})	-1,08
Total sum of residues (for E_a)	3,35E+07
Total sum of residues (for k_{ref})	4,59E-05

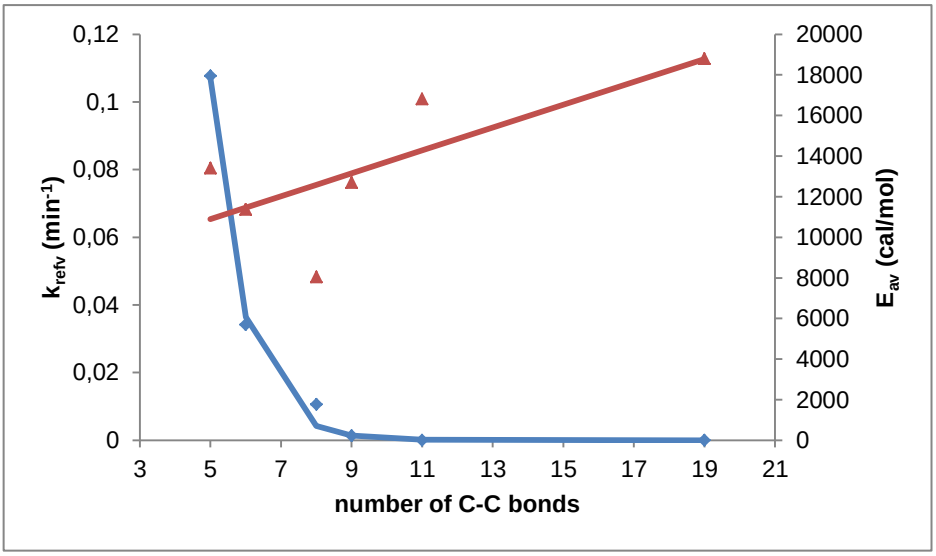

Figure 4.12 - Kinetic parameters' values for the different paraffins: k_{refv} from individual fitting (blue symbols) and from global fitting (blue line) and E_{av} from individual fitting (red symbols) and from global fitting (red line); global laws: linear for E_{av} and exponential for k_{refv}, method II.

From the results in Table 4.9, it is possible to write the equations of the global laws found in this attempt:

$$E_{av}(cal/mol) = 8083{,}34 + 563{,}17.n_l$$

$$k_{refv}\ (min^{-1}) = 23{,}64.e^{(-1{,}08.n_l)}$$

Once determined the equations of the global laws, the simulations were performed using the stochastic model program and are presented in Figure 4.13.

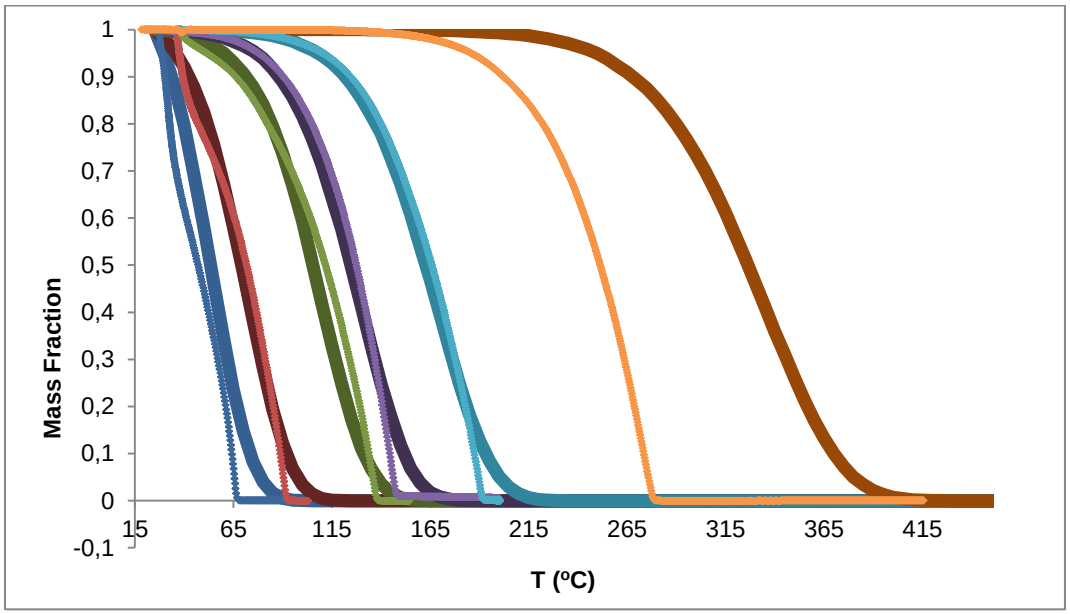

Figure 4.13 - Experimental rates of vaporization and simulated [k_{refv} exponential; E_{av} linear; method II) vaporization curves, respectively, for: n-hexane (blue dots and line); n-heptane (red dots and line); n-nonane (green dots and line); n-decane (violet dots and line); n-dodecane (light blue dots and line) and n –icosane (orange dots and line)].

Observing Figure 4.13 it can be seen that the fittings there presented are quite satisfactory, except for the case of n-icosane. Comparing these results with the ones obtained for the same type of functions but using method I, it is noticeable that, for all compounds (not for n-C20), the curves present a better overlapping, i.e, in a bigger extension. Still it's noteworthy that the n-dodecane fitting is better than in the latter attempt. However, the vaporization temperatures given for these simulations are not so close of the ones encountered in experimental data. In spite of the relatively better curve's overlapping and in addition to the vaporization temperatures issue, there is a main shortcoming that, in a general way, makes this fitting unsuitable: the inability of fit the n-C20 simulation evaporation rate with the experimental data. In fact, its vaporization occurs at much higher temperatures than what is verified experimentally.

4.4.4. **Exponential function for the rate constant at the reference temperature and function defined by segments for the activation energy**

Even though, at this point, there have been already obtained various sets of global laws that, in some cases, provided quite good fittings, the global functions for the activation energy used (linear, quadratic and 3rd degree polynomial) never presented the same trends than the distribution of the activation energy values from the individual fitting (see Figure 4.7 and Figure 4.12).

Considering this handicap, as a last attempt, a function defined by segments for E_{av} is tested having the purpose explained. Thereby, the generic form of such correlations is:

$$E_{av} = \begin{cases} a_{1\_E_a} + b_{1\_E_a}.n_l, & n_l < n_{0\_E_a} \\ \dfrac{a_{2\_E_a}.\left(n_l - n_{0\_E_a}\right)}{b_{2\_E_a} + \left(n_l - n_{0\_E_a}\right)}, & n_l \geq n_{0\_E_a} \end{cases}$$

Eq. 4.13

$$k_{refv} = a_{\_kref}.e^{\left(b_{\_kref}.n_l\right)}$$

Eq. 4.14

a. Method I

Chosen the new types of function to be tested, the current procedure has been applied and the results are presented in Table 4.10.

Table 4.10 - Global fitting results (exponential function for k_{ref}; function defined by parts for E_a; method I)

Global fitting results	
$a_1\_E_a$ (cal.mol^{-1})	5723,81
$b_1\_E_a$ (cal.mol^{-2})	67,88
$a_2\_E_a$ (cal.mol)	4296,96
$b_2\_E_a$ (mol)	1,02
$n_0\_E_a$ (mol)	8,00
a_{kref} (min^{-1})	14,59
b_{kref} (mol^{-1})	-0,84
Total sum of residues	7,83

Therefore, the global laws are:

$$E_{av}(cal/mol) = \begin{cases} 5723{,}81 + 67{,}88.n_l, & n_l < 8{,}00 \\ \dfrac{4296{,}96.(n_l - 8{,}00)}{1{,}02 + (n_l - 8{,}00)}, & n_l \geq 8{,}00 \end{cases}$$

$$k_{refv}\ (min^{-1}) = 14{,}59.e^{(-0{,}84.n_l)}$$

Thereafter are presented the simulated curves obtained by means of the stochastic model (see Figure 4.14)

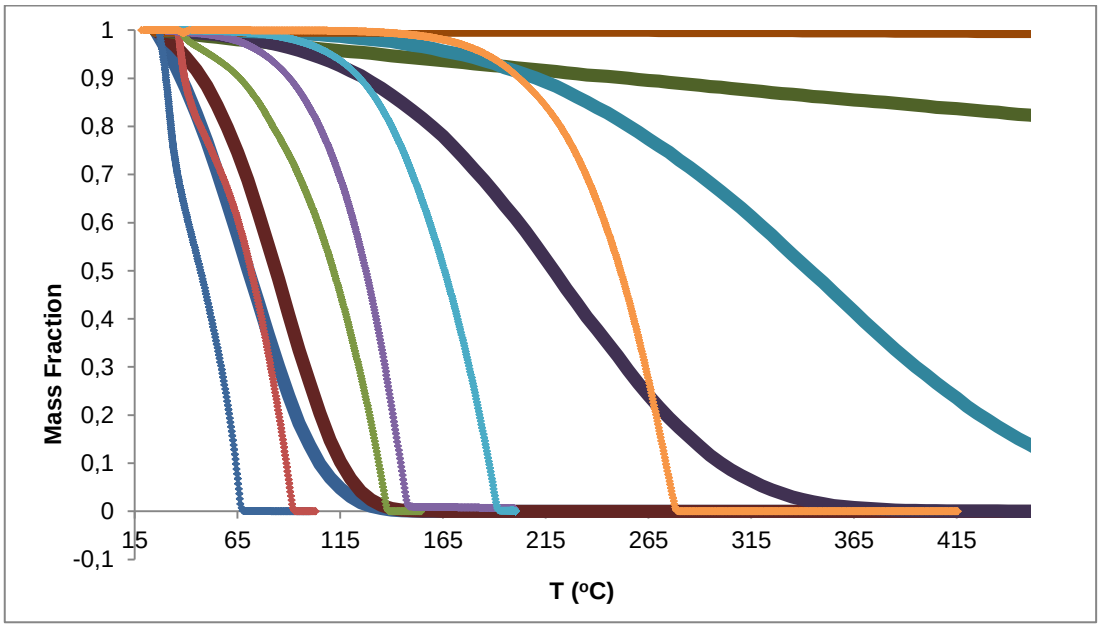

Figure 4.14 -Experimental rates of vaporization and simulated [k_{refv} exponential; E_{av} function defined by segments; method I) vaporization curves, respectively, for: n-hexane (blue dots and line); n-heptane (red dots and line); n-nonane (green dots and line); n-decane (violet dots and line); n-dodecane (light blue dots and line) and n –icosane (orange dots and line)].

According to Figure 4.14, it is clear that the global laws for vaporization here found are not suitable at all to describe the mentioned process in paraffins' pyrolysis. For all the different compounds there is no overlap between simulated and experimental evaporation curves. Besides, from the figure, it can be found that there is an inversion in the simulated curves (i.e., a smaller paraffin evaporates at higher temperatures than other with less bonds in its chain – see the example of n-C9 in which the vaporization occurs at a more elevated temperature than n-C10 and n-C12 -). It is also noteworthy that, in addition to all shortcomings verified, all the hydrocarbons, according to the simulation, evaporate at much higher temperatures. Note, for example, the case of n-C20, where no mass loss into the gas phase is observed until 415 ^{o}C[13].

b. Method II

Applying the method II procedure and considering the type of functions chosen in this sub-chapter, the following results were obtained (Table 4.11). In Figure 4.15 it can also be seen the kinetic parameters from both individual and global fittings.

[13] Remember that the approximate temperature for end of vaporization estimated from experimental data is 276,9^{o}C.

Table 4.11 global fitting results (exponential function for k_{ref}; function defined by parts for E_a; method II)

Global fitting results	
$a_1\_E_a$ (cal.mol^{-1})	-2034,39
$b_1\_E_a$ (cal.mol^{-2})	23583,73
$a_2\_E_a$ (cal.mol)	20468,02
$b_2\_E_a$ (mol)	0,90
$n_0\_E_a$ (mol)	7,43
a_k_{ref} (min^{-1})	6,64
b_{kref} (mol^{-1})	-0,91
Total sum of residues (for Ea)	1,44E+06
Total sum of residues (for kref)	2,06E-07

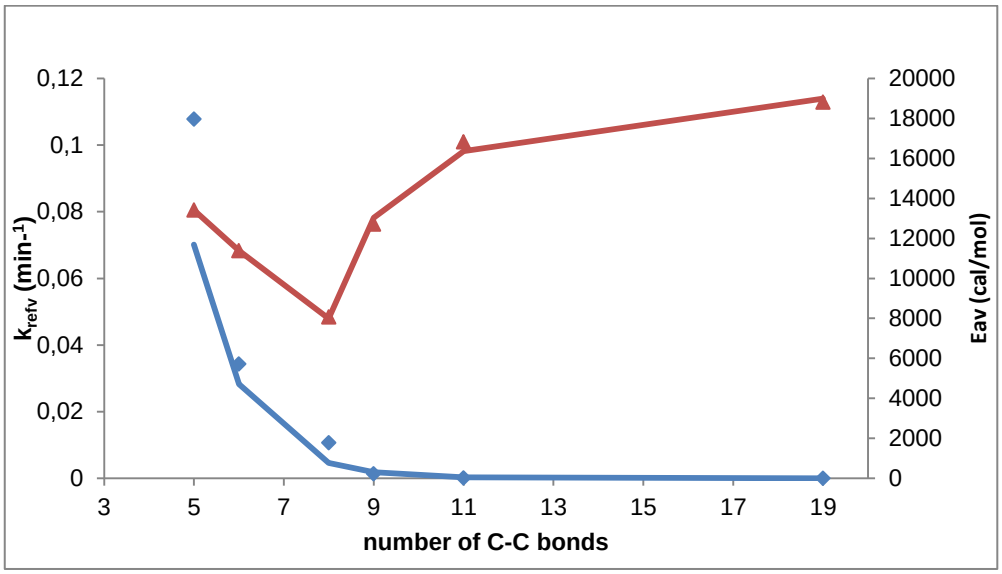

Figure 4.15 - kinetic parameters' values for the different paraffins: k_{refv} from individual fitting (blue symbols) and from global fitting (blue line) and E_{av} from individual fitting (red symbols) and from global fitting (red line); global laws: function defined by segments for E_{av} and exponential for k_{refv}, method II.

Considering Table 4.11, it can be concluded that the global laws are:

$$E_{av}(cal/mol) = \begin{cases} 23583{,}73 - 2034{,}39.n_l, & n_l < 7{,}43 \\ \dfrac{20468{,}02.(n_l - 7{,}43)}{0{,}90 + (n_l - 7{,}43)}, & n_l \geq 7{,}43 \end{cases}$$

$$k_{refv}\ (min^{-1}) = 6{,}64.e^{(-0{,}9.n_l)}$$

From the previous equations, it was possible to simulate the evaporation rate curves, shown in Figure 4.16.

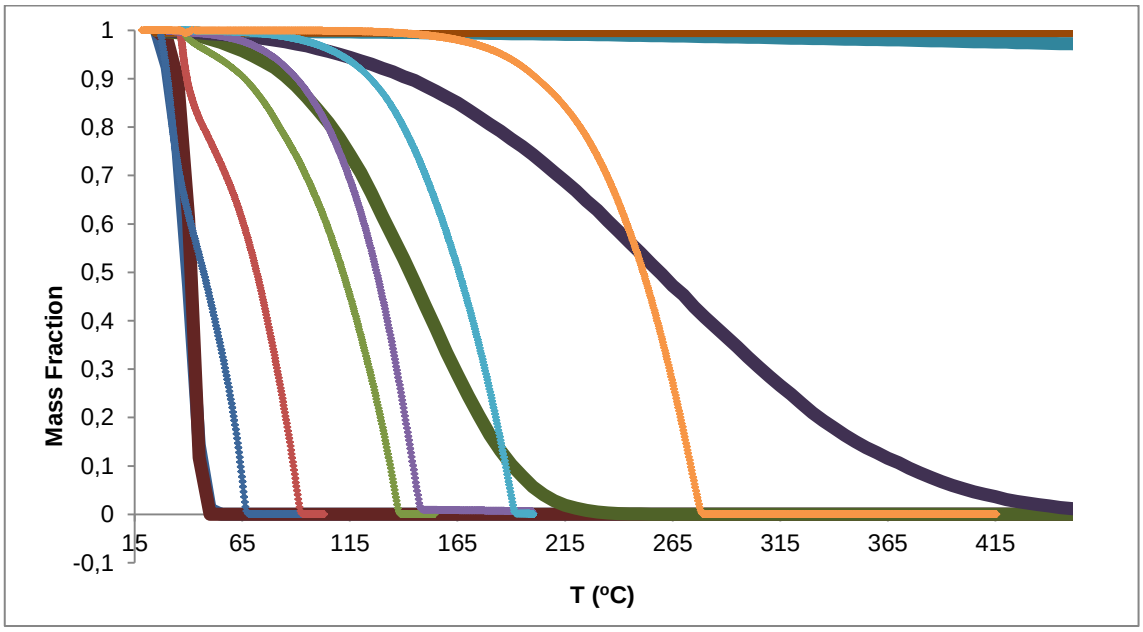

Figure 4.16 - Experimental rates of vaporization and simulated [k_{ref} exponential; E_a function defined by parts; method II) vaporization curves, respectively, for: n-hexane (blue dots and line); n-heptane (red dots and line); n-nonane (green dots and line); n-decane (violet dots and line); n-dodecane (light blue dots and line) and n –icosane (orange dots and line)].

A closer look to the graphic presented enables the perception of two distinct trends in the simulated curves: the first comprises the curves for n-C6 and n-C7 (where $n_l = 5;6 < n_{0\_E_a} = 7{,}43$), covered by the first segment of the global law for E_{av}; and a second trend for the other paraffins ($n_l = 8;9;11;19 \geq 7{,}43 = n_{0\_E_a}$). For the first trend, the simulated curves for both n-hexane and n-heptane, in addition to be very close to each other, in terms of temperature, present lower vaporization temperatures than those found in the data. On the other hand, for the second trend of the simulated curves, they present exaggerated high temperatures. Note, for example, that for n-decane the vaporization is completed about the 450^{o}C and for both n-dodecane and n-icosane, even though there are no further information, the vaporization may occur for temperatures high above the 450 ^{o}C.

4.5. Selecting the set of global laws providing the best fitting

After the presentation of all the attempts performed to find a global law for k_{refv} and E_{av}, one must select the set that provided the best fittings.

The main criteria used for this selection were not only the capacity of the equations to enable the stochastic model to calculate rates of vaporization that can best superimpose the experimental curves, especially in the portion where the vaporization occurs and, consequently, that have the vaporization temperatures closer than the ones found experimentally, but also to produce consistent results (e.g. ensure that the larger the paraffins are, the higher the vaporization temperature is).

Table 4.12 is presented below, summarizing the characteristics of each simulation executed.

Table 4.12 - simulation charecteristics summary

		Simulation Characteristics	
Function for E_{av}	**Function for k_{refv}**	**Method I**	**Method II**
Linear	**Exponential**	• Good fitting of simulated to experimental curves • Good overlapping in the vaporization portion of the curves • Closer vaporization temperatures obtained • Consistent vaporization results for higher molecules	• Very good fitting of simulated to experimental curves, except for n-C20 • Slightly higher vaporization temperatures • Inability to fit the experimental data from n-C20
quadratic	**exponential**	• Very good fitting of simulated to experimental curves • Inconsistent vaporization results for higher molecules	• Very good fitting of simulated to experimental curves • Inability to fit the experimental data from and n-C20
3rd degree polynomyal	**exponential**	• Very good fitting of simulated to experimental curves • Inconsistent vaporization results for higher molecules	• No global correlation obtained
defined by segments	**exponential**	• No overlapping between simulated and experimental curves • Much higher temperatures of vaporization • Inversion in the temperature order of vaporization	• No overlapping between simulated and experimental curves • Fitting of n-C6 and n-C7 (are coincident and the vaporization temperatures are lower) • Other paraffins curves present very high vaporization temperatures

After analyzing Table 4.12 and all the information from the previous sub-chapters, the selected global laws to describe paraffins' vaporization are the following (linear function for E_{av}; exponential function for k_{refv}; method I):

$$E_{av}(cal/mol) = 8280{,}77 + 1512{,}05.n_l$$

$$k_{refv}\ (min^{-1}) = 440{,}14.e^{(-1{,}76.n_l)}$$

Among the methodologies used to determinate the different global correlations, it has been shown that the one which permitted better results was the one-step fitting (method I). This would be expected since it is always better to perform a single-step fitting rather than a multiple-step one.

4.6. Using the global laws obtained to fit mixtures of hydrocarbons vaporization

In the previous sections it has been shown that a correlation between the chain vaporization kinetic parameters of pure hydrocarbons and the number of C-C bonds in their chain exists and, when introduced in the stochastic model, can produce reliable results that can fit the experimental ones.

In order to investigate if that correlation is also able to predict the vaporization rate curves of mixtures of hydrocarbons some vaporization kinetics of hydrocarbons mixtures assays have been performed.

In this chapter the experimental data obtained from the present experiments as well as the fitted curves using the information from the global correlation chosen will be presented

4.6.1. **Experimental data**

In the same manner that is shown in section 4.1, the data were obtained from the same TG/DSC apparatus and were exported using the software already mentioned. Also the data contain the values of time (min), weight (mg), heat flow (mW) and the temporal derived of the weight (mg/min). Once more, to construct the vaporization rate curves, data were processed as mass fraction (Eq. 4.1) which has been plotted against temperatures.

4.6.2. **Fitting the experimental data**

In this fitting, the values of the global kinetic parameters obtained from the correlation found in sub-chapter 4.5 are used to calculate the vaporization kinetics of each of the hydrocarbons presents in the mixture.

Recalling what have been outlined in section 4.1, the mass variation with the time is given by a first-order kinetics[14], written as:

$$\frac{dm_j}{dt} = -k(T)_j . m_j$$

Eq. 4.15

[14] It has been assumed that no interactions between the two compounds take place and so a first-order is likely to be adapted to the mixture's vaporization kinetics.

where the subscript $j = H\ or\ L$ refers to the heavier hydrocarbon in the mixture and the subscript L refers to the lighter one. The mass variation with the time/temperature is estimated separately for the two compounds since each one of these variations will be calculated using the specific compound global kinetic parameter.

Reminding that the temperature-dependent rate constant of vaporization follows an Arrehnius law, the mass variation with time (and simultaneously with the temperature) is given by Eq. 4.16:

$$\frac{dm_j}{dt} = k_{ref,j}.e^{-\left(\frac{E_{a,j}}{R}\left(\frac{1}{T}-\frac{1}{T_{ref}}\right)\right)}.m_j$$

Eq. 4.16

where $j = H\ or\ L$, i.e, corresponds to the heavier and to the lighter hydrocarbon, respectively. Thus, applying Euler's method is possible to compute the mass fraction of each of the hydrocarbons in the mixture:

$$m_j\ (t + \Delta t) = m_j\ (t) + \left(\frac{dm_j}{dt}\right)_{t+\Delta t}.\Delta t$$

Eq. 4.17

Once the values of m_H and m_L are calculated, the modelled total mass of the sample in this experiments can be easily determined (Eq. 4.18) and then processes as mass fraction to plot the curves vs the assay's temperature (Eq. 4.19):

$$m_{mod\ mixt}(t) = m_H(t) + m_L(t)$$

Eq. 4.18

$$X_{mod\ mixt} = \frac{m_{mod\ mixt}(t)}{m_{0\ mixt}}$$

Eq. 4.19

4.6.3. **Vaporization of hydrocarbons mixtures' modelling**

All the vaporizations of the mixtures here studied have been performed in the TG/DSC apparatus, according to the procedure exposed in the section 2.2. No gas products were collected.

a. Mixture of n-decane and n-dodecane

In Figure 4.17, the experimental vaporization curves for n-decane, n-dodecane and for the blend of n-decane and n-dodecane are presented, as well as the modeled curves for the same assays.

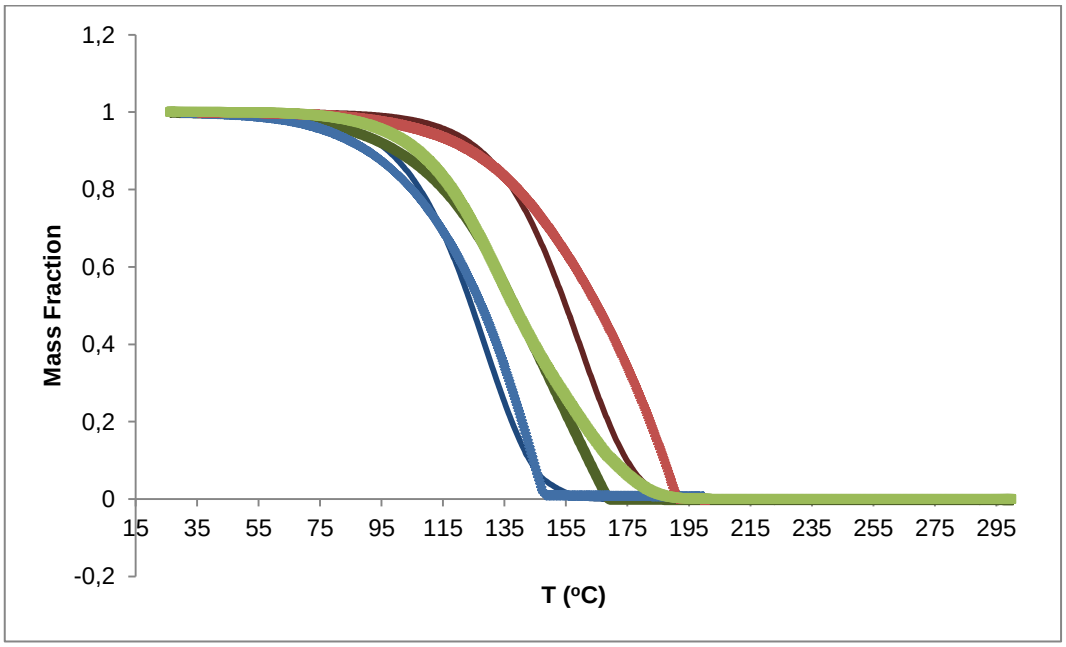

Figure 4.17 - experimental and modeled vaporization curves, respectively, for: n-decane [blue dots and line); n-dodecane (red dots and line); n-decane + n-dodecane (green dots and line)].

It would be expected that in the modeled curve representing the mixture vaporization there were two different sections: one corresponding to the vaporization of the lighter hydrocarbon (n-C10), for lower temperatures, and another representing the heavier hydrocarbon vaporization (n-C12), for higher temperatures. Though this is not much perceptible, it is still noticeable two segments with different decays: one from 26^{o}C to around 140^{o}C and another from there on. Probably they're not perceptible due to the similar composition of the two hydrocarbons present, both with vaporization temperatures not too far from one another.

Comparing with the experimental curves for pure compounds, in the mixture experimental data, the vaporization temperatures are only slightly higher. Nevertheless, the results from this experiment are still consistent and can be considered acceptable.

In this case, it can be observed a quite satisfactory agreement between the experimental data and the model results for the vaporization of the mixture of hydrocarbons. Both of the curves overlap in almost all their extension and can be concluded, for this case, that the experimental data on vaporization with mixtures of hydrocarbons can be predicted within a reasonable degree of accuracy, using the global correlation found.

b. Mixture of n-decane and n-icosane

The experimental evaporation rates for n-decane, n- icosane and the mixture of both are presented in Figure 4.18 as well as the respective modeled ones.

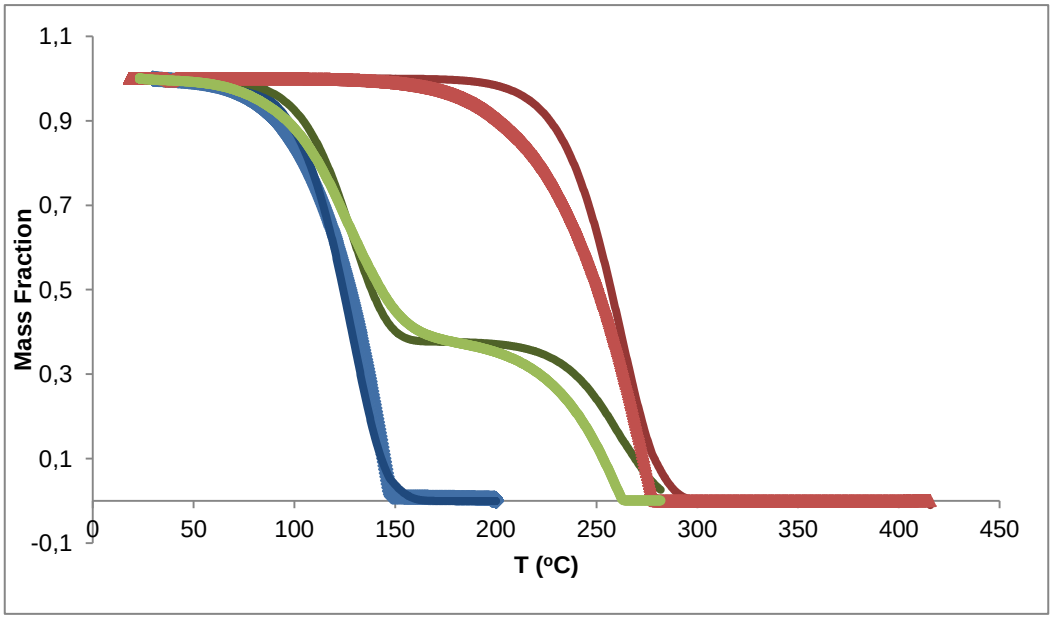

Figure 4.18 - experimental and modeled vaporization curves, respectively, for: n-decane [blue dots and line); n-icosane (red dots and line); n-decane + n-icosane (green dots and line)].

Considering Figure 4.18 and more specifically the modelled evaporation rate curve, it is easily noticeable that for this specific mixture of hydrocarbons there are two different segments that are related with the vaporization of n-C10 and n-C20.

In the experimental curve for the blend such progress is also readily perceptible. Regarding this curve, the vaporization of n-C10 occurs at a temperature very similar to the one found in experimental data whereas for n-C20, the vaporization occurs at slightly lower temperatures when compared with the data of the pure compounds, but still not with a significant difference.

The experimental and modelled temperatures of vaporization for each paraffin are similar and the curves are superimposable in almost their whole extension. Therefore there's the model used is capable of accurately describing the data and, consequently, the global correlation is able to predict the vaporization kinetics of the present blend.

4.6.4. **Conclusions**

From the results presented we can conclude that the evaporation rate laws obtained through the methodology described in this chapter are capable of describe the evaporation of pure hydrocarbons as well as of the mixtures that were tested. These equations will be used hereafter for the stochastic model.

5. THERMAL AND CATALYTIC DEGRADATION OF HIGH-DENSITY POLYETHYLENE

Once the global correlations for vaporization are known and this process is adequately described, the cracking phenomenon has to be investigated in order to have a model with the ability to predict the DSC/TG simultaneous results for the whole polyethylene degradation. In this way, the present chapter is dedicated to the study of the cracking process.

. In the computational model developed, one has to know and then insert the values for the kinetic constant of the HDPE degradation reaction as well as its activation energy providing the best fitting. For this purpose a study on how the values of the latter parameters affect the simulated degradation rate curves and the DSC signal has been carried out.

After such study was performed, the best fitting for both thermal and catalytic degradation experiments has been chosen and some additional improvements in the DSC curves overlapping varying the values of the C_p, ΔH_{C-C} and ΔH_{vap} have been made.

5.1. Effect of the constant rate and the activation energy of PE degradation in TG and DSC simulated results

The experimental results used in this study to be compared with the simulated curves were obtained from the thermal and catalytic cracking of HDPE experiments whose procedure and experimental conditions are mentioned in subchapter 2.2.

The simulations from both thermal and catalytic degradation were all performed under the same conditions, excepting, obviously to the values of k_{ref} and E_a, whose variation effect is presently studied. The thermodynamic parameters used are only indicative values. These conditions are listed in Table 5.1.

Table 5.1 - simulation conditions used for all simulations performed in thermal and catalytic degradation of HDPE studies (T_i – initial simulation temperature; T_f – final simulation temperature; β – heating rate; dt – integration step; C_p – average heat capacity; $\Delta H_{(C-C)}$ – average C-C bond enthalpy; k – cracking kinetic constant rate; ΔH_{vap} – average vaporization enthalpy; nr. bonds – number of bonds per molecule; nr. molecules – number of molecules used in the simulation).

Simulation conditions	
T_i (^oC)	25
T_f (^oC)	700
β ($^oC.min^{-1}$)	10
dt (min)	0,025
C_p ($cal.g^{-1}.^oC^{-1}$)	1,5
$\Delta H_{(C-C)}$ ($cal.mol^{-1}$)	20000
k (min^{-1})	variable
Ea ($cal.mol^{-1}$)	variable
ΔHvap ($cal.mol^{-1}$)	277,876
Nr. bonds[15]	21500
Nr. molecules	40

5.1.1. **Thermal degradation**

From previous works on simultaneous TG/DSC analysis of HDPE thermal and catalytic degradation (Coelho, Costa et al. 2012) the values found for the thermal degradation constant reference rate and activation energy are $3{,}74 \times 10^{-5}\, min^{-1}$ ($\approx 4 \times 10^{-5}\, min^{-1}$) and $26529{,}69\, cal.mol^{-1}$ ($\approx 30000\, cal.mol^{-1}$), respectively. These were, then, used as a starting point values to elaborate the present study. In Table 5.2 are presented the values for the kinetic parameters inserted in the program's interface to perform the simulations carried out. The nine assays/simulations performed are listed in Table 5.3.

[15] The number of bonds considered for a HDPE molecule was determined from supplier's molecular weight information: $\overline{\mathrm{M}}(\mathrm{HDPE}) = 300\,\mathrm{kDa}$.Then, knowing the molecular weight of one monomer, ethylene, it is simple to calculate the number of bonds of this polymer: $\frac{300\,000\, g.mol^{-1}}{14\, g.mol^{-1}} = 21428{,}57 \approx 21500\, bonds$.

Table 5.2 – values of the kinetic parameters used for thermal degradation of PE simulations.

Degradation refrence constant rate (k_{ref})		**Activation energy of degradation (E_a)**	
parameter value (min^{-1})	parameter designation	parameter value ($cal.mol^{-1}$)	parameter designation
2,00E-05	k_{-1}	20000	E_{a-1}
4,00E-05	k_0	30000	E_{a0}
8,00E-05	k_1	40000	E_{a1}

Table 5.3 – values of the kinetic parameters used in each simulation performed in thermal degradation of PE.

Parameters designation	**E_{a-1}**	**E_{a0}**	**E_{a1}**
k_{-1}	Assay nr. 1	Assay nr. 2	Assay nr. 3
k_0	Assay nr. 4	Assay nr. 5	Assay nr. 6
k_1	Assay nr. 7	Assay nr. 8	Assay nr. 9

Following, the simulation results from all the assays performed (both from TG and DSC signals), as well as the experimental results, are presented in Figure 5.1.

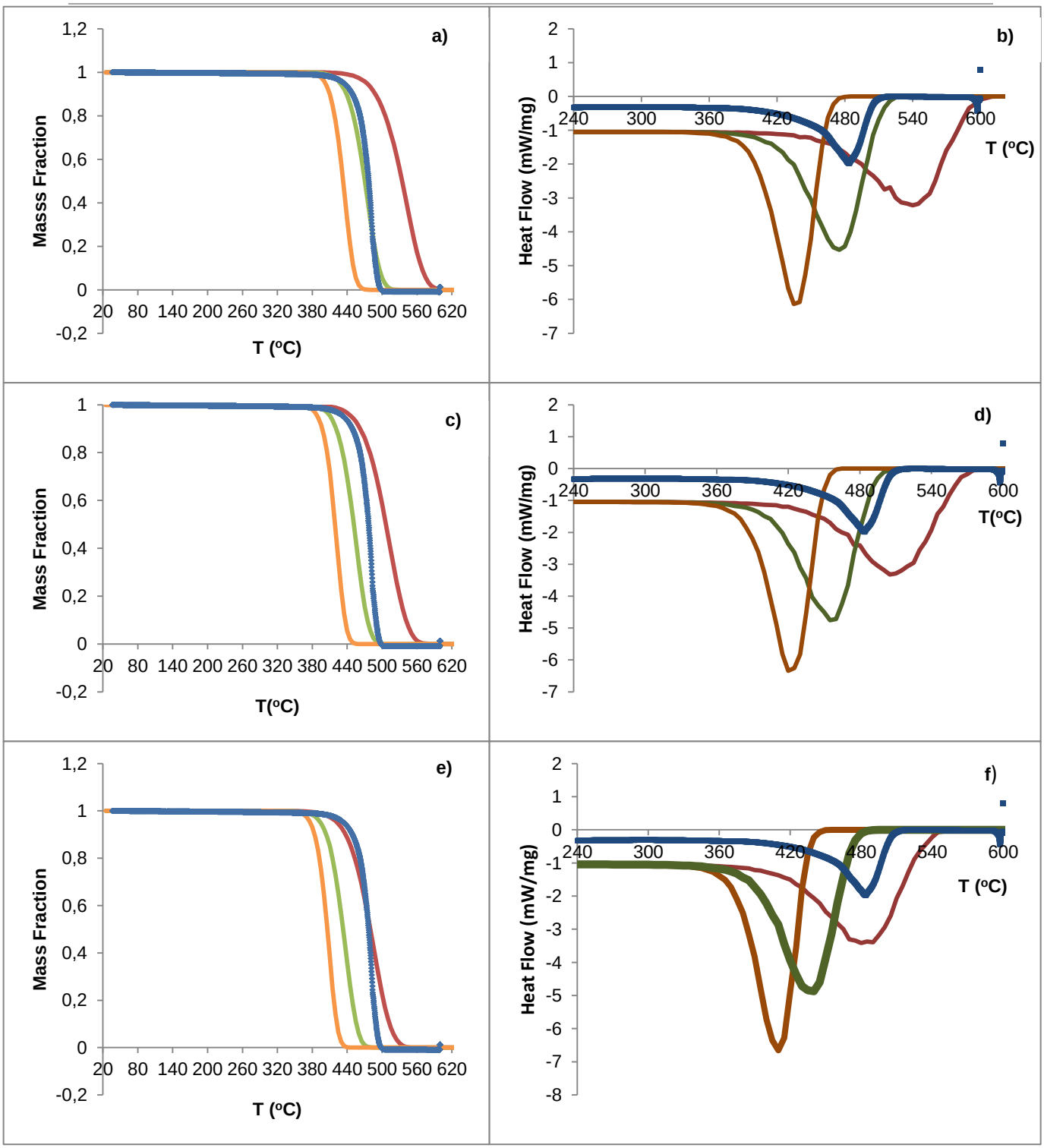

Figure 5.1 - a): HDPE thermal degradation curves: experimental (blue dots), assay nr. 1 (red line), assay nr. 2 (green line) and assay nr. 3 (orange line); b) DSC signals: experimental (blue dots), assay nr. 1 (red line), assay nr. 2 (green line) and assay nr. 3 (orange line); c) HDPE thermal degradation curves: experimental (blue dots), assay nr. 4 (red line), assay nr. 5 (green line) and assay nr. 6 (orange line); d) DSC signals: experimental (blue dots), assay nr. 4 (red line), assay nr. 5 (green line) and assay nr. 6 (orange line); e) HDPE thermal degradation curves: experimental (blue dots), assay nr. 7 (red line), assay nr. 8 (green line) and assay nr. 9 (orange line); f) DSC signals: experimental (blue dots), assay nr. 7 (red line), assay nr. 8 (green line) and assay nr. 9 (orange line)

Observing it is noticeable that the kinetic parameters variation does affect the simulated curves both for TG and DSC experiments. In Table 5.4 and Table 5.5 there is a summary of such effects.

Table 5.4 – Effect of the kinetic parameters variation on TG simulated curves for PE thermal degradation.

Kinetic Parameter Variation		Effect on TG simulated curves behaviour
k_{ref} fixed	**E_a variable**	increase in activation energy leads to lower degradation temperatures
k_{ref} variable	**E_a fixed**	increase in constant rate energy leads to lower degradation temperatures

Table 5.5 - - Effect of the kinetic parameters variation on DSC simulation signals for PE thermal degradation.

Kinetic Parameter Variation		Effect on simulated DSC signal behavior		
		Peak position	**Peak width**	**Peak intensity**
k_{ref} fixed	**E_a variable**	increase in activation energy shifts the peak to lower degradation temperatures	increase in activation energy leads to narrower peaks	increase in activation energy of degradation leads to an increase in peak intensity
k_{ref} variable	**E_a fixed**	increase in constant rate of degradation shifts the peak to lower degradation temperatures	variation in constant rate of degradation values does not affect peak width	increase in constant rate of degradation leads to an increase in peak intensity

Concerning the TG simulated curves, as it is said in Table 5.4 and can be concluded from , when the value of the activation is fixed and there is an increment in the reference constant rate's value, there's also an increase in rate of the whole degradation process which leads, in turn, to a lower-temperature mass loss, as it would be expected. On the other hand, when the value of the reference constant rate is fixed and one varies the activation energy's value, a situation unexpected occurs. As the activation energy increases, one should expect higher vaporization temperatures since there's a higher energetic barrier to the reaction to occurs. On contrary, what is observed from is that the higher the activation energy is the lower the degradation takes place. This evidence can be graphically explained observing the plot of an Arrhenius law linearized (

Eq. 5.1 and Figure 5.2):

$$\ln(k) = ln(k_{ref}) - \frac{E_a}{R}.\left(\frac{1}{T} - \frac{1}{T_{ref}}\right)$$

Eq. 5.1

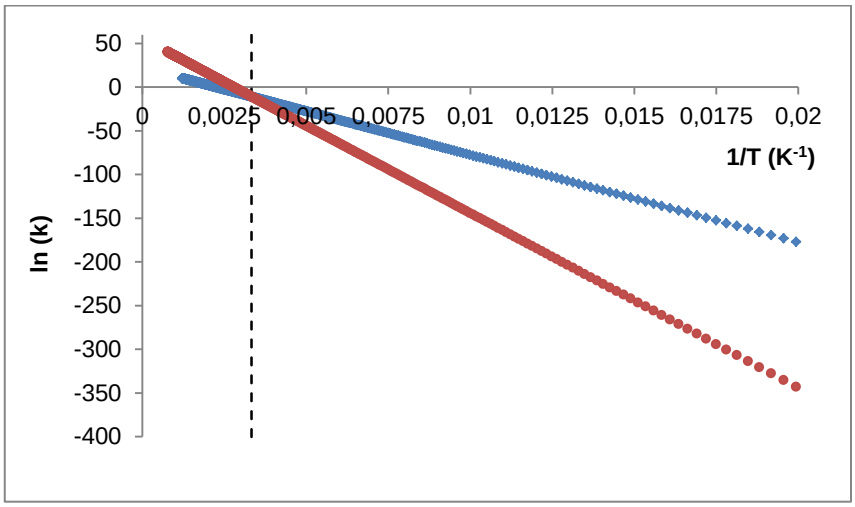

Figure 5.2 - Blue symbols: values of ln(k) vs (1/T) for the thermal degradation of HDPE with k_{ref}= 2x10^{-5} min^{-1} and E_a = 20000 cal/mol; red symbols: values of ln(k) vs (1/T) for the thermal degradation of HDPE with k_{ref}= 2x10^{-5} min^{-1} and E_a = 40000 cal/mol; vertical dashed line: represents the fixed reference temperature (300 K ⇔ 1/T ≈ 0,0033 K^{-1}).

Since the temperature in which the degradation of PE starts to happen (minimum temperature of 633,15 K), in all the cases, is significantly greater than the reference temperature chosen (300 K; left region from the dashed line in Figure 5.2), for such temperature, when the slope of the linearized Arrhenius law is higher (greater values of Ea; red symbols distribution from Figure 5.2), the value of ln(k_{ref}) (ordinate axis in Figure 5.2) is also higher and, therefore, the global rate of degradation, k, is going to be superior . Thus, the temperature at which it starts will be logically lower.

Regarding the DSC simulated signals, their progress relating to peak position (in terms of degradation temperatures) is analogous to TG curves and the enlightenment outlined explains it since the mass loss associated with the polymer's degradation is accompanied by the emergence of one endothermic peak in the DSC curves. In relation to peak intensity, it is clear from that in both cases (k fixed, E_a variable or k variable; E_a fixed) that as any of the kinetic parameters increases there is an increment in then peak intensity as well. The kinetic parameters here manipulated are associated with the cracking process only. Thus, the peak intensity on DSC curve is only due to the variation in the cracking term of the heat flow, remaining constant the terms of heating and vaporization. Consequently, for a fixed value of activation energy, when the rate of degradation is augmented (increase in k_{ref} values) bond breaking per unit of time is more likely to occur and, in turn, there is more energy associated, leading to an increase in peak intensity. For the E_a variation, keeping k_{ref} values fixed, because the degradation temperatures are higher than the reference one (see Figure 5.2 and the enlightenment outlined for TG curves' progress) it is also natural that the number of bonds broken per time unit is greater, leading, in the same way, to an increase in peak intensity. Relating to peak width, it seems that the variation of the rate constant at the reference temperature does not affect significantly this curve characteristic, whereas an increment in the activation energy value has a more significant effect. In fact, according to literature (Marcilla, Reyes-Labarta et al. 2001), the width of the

peak in a DSC curve is more sensitive to E_a variation. When its value is higher, a faster bond breaking phenomenon occurs, what is expected since, as shown previously (see Figure 5.2), an increase of such values conducts to a higher rate of cracking.

5.1.2. **Catalytic degradation**

Likewise what has been done for the PE depolymerization kinetic parameters effect on TG and DSC simulated curves in thermal degradation, in this case, the starting point values used to performed the study were taken from literature, having ZSM-5 zeolite as catalyst: $1{,}06 \times 10^{-3}\, min^{-1}$ ($\approx 1 \times 10^{-3}\, min^{-1}$) and $14340{,}34\, cal.mol^{-1}$ ($\approx 15000\, cal.mol^{-1}$) (Coelho, Costa et al. 2012). The others parameter values used are listed in Table 5.6 and the assays performed are presented in Table 5.7.

Table 5.6 - Values of the kinetic parameters used for catalytic degradation of PE simulations

Degradation reference constant rate (k_{ref})		**Activation energy of degradation (E_a)**	
parameter value (min^{-1})	parameter designation	parameter value ($cal.mol^{-1}$)	parameter designation
5,00E-04	k_{-1}	10000	E_{a-1}
1,00E-03	k_0	15000	E_{a0}
2,00E-03	k_1	20000	E_{a1}

Table 5.7 - Values of the kinetic parameters used in each simulation performed in catalytic degradation of PE.

Parameters designation	**E_{a-1}**	**E_{a0}**	**E_{a1}**
k_{-1}	Assay nr. 1	Assay nr. 2	Assay nr. 3
k_0	Assay nr. 4	Assay nr. 5	Assay nr. 6
k_1	Assay nr. 7	Assay nr. 8	Assay nr. 9

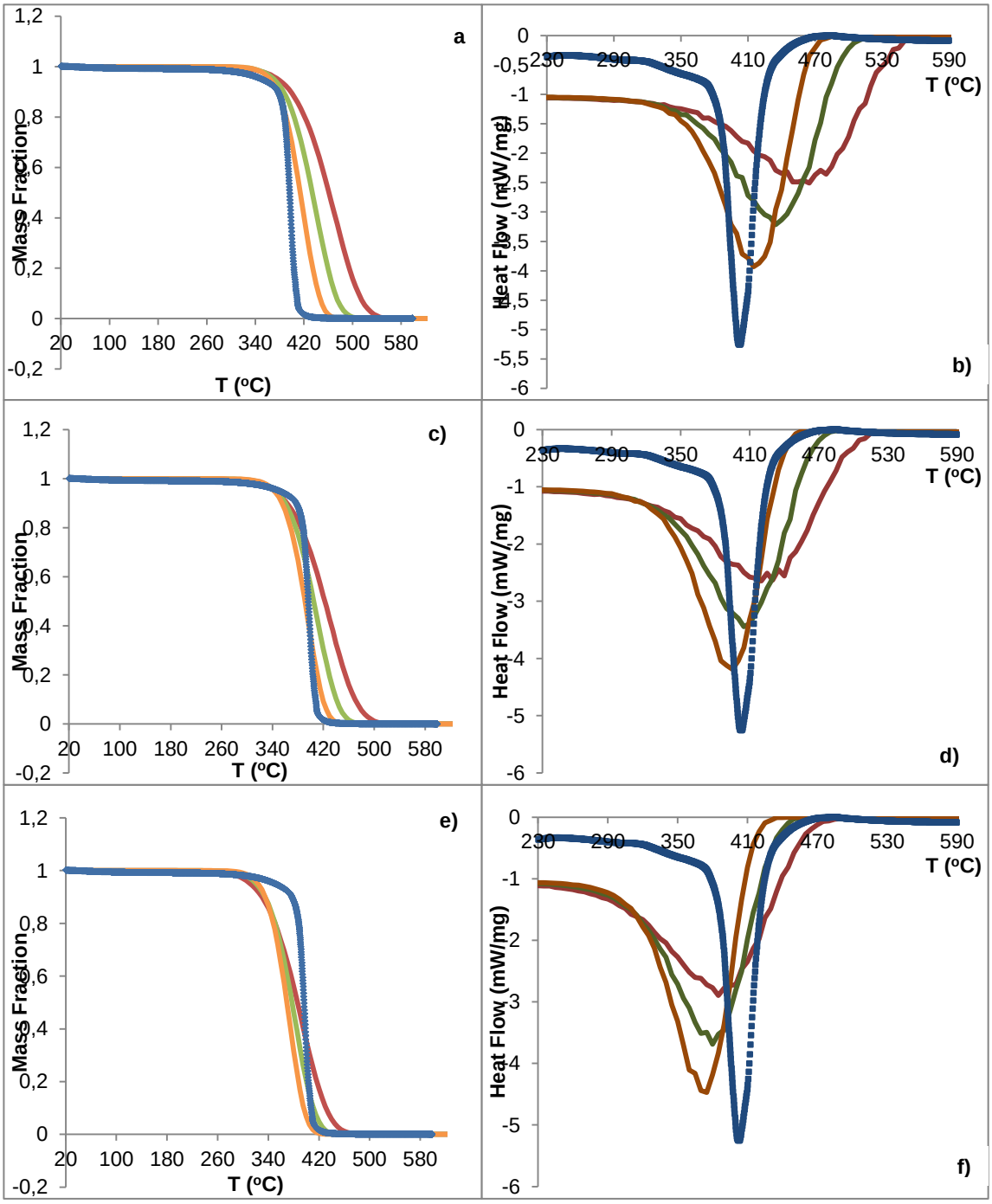

Figure 5.3 - HDPE catalytic degradation curves: experimental (blue dots), assay nr. 1 (red line), assay nr. 2 (green line) and assay nr. 3 (orange line); b) DSC signals: experimental (blue dots), assay nr. 1 (red line), assay nr. 2 (green line) and assay nr. (orange line); c) HDPE catalytic degradation curves: experimental (blue dots), assay nr. 4 (red line), assay nr. 5 (green line) and assay nr. 6 (orange line); d) DSC signals: experimental (blue dots), assay nr. 4 (red line), assay nr. 5 (green line) and assay nr. 6 (orange line); e) HDPE catalytic degradation curves: experimental (blue dots), assay nr. 7 (red line), assay nr. 8 (green line) and assay nr. 9 (orange line); f) DSC signals: experimental (blue dots), assay nr. 7 (red line), assay nr. 8 (green line) and assay nr. 9 (orange line).

Observing Figure 5.3 and comparing it with Figure 5.1, it is perceptible that the effect of the kinetic parameters variation in the case of catalytic degradation of PE in both TG and DSC simulated curves is the same observed in the thermal degradation (see Table 5.4 and Table 5.5). The differences found in the first assays when compared with those from thermal degradation are the lower temperatures of degradation (corresponding to lower-temperatures decays in TG curves and also lower temperatures for peak position is DSC curves) and the less amount of energy associated (less intense peaks in DSC curves). Such differences are consequence of the use of catalyst which reduces the process temperatures and, consequently, saves energy (Coelho 2008, Coelho, Costa et al. 2010, Coelho, Fonseca et al. 2010, Contreras, Garcia et al. 2012, Marcilla, Gómez-Siurana et al. 2007, Neves, Botelho et al. 2007, Marcilla, Gómez-Siurana et al. 2007).

5.2. Selecting the best kinetic and thermodynamic parameters to simulate thermal and catalytic degradation of HDPE

Concerning all the simulation performed in the previous sub-chapter, one has chosen those whose curves can be best superimposable to experimental data as the ones that can predict the thermal and catalytic processes in a best degree of accuracy.

Thereby, the best fittings are assay nr. 2 ($k = 2 \times 10^{-5}\, min^{-1}$ and $E_a = 30\,000\, cal.mol^{-1}$) for thermal degradation and assay nr.6 ($k = 1 \times 10^{-3}\, min^{-1}$ and $E_a = 20\,000\, cal.mol^{-1}$) catalytic degradation, whose curves are depicted below (Figure 5.3 and Figure 5.4, respectively).

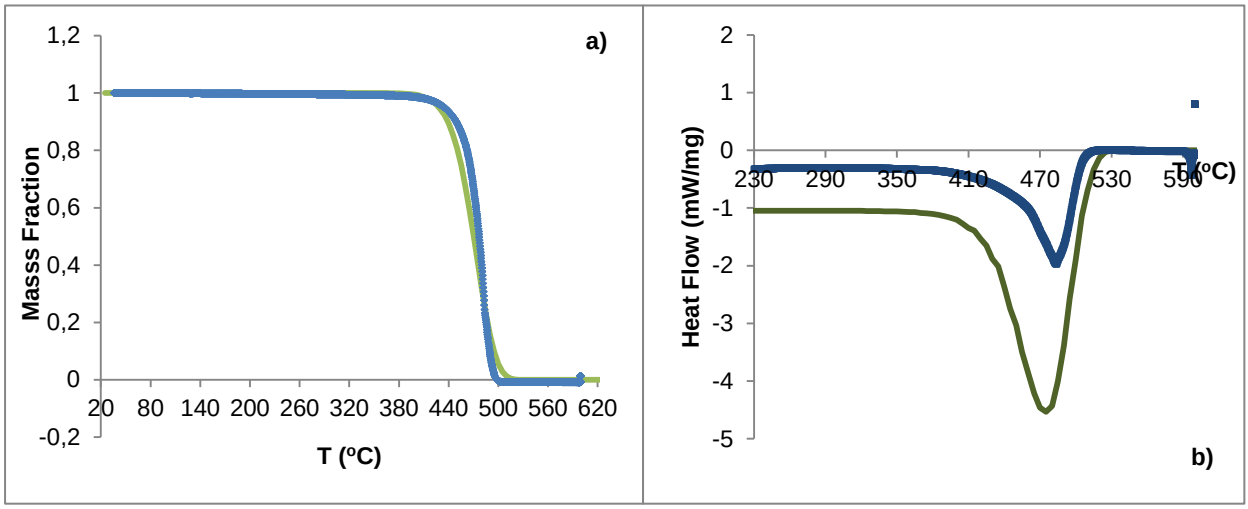

Figure 5.4 - Best fitting obtained using the stochastic model for thermal degradation of HDPE [k_{ref} = 2 x 10^{-5} min^{-1} and E_a = 30 000 $cal.mol^{-1}$): a) experimental TG curve (blue dots) and simulated TG curve (green line); b) experimental DSC curve (blue dots) and simulated DSC curve (green line)].

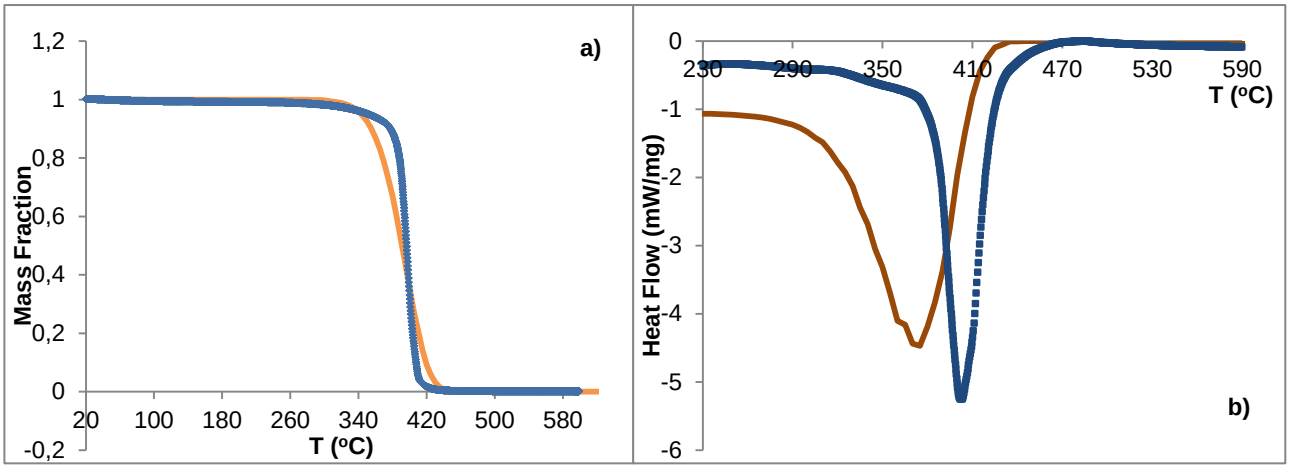

Figure 5.5 - Best fitting obtained using the stochastic model for catalytic degradation of HDPE [k_{ref} = 1 x 10^{-3} min^{-1} and E_a = 20 000 $cal.mol^{-1}$): a) experimental TG curve (blue dots) and simulated TG curve (orange line); b) experimental DSC curve (blue dots) and simulated DSC curve (orange line)].

As it can be seen for both cases, the simulated curves (especially the DSC signals), even though these are the best fitting obtained, are still not perfectly fitted. In this way, some improvements in the kinetic and thermodynamic parameters have been performed.

With the knowledge achieved in sub-chapter 5.1 about the influence of the kinetic parameters on curves progress, different values have been tested. When the variation of such parameters values starts to have no influence in curve's trend for the case of DCS signal), a trial and error method for the

thermodynamic parameters ($C_p, \Delta H_{vap}$ and ΔH_{C-C}) have been applied in order to acquire the best overlapping between the graphics.

As explained above the heat flow calculated by the model to plot the DSC curves has three components: one due to heating of the sample (Eq. 5.2), another correspondent to vaporization (Eq. 5.3) and a last one concerning bonds breaking (Eq. 5.4).

$$m_{heat}.C_p \quad \textbf{Eq. 5.2}$$

$$m_v.\Delta H_{vap} \quad \textbf{Eq. 5.3}$$

$$n_b.\Delta H_{C-C} \quad \textbf{Eq. 5.4}$$

where:

m_{heat}: mass of bonds heated per time unit (g.K.min^{-1})

C_p: average heat capacity (cal.g^{-1}.K^{-1})

m_v:mass of bonds evaporated per time unit (g.min-1)

ΔH_{vap}: average enthalpy of vaporization (cal.g^{-1})

n_b: number of bonds broken per time unit (mol.min^{-1})

ΔH_{C-C}: average C-C bond enthalpy (cal.mol^{-1}).

Understanding what are the terms involved on heat flow calculation and the corresponding thermodynamic parameters, it is easier to change its values and fit the DSC simulated curves to the experimental ones.

The heating term is predominant, logically, where no vaporization and bond breaking takes place and, therefore, by changing $C_p$value it is possible to fit the first segment of the curve (before the DSC peak emergence). If a lower value is used, the first plateau in the curve will be shifted for lower energy values. On the other hand, the terms related to vaporization and bond breaking are associated with peak intensity since this is the region on DSC graphic where such process occurs. If one increases the values of ΔH_{vap} and ΔH_{C-C}, more energy will be associated to these processes and more intense the peak will be.

Considering the information obtained in sub-chapter 5.1 and the elements outlined previously, several attempts to obtain the best fitting were executed. Nevertheless, only the bests are presented below as well as the kinetic and thermodynamic values used and the other simulation conditions (see Figure 5.6 and Table 5.8; Figure 5.7 and Table 5.9).

Table 5.8 - simulation conditions used for the best fitting performed for the thermal degradation of HDPE (T_i – initial simulation temperature; T_f – final simulation temperature; β – heating rate; dt – integration step; C_p – average heat capacity; $\Delta H_{(C-C)}$ – average C-C bond enthalpy; k_{ref} – cracking kinetic constant rate at reference temperature; ΔH_{vap} – average vaporization enthalpy; nr. bonds – number of bonds per molecule; nr. molecules – number of molecules used in the simulation).

Simulation conditions	
T_i (^oC)	25
T_f (^oC)	700
β ($^oC.min^{-1}$)	10
dt (min)	0,025
C_p ($cal.g^{-1}.^oC^{-1}$)	**0,45**
$\Delta H_{(C-C)}$ ($cal.mol^{-1}$)	**1000**
k_{ref} (min^{-1})	**1 E -05**
E_a ($cal.mol^{-1}$)	**32000**
ΔH_{vap} ($cal.mol^{-1}$)	**138**
Nr. bonds	21500
Nr. molecules	40

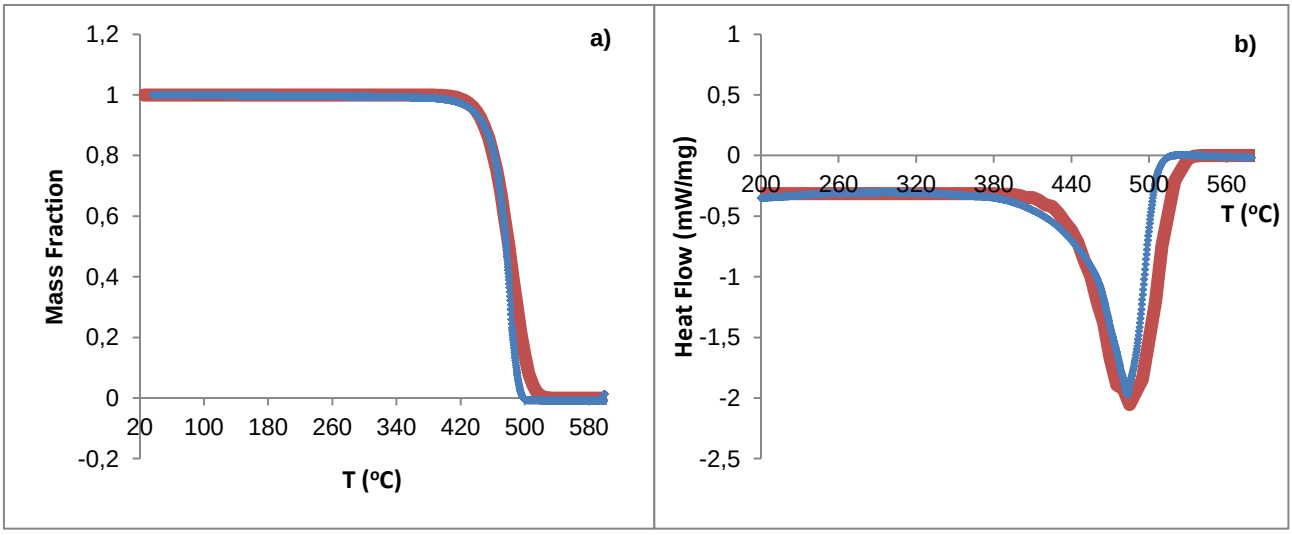

Figure 5.6 – best fitting provided by the stochastic model developed for HDPE thermal degradation: a) TG experimental (blue dots) and simulated (red line) curves; b) DSC experimental (blue dots) and simulated (red line) curves.

Table 5.9 - simulation conditions used for the best fitting performed for the catalytic degradation of HDPE (T_i – initial simulation temperature; T_f – final simulation temperature; β – heating rate; dt – integration step; C_p – average heat capacity; $\Delta H_{(C-C)}$ – average C-C bond enthalpy; k_{ref} – cracking kinetic constant rate at reference temperature; ΔH_{vap} – average vaporization enthalpy; nr. bonds – number of bonds per molecule; nr. molecules – number of molecules used in the simulation).

Simulation conditions	
T_i (^oC)	25
T_f (^oC)	700
β ($^oC.min^{-1}$)	10
dt (min)	0,025
C_p ($cal.g^{-1}.^oC^{-1}$)	**0,55**
$\Delta H_{(C-C)}$ ($cal.mol^{-1}$)	**1000**
k_{ref} (min^{-1})	**4,5 E -04**
E_a ($cal.mol^{-1}$)	**29000**
ΔH_{vap} ($cal.mol^{-1}$)	**325**
Nr. bonds	21500
Nr. molecules	40

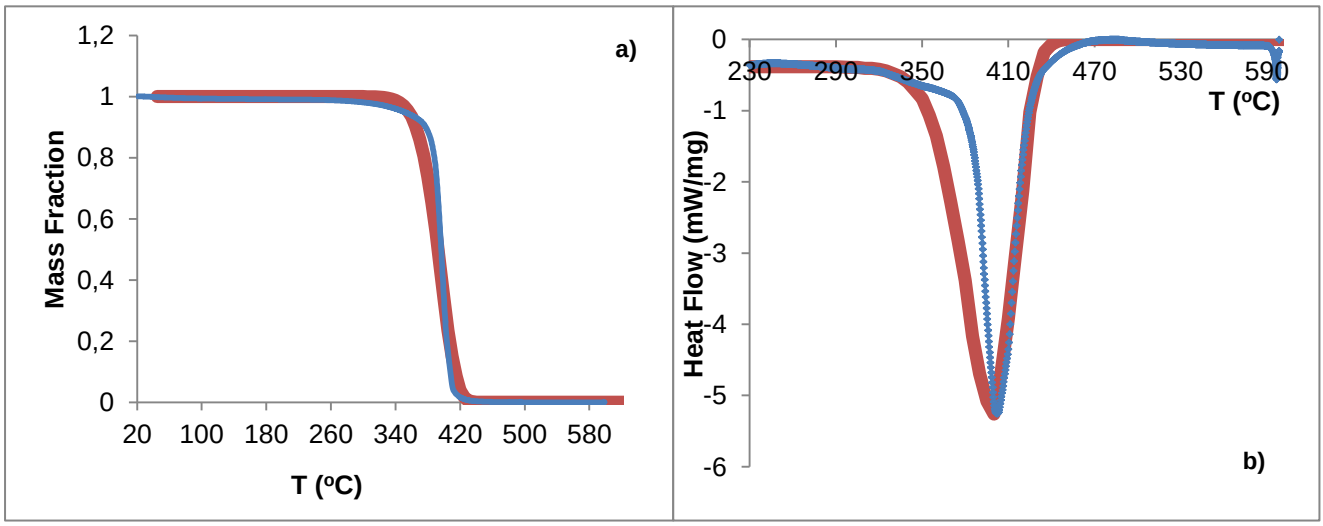

Figure 5.7 - best fitting provided by the stochastic model developed for HDPE catalytic degradation: a) TG experimental (blue dots) and simulated (red line) curves; b) DSC experimental (blue dots) and simulated (red line) curves.

From Figure 5.6 and Figure 5.7 it is noticeable that this changes (such as the variation of the kinetic and thermodynamic parameters) resulted in better fittings.

One thing that can be concluded with this study is that a first-order kinetics in order to the number of bonds broken in PE chain is well applied to the thermal and catalytic degradation of HDPE process

6. MOLECULAR SIMULATION

6.1. Fundamentals[16]

Molecular and quantum mechanics calculations are two methods commonly used to establish molecular geometries and conformations. Quantum mechanics calculations, in turn, are also being more and more frequently used to supply thermochemical and kinetic data, not only to interpret the existing information, but also to supplement or even replace it. The advances in computer software have also influenced these models development, making them a powerful tool for chemists.

Molecular mechanics methods describe a molecule in terms of "connected atoms" and geometry in terms of distortions from "ideal" (equilibrium) bond distances, bond angles and dihedral angles, together with an account of non-bonded van der Waals and Coulombic interactions. Thus, the energy of a molecule, according to this method, is described in terms of a sum of the contributions from the previous first three items, together with contributions due to non-bonded interactions (van der Waals and Coulombic). Calculation methods based on molecular mechanics, due to its nature, would not be expected to yield accurate results.

On the other hand, quantum mechanics for molecular calculations describe molecules in terms of the interactions between nuclei and electrons and the geometry is based on minimum energy arrangements of nuclei. The base of quantum methods is the Schrödinger equation, which gives simultaneously the energy and describes the motion of an electron in an atomic system. For the simplest case, the hydrogen atom (one particle in three dimensions), Schrödinger equation can be solved exactly and written as follows (Eq. 6.1):

$$\left[\frac{-h^2}{8.\pi^2.m_e}\nabla^2 - \frac{Z.e^2}{r}\right] = \Psi(x,y,z) = E\Psi(x,y,z)$$

Eq. 6.1

where the first and second terms within the square brackets represent, respectively, the kinetic and the potential energy of an electron of mass m_e, a distance r from the nuclear charge Z (in this case, $Z = 1$) and a charge e; h is Planck's constant. E represents the energy of the electron and Ψ is a function of atomic coordinates that describes its motion (wavefunction).

In this work, the molecular simulation study was developed using *PC SPARTAN PRO 6* ® software that provides several models to perform the calculations. Some are based on molecular mechanics but the majority is based on quantum mechanics. All quantum models used in the software resort to Schrödinger equation for many-electrons, which, unlike Eq. 6.1, cannot be exactly solved, even for the simplest many-electrons system. Therefore, some approximations and simplifications have to be assumed to provide practical methods. Such assumptions are applied in the model that was used to perform the present study – PM3 semi-empirical method – and will be outlined below.

16 This sub-chapter is based on the following reference: (Hehre, Yu et al. 1998).

In a many-electron system, where there are interactions between the nuclei, the electrons and between the electrons and the nuclei, the first way to simplify Schrödinger equation is to assume that the nuclei do not move – Born-Oppenheimer Approximation. Still, the Schrödinger equation cannot be solvable for more than a single electron and further approximations need to be applied. Another assumption adopted in this type of models is the Hartree-Fock Approximation which consists in the replacement of the many-electron wavefunction by a product of one-electron wavefunctions. This simplification involves a single-determinant of one-electron functions. Thus, the Hartree-Fock approximation leads to a set of coupled differential equations, each involving a single electron. In this way, the equations can already be solved. Nevertheless, it is advantageous to introduce one additional approximation: the Linear Combination of Atomic Orbitals (LCAO) Approximation. This assumption follows from the notion that the one-electron solutions for many electrons will resemble the one-electron solutions (for the hydrogen atom). Since molecules are made up of atoms, the molecular solutions can be, in the same way, made up of atomic solutions. These atomic solutions are expressed as linear combinations of a finite set of basis functions, ϕ, usually centered at the nuclear positions and then named atomic orbitals. Therefore, the molecular wave function can be expressed according to Eq. 6.2:

$$\Psi_i = \sum_{\mu}^{atomic\ orbitals} c_{\mu_i}.\phi_i$$

Eq. 6.2

PM3 semi-empirical method, the one used in this work, follows directly from Hartee-Fock models but have more simplifications applied. The simplifications are:

- Restriction of the treatment to valence electrons only (the inner shells are considered to be part of the fixed core);
- Restriction of the basis set to a minimal representation[17] (for main group elements, comprises a single s-type function and a set of p-type functions, e.g. for a first-row element: 2s, $2p_x$, $2p_y$ and $2p_z$);
- No-overlapping of the atomic orbitals associated to different atomic centres (known as the Neglect of Diatomic Differential Overlap Approximation);
- Further approximations can be introduced to simplify the overall calculation and, above all, to enable the introduction of semi-empirical parameters. For this specific method, the parameters for transition metals are based only on reproducing equilibrium geometry

17 See (Hehre, Yu et al. 1998) for more examples and exceptions.

6.2. Molecular Simulation Study

As been said in sub-chapter 3.2, in the stochastic model developed, it has been assumed that the probability of a given bond breaking is always the same, regardless of the bond's position in the molecule with the exception of the terminal bonds. However, some authors, like (Ziff, McGrady 1986), claim that in many polymeric systems, the occurrence of bonds breakage depend upon the position of the bond within the chain and/or the total length of the chain.

In order to investigate this issue, a molecular simulation has been performed. On such simulation, the polyethylene chain was mimicked by an n-decane molecule and the zeolite catalysts generally employed in the catalytic cracking process have been mimicked by a Brønsted acidic site. The mechanism employed in this cracking reaction was a protolytic scission.

Using the PM3 semi-empirical model from *PC SPARTAN PRO 6* ® software, the activation energy (according to Eq. 6.3) of the scission reaction have been determined by varying the bond position on decane molecule's chain.

$$Cleavage\ Activation\ Energy = Heat\ of\ Formation\ (transition\ state) - Heat\ of\ formation\ (reagent)$$

Eq. 6.3

6.2.1. Selecting a Model

Following is presented a relation between the several methods existing in *PC SPARTAN PRO 6* ® software and them performances according to the task desired (Table 6.1).

Table 6.1 – performance and cost of some models existing in *PC SPARTAN PRO 6* ® software [adapted from (Hehre, Yu et al. 1998)].

	Molecular	Semi-	Density functional		Hartree-	
Task	**Mechanics**	**Empirical**	**SVWN**	**pBP**	**Fock**	**MP2**
geometry (organics)	GC	G	G	G	G	G
geometry (transition metals)	P	G	G	G	P	?
transition-state geometry	N/A	G	G	G	G	G
conformation	G	P	GC	G	GC	G
thermochemistry (non *isodemic*)	n.a.	P	GC	G	GC	G
thermochemistry (*isodemic*)	n.a.	P	G	G	G	G
cost	very low	low	moderate	moderate	High	very high

G = good; GC = good with cautions application; P = poor; ? = unknown; n.a. = not applicable.

In the present study, the main goal is to obtain the activation energies of the scission reactions initiated in different bonds' positions along the n-decane molecule chain. Thus, the obtaining of equilibrium geometry for the reagent and the product, finding the correct transition state for each

reaction and the calculation of heat of formation values for each chemical intervenient are required. Taking a look to Table 6.1, it is noticeable that semi-empirical methods are able to calculate equilibrium and transition-state geometries with good accuracy. Nevertheless, the calculation of thermochemical parameters such as the heat of formation can only be poorly obtained by these methods. Even though this drawback, a semi-empirical PM3 model has been chosen to perform the actual study since only an approximate value of the heat of formation is needed to give a general idea and, above all, due to the low cost associated with the model when comparing to more complex ones (e.g. Hartree-Fock, MP2).

6.2.2. **Procedure**

a. Equilibrium geometry calculations

For each reactant and product of the several scissions performed in the software *PC SPARTAN PRO 6* ®, a molecular model has been constructed. After that, an equilibrium geometry has been calculated, following the steps: Menu Setup → Calculations and then adding the information as shown below (Figure 6.1):

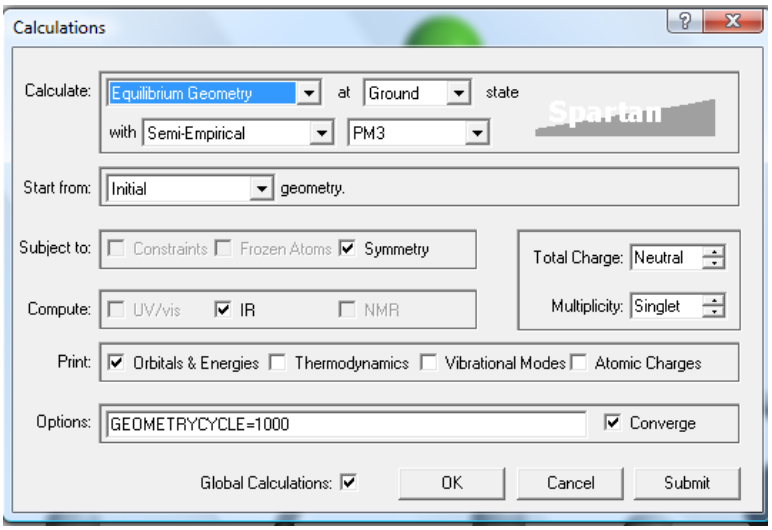

Figure 6.1 – *PC SPARTAN PRO 6* software commands to calculate an equilibrium geometry.

b. Transition-state geometry

Firstly a transition state geometry for one specific case (scission in position 5) among all the scissions performed has been found according to the following steps:

- Use the molecular model of the reagents (after geometry optimization) (see Figure 6.2);

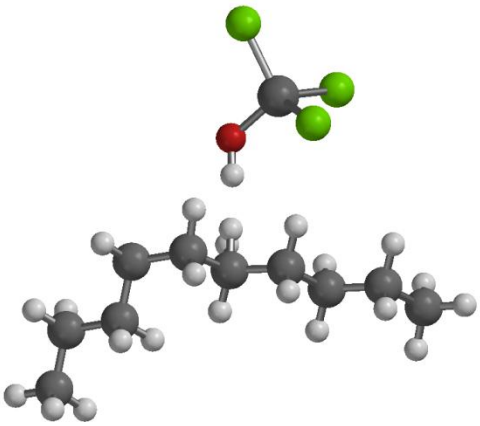

Figure 6.2 – Molecular models used in the software that represent the regents from all scission reactions (green spheres: chloride atoms; dark grey sphere in acidic sire representation: silicon atom; red sphere: oxygen atom; dark grey spheres: carbon atoms; white spheres: hydrogen atoms).

- Constraint the following bonds (marked in Figure 6.3) using the button on toolbar and by writing the distance to be imposed in a bond between two atoms[18]. For each time a set of bonds is constraint, calculate the equilibrium molecular geometry and display an IV spectrum (see Figure 6.4) and display the last one.(see Figure 6.5);

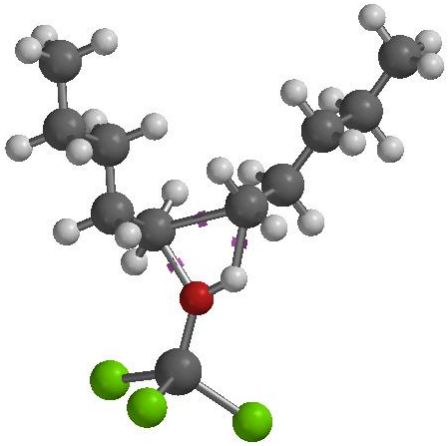

Figure 6.3 – Molecular model of a transition-state complex associated to the scission of the bond in position 5 (illustrates the action of constraining bonds).

[18] The bonds supposed to break must be stretched (by increasing the distance between the atoms) and the ones supposed to form must be shortened (by decreasing the distance between the atoms).

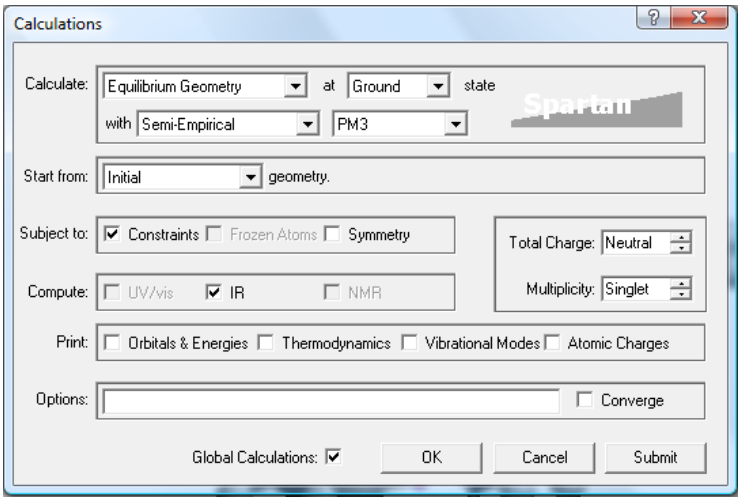

Figure 6.4 – Commands used in *PC SPARTAN PRO 6* software to perform an equilibrium geometry optimization subjected constraints and additional IV spectrum request.

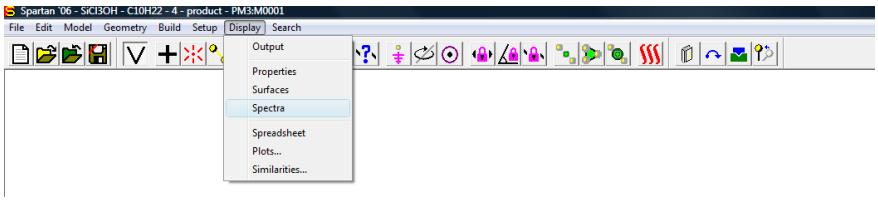

Figure 6.5 – How to display a IV spectrum in *PC SPARTAN PRO 6* software.

• By means of a trial-and-error method, repeat the latter step until only a negative vibration (marked with the letter i before the frequency value) in IV spectrum is found (see Figure 6.6);

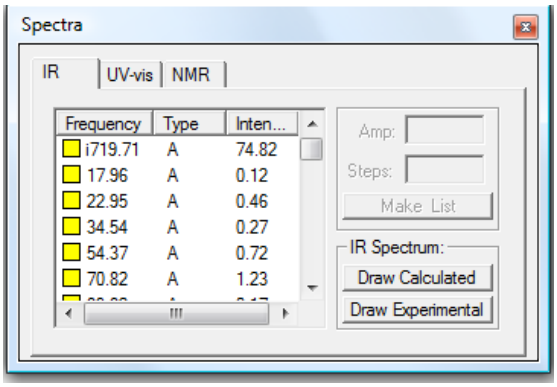

Figure 6.6 – Illustration of a single-negative frequency in a IV spectrum.

• Once it is found, a confirmation if the vibration is the correct for the reaction in study (i.e., this negative vibration must be the one characterized by stretching the bonds to be broken and shortening the ones to be formed) has to be done. If it is so, a transition- state geometry has been found. The next step is to perform a transition state geometry optimization, using the following commands (see Figure 6.7);

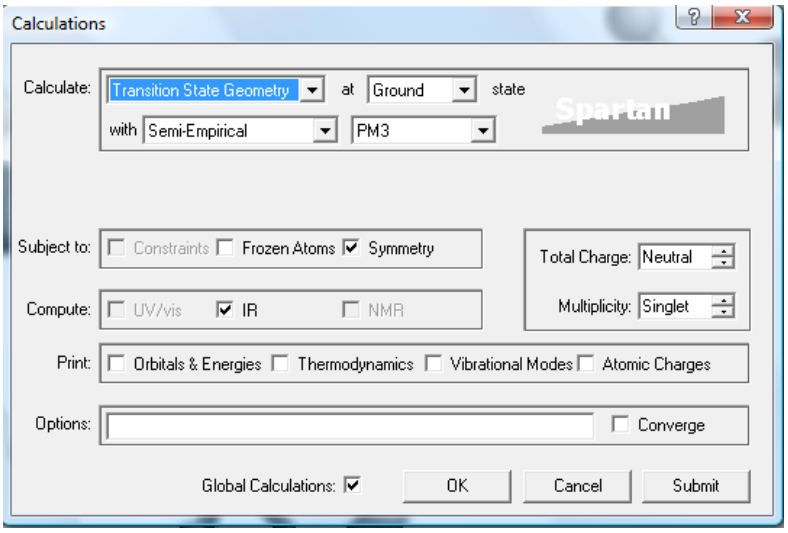

Figure 6.7 – Commands used in *PC SPARTAN 6* ® software to optimize a transition state-geometry, including an IV spectrum request.

- After finding the transition-state complex for one specific scission, the others are easily determined by constructing the respective molecular model from the transition-state complex already determined and by performing the latter step.

c. Heat of formation's calculation

For all molecular simulations performed, the heat of formation is an output data and it can be requested as follows: Menu Display → Output. Then, a window with several values is opened and the heat of formation value can be consulted (see Figure 6.8).

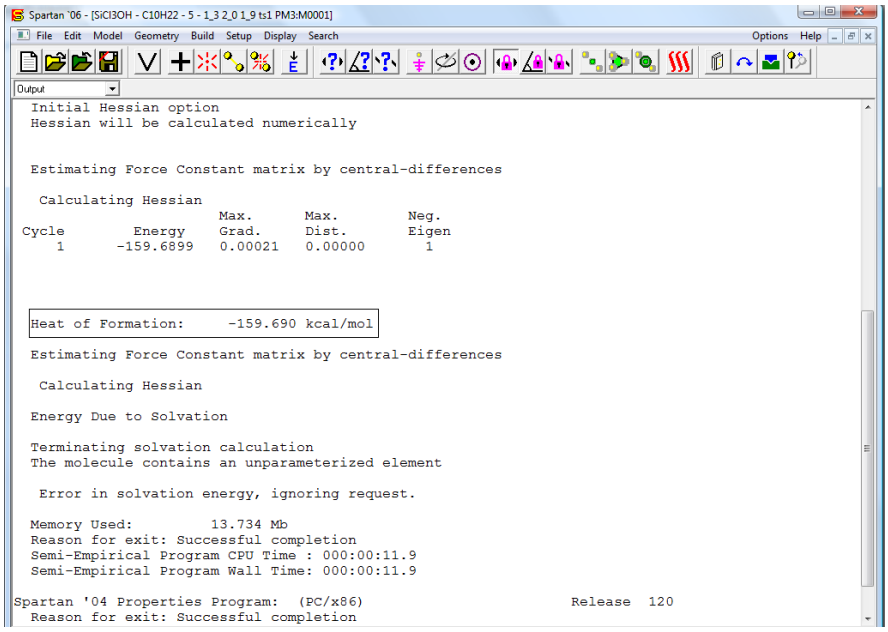

Figure 6.8 – Output data from a molecular simulation.

6.2.3. **Simulation Results**

In Table 6.2, the several cleavage products obtained are listed:

Table 6.2 – relation between the bond- chain position where scission occurs and the products formed, for all molecular simulations carried out.

Scission bond chain position	Scission Products
1	1 nonane molecule + 1 methyl radical adsorbed in the zeolite surface
2	1 octane molecule + 1 ethyl radical adsorbed in the zeolite surface
3	1 heptane molecule + 1 propyl radical adsorbed in the zeolite surface
4	1 hexane molecule + 1 butyl radical adsorbed in the zeolite surface
5	1 penthane molecule + 1 penthyl radical adsorbed in the zeolite surface
6	1 butane molecule + 1 hexyl radical adsorbed in the zeolite surface
7	1 propane molecule + 1 heptyl radical adsorbed in the zeolite surface
8	1 ethane molecule + 1 octyl radical adsorbed in the zeolite surface
9	1 methane molecule + 1 nonyl radical adsorbed in the zeolite surface

According to Eq. 6.3 and from the output data on the heat of formation, it was possible to calculate the activation energy associated to each one of the cracking reactions simulated. These values are presented in Table 6.3 and plotted in Figure 6.9.

Table 6.3 – activation energy values calculated with base on *PC SPARTAN 6* ® software for the zeolite-catalyzed cracking reaction along the bonds in an n-decane chain

Cleavage bond chain position	Reagent Heat of formation ($kJmol^{-1}$)	Transition state Heat of formation ($kJmol^{-1}$)	Overall Reaction Activation energy ($kJ.mol^{-1}$)
1	-1103,871	-665,444	438,427
2	-1106,193	-668,57	437,623
3	-1105,359	-668,062	437,297
4	-1106,522	-668,285	438,237
5	-1106,492	-668,143	438,349
6	-1106,422	-668,394	438,028
7	-1105,783	-667,955	437,828
8	-1107,304	-673,083	434,221
9	-1107,123	-667,354	439,769

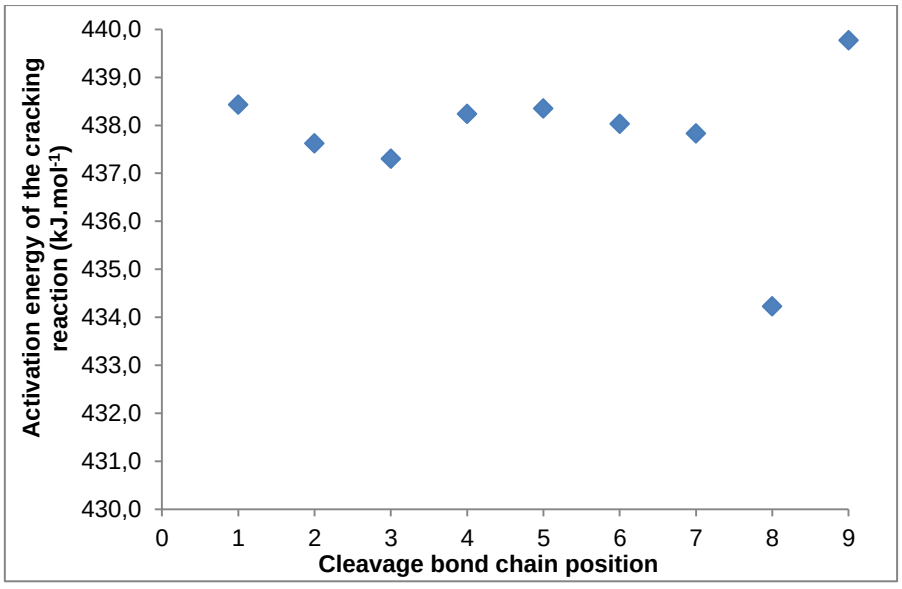

Figure 6.9 – Distribution of the activation energy calculated with base on *PC SPARTAN 6* ® software for the zeolite-catalyzed cracking reaction along the bonds in an n-decane chain.

Observing Table 6.3 and Figure 6.9, it is noticeable that the activation energies have not the same precise value, depending on the position in the chain of the broken bond. Thus, it can be said that the probability of cracking to occur is not exactly the same for all bonds. Surprisingly, the values

are very close to each other. Even though this little discrepancy, it is still perceptible that bond breakages occurred on chain ends present the higher values, meaning that is energetically more complicate to break these bonds (1 and 9) and, thus, their cracking are less likely to occur. What was not also expected is that at the central positions (4, 5 and 6) cracking presents the second higher values of activation energy, when it is known that, according to literature (Ziff, McGrady 1986), in these positions the probability to crack would be the greatest. Other aspect that also is not consistent is the fact that for position 8, there is the lowest value of cracking activation energy.

Generally, one can say that the probability to crack must not be the same according to the position of the bond that cracks in the whole chain. Nevertheless, these results must be cautiously interpreted since, as it was mentioned in sub-chapter 6.2.1, semi-empirical methods cannot predict accurately thermochemical data like heat of formation.

7. CONCLUSIONS

7.1. Main Achievements

7.1.1. General achievements on Stochastic Model

The first item to be concluded is that the main goal of this work was attained, i.e., the development of a stochastic model to predict the thermal and catalytic degradation in DSC/TG simultaneous assays was achieved. Such model is based in simple assumptions and still presents some limitations (e.g. an incorrect product distribution when compared to experimental data). However, it can produce quite good results regarding TG and DSC curves.

This stochastic model presents some advantages over other models previously developed, namely the deterministic ones. Firstly, there is no need of using experimental data to obtain the simulated curves. Instead, to perform a simulation, one has only to introduce information of the number of bonds of the molecule in study, the number of molecules which are involved and a few experimental conditions associated with the DSC/TG experiments (the heating rate, the temperature range in which the assay is performed and the integration step) and, finally, the thermodynamic and kinetic parameters. Therefore, in relation to experimental data usage, one can say that the present model is autonomous, unlike the available deterministic models. Moreover, the interface where the program code is implemented (Microsoft Excel spreadsheet with Visual Basic) makes it very simple to use, since its availability is increased its and complexity, in terms of the user's point of view, is lower. At last but not the least, the fact of using a stochastic model in the prediction of HDPE degradation allows the insertion of the randomness inherent in chemical reactions, especially in the case of polymerization/depolymerization processes, where populations of different chemical species are present. Summarizing, the utilization of a stochastic provides a more realistic simulation method.

Such a stochastic model can become a powerful tool for further engineering calculations and for an eventual industrial implementation of the HDPE catalytic degradation.

7.1.2. Vaporization Kinetics

The present work showed, from the individual fittings performed that a first-order kinetics (in order to paraffin's mass) can produce quite good fittings to experimental rates of vaporization obtained from TG/DSC experiments.

From the global fittings performed, it was also found a set of mathematical functions which provides the values of the kinetic parameters of vaporization (k_{refv} and E_{av}) from the number of C-C bonds in any given hydrocarbon chain. Two methods to estimate the functions coefficients were used (one-step fit and two-steps fit), being the one-step fit the one which presented better results. The values of the kinetic parameters for each compound are used to calculate the rates of vaporization and to include in the program's code for further simulation. Among the type of functions tested as

global rules of vaporization (exponential functional for k_{refv}; linear function, quadratic function, third-degree function and function defined by segments for E_{av}), the set which presented the best results was the exponential function for k_{refv} and the linear function for E_{av} and they are written as:

$$k_{refv,300K}\ (min^{-1}) = \ 440{,}14.\, e^{-1{,}76.n_l}$$
$$E_{av}(cal.mol^{-1}) \ = \ 8280{,}27 + 1512{,}12.\, n_l$$

This selection was based on the ability of the functions to provide the best fitting to the vaporization experimental data for each paraffin studied and the production of consistent results in the simulation of higher hydrocarbons vaporization (> n-C20).

The previous mathematical rules were not only tested for the vaporization of pure hydrocarbons, but also in the vaporization of hydrocarbons blends. For that, the following mixtures were used: n-C10 (37,7% (w/w)) + n-C12 (62,3% (w/w)) and n-C10 (50,9% (w/w) + n-C20 (49,1% (w/w). The modeling performed using the rate of vaporization calculated from the kinetic parameters obtained by means of the mathematical rules showed that these set of global laws allow the fitting of the blends of hydrocarbons vaporization in a good degree of accuracy.

7.1.3. **Thermal and Cracking Degradation**

For thermal and catalytic degradation of HDPE, this work showed that a first-order kinetics in order to the number of C-C bonds broken is adequate to the process. For that, the correct values of k_{ref} and E_a had to be found. Thus, a comprehensive study on how these parameters influenced the TG and DSC curves was done.

For the thermal degradation the following values of k_{ref} were used as starting points: $2x10^{-5}$ min^{-1}, $4x10^{-5}$ min^{-1}, $8x10^{-5}$ min^{-1}; and the values of E_a used were: 20 000 cal/mol, 30 000 cal/mol, 40 000 cal/mol. In the case of the catalytic cracking, the values of kref used in simulations were: $5x10^{-4}$ min^{-1}, $1x10^{-3}$ min^{-1}, $2x10^{-3}$ min^{-1}, whereas the values used for the E_a were: 10 00 cal/mol; 15 000 cal/mol, 20 000 cal/mol. The main conclusions of the study are as follows:

- **TG curves**: when k_{ref} is fixed, an increase in E_a leads to lower degradation temperatures;
- **TG curves**: when E_a is fixed, an increase in k_{ref} leads to lower degradation temperatures;
- **DSC curves – peak position**: when k_{ref} is fixed, an increase in E_a shifts the peak to lower temperatures; when E_a is fixed an increase in k_{ref} has the same effect;
- **DSC curves – peak intensity**: when k_{ref} is fixed, an increase in E_a leads to an increase in peak intensity; when E_a is fixed, increasing k_{ref} has the same effect;
- **DSC curves – peak width**: when k_{ref} is fixed, an increase in E_a leads to narrower peaks; when E_a is fixed, the variation of k_{ref} does not affect peak width.

Among the simulations performed, some additional improvements have been made through manipulation of the thermodynamic parameters and the best fittings found were the ones which are associated the following parameters:

- **Thermal degradation** of HDPE: C_p = 0,45 cal.g^{-1}.^{o}C^{-1}; $\Delta H_{(C-C)}$ = 1000 cal/mol; k_{ref} = 1,0 x10^{-5} min^{-1}; E_a = 32 000 cal/mol; ΔH_{vap} = 138 cal/mol.

- **Catalytic degradation** of HDPE: C_p = 0,55 cal.g^{-1}.^{o}C^{-1}; $\Delta H_{(C-C)}$ = 1000 cal/mol; k_{ref} = 4,5 x10^{-5} min^{-1}; E_a = 29 000 cal/mol; ΔH_{vap} = 325 cal/mol.

As expected, due to catalysis influence, the k_{ref} value for thermal degradation is lower than for catalytic degradation (1,0 x10^{-5} min^{-1} vs. 4,5 x10^{-5} min^{-1}) and the value of E_a for thermal degradation, in turn, is higher than the one for the catalytic process (32 000 cal/mol vs. 29 000 cal/mol).

7.1.4. **Molecular Simulation**

The PM3 semi-empirical method (from *PC SPARTAN PRO 6* ® software) applied in molecular simulation of the cracking process of a molecule of n-decane (mimicking a PE molecule) with a protonic acid site (mimicking the action of a zeolite catalyst) allowed the calculation of the activation energy values involved in the cleavage of the bonds in different positions of the main chain.

Even though the values obtained are not very feasible, because of the poor ability of the method to make thermochemical calculations, it is obvious that the activation energy values of bond breakage are different from position to position of the bonds in the main chain. Thus, also the probability of bond breakage will be different, which is not in agreement with one of the assumptions of the model here developed.

7.2. Future work

As it has been seen previously, a reliable and realistic stochastic model was developed in this work. Nevertheless, there are still some drawbacks associated with it.

The first issue that has to be solved concerns the product distribution. Even though this task is out of the scope of the work, it was possible to note, during simulations performance, that the product distribution supplied by the model does not corresponded at all to the one from experimental data. Thus, further improvements need to be introduced in the program's code. This discrepancy in the products obtained may occur due to complex reaction mechanism involved in thermal or catalytic

cracking. Perhaps additional reactions take place in the gas phase after vaporization occurrence that are not being accounted at the present. It has been already uncovered, through the molecular simulations study performed, that bond cleavage probability assumption does not corresponds to reality. Instead, the probability of a bond to break seems to be independent of bonds position. Nevertheless, more rigorous calculations using more complex molecular simulation methods (e.g. Hartree-Fock methods) should be used to ensure this fact.

Some additional studies on fitting catalytic degradation with different catalysts cracking experimental data (e.g. HY zeolite and with mesoporous catalysts such as MCM-41 and pillared clays) must be performed since that other mechanisms are involved and, probably, the first-order kinetic adopted is no longer valid.

The model will also have to be improved in terms of the account for the possible deactivation endured by the catalyst during the reaction.

REFERENCES

ALFONSI, A., CANCÈS, E., TURINICI, G., DI VENTURA, B. and HUISINGA, W., 2005. Adaptive simulation of hybrid stochastic and deterministic models for biochemical systems. *Eric Cancès & Jean-Frédéric Gerbeau, Editors,* **14**, pp. 1.

ASSOCIATION OF PLASTICS MANUFACTURERS IN EUROPE (APME), 2010. *Association of Plastics Manufacturers in Europe (APME) - Plasics - the facts 2010: an analysis of European plastics, production, demand and recovery for 2009.*

BOCKHORN, H., HORNUNG, A. and HORNUNG, U., 1999. Mechanisms and kinetics of thermal decomposition of plastics from isothermal and dynamic measurements. *Journal of Analytical and Applied Pyrolysis,* **50**(2), pp. 77-101.

BUEKENS, A.G. and HUANG, H., 1998. Catalytic plastics cracking for recovery of gasoline-range hydrocarbons from municipal plastic wastes. *Resources, conservation and recycling,* **23**, pp. 163.

CEAMANOS, J., MASTRAL, J.F., MILLERA, A. and ALDEA, M.E., 2002. Kinetics of pyrolysis of high density polyethylene. Comparison of isothermal and dynamic experiments. *Journal of Analytical and Applied Pyrolysis,* **65**(2), pp. 93-110.

COELHO, A., 2008. *Applications of zeolites and other acid catalysts for liquid fuels production from recyclable plastics*, Faculdade de Ciência e Tecnologia/ Universidade Nova de Lisboa.

COELHO, A., COSTA, L., MARQUES, M.M., FONSECA, I., LEMOS, M.A. and LEMOS, F., 2010. Using simultaneous DSC/TG to analyze yhe kinetics of polyethylene degradation - catalytic cracking using HY and HZSM-5 zeolites. *React Kinet. Mech. Catal.,* **99**, pp. 5.

COELHO, A., COSTA, L., MARQUES, M.M., FONSECA, I.M., LEMOS, M.A.N.D.A. and LEMOS, F., 2012. The effect of ZSM-5 zeolite acidity on the catalytic degradation of high-density polyethylene using simultaneous DSC/TG analysis. *Applied Catalysis A: General,* **413–414**(0), pp. 183-191.

COELHO, A., FONSECA, I.M., MATOS, I., MARQUES, M.M., BOTELHO DO REGO, A.M., LEMOS, M.A.N.D.A. and LEMOS, F., 2010. Catalytic degradation of low and high density polyethylene using ethylene polymerization catalysts: Kinetic studies using simultaneous TG/DSC analysis. *Applied Catalysis A: General,* **374**(1–2), pp. 170-179.

CONTRERAS, F., GARCIA, F., PLAZA, H. and COVARRUBIAS, C., 2012. Energy optimisation and catalytic degrdation of plastic waste. *Seguridad y Medio Ambiente (Fundació Mapfre),* **125**.

FERNANDES JR, V.J., ARAUJO, A.S. and FERNANDES, G.J.T., 1997. Catalytic degradation of polyethylene evaluated by TG. *Journal of Thermal Analysis and Calorimetry,* **49**, pp. 255.

FONT, R., GÓMEZ-RICO, M.F. and ORTUÑO, N., 2011. Analysis of the vaporization process in TG apparatus and its incidence in pyrolysis. *Journal of Analytical and Applied Pyrolysis,* **91**(1), pp. 89-96.

GALINA, H. and LECHOWICZ, J., 1998. An algorithm for Monte Carlo modeling of degradation of polymer networks. *Computer Chemistry,* **22**(1), pp. 39.

GARCÍA, R.A., SERRANO, D.P. and OTERO, D., 2005. Catalytic cracking of HDPE over hybrid zeolitic–mesoporous materials. *Journal of Analytical and Applied Pyrolysis,* **74**(1–2), pp. 379-386.

GARFORTH, A., ALI, S., HERNANDEZ-MARTÍNEZ, J. and AKAH, A., 2005. Feedstock recycling of polymer wastes. *Current Opinion Solid State Matter Science,* **74**, pp. 379.

GARFORTH, A., FIDDY, S., LIN, Y.-., GHANBARI-SIAKHALI, A., SHARRATT, P.N. and DWYER, J., 1997. Catalytic degradation of high density polyethylene: An evaluation of mesoporous and microporous catalysts using thermal analysis. *Thermochimica Acta,* **294**(1), pp. 65-69.

GEORGIEV, D., BOGDANOV, B., ANGELOVA, K., MARKOVSKA, I. and HRISTOV, Y., 2009. Synthetic zeolites: structure, classification, current trends in zeolite synthesis - review, PROF. DR. ASSEN ZLATAROV UNIVERSITY, BOURGAS, BULGARIA, ed. In: *International Science conference: "Economics and Society development on the Base of Knowledge"*, 4th-5th July, 2009, Stara Zagora, Bulgaria 2009, pp. 1.

GILLESPIE, D.T., 2007. Stochastic simulation of chemical kinetics. *Annu. Rev. Phys. Chem.,* **58**, pp. 35.

GOBIN, K. and MANOS, G., 2004. Polymer degradation to fuels over microporous catalysts as a novel tertiary plastic recycling method. *Polymer Degradation and Stability,* **83**(2), pp. 267-279.

GOBIN, K. and MANOS, G., 2004. Thermogravimetric study of polymer catalytic degradation over microporous materials. *Polymer Degradation and Stability,* **86**(2), pp. 225-231.

GUISNET, M. and RAMÔA, F.R., 2004. *Zeólitos: um nanomundo ao serviço da catálise.* Lisbon: Serviço de Educação e Bolsas - Fundação Calouste Gulbenkian.

HAAG, W.O., LAGO, R.M. and WEISZ, P.B., 1984. The active site of acidic aluminosilicate catalysts. *Nature,* **309**, pp. 589.

HEHRE, W.J., YU, J., KLUNZINGER, P.E. and LOU, L., 1998. *A brief guide to Molecular Mechanics and Quantum Chemical Calculations.* Irvine, CA, USA: Wavefunction, Inc.

KOTREL, S., KNÖZINGER, H. and GATES, B.C., 2000. The Haag-Dessau mechanism of protolytic cracking of alkanes. *Microporous and Mesoporous Materials,* **35-36**(0), pp. 11-20.

LACHOR, P., KRZYSTOF, P. and POLÁNSKI, A., 2011. Deterministic models and stochastic simulations in multiple reaction models in systems biology. *Journal of Biotechnology, Computational Biology and Bionanotechnology,* **93(2)**, pp. 265.

MARCILLA, A., BELTRÁN, M.I. and NAVARRO, R., 2009. Thermal and catalytic pyrolysis of polyethylene over HZSM5 and HUSY zeolites in a batch reactor under dynamic conditions. *Applied Catalysis B: Environmental,* **86**, pp. 79.

MARCILLA, A., GÓMEZ-SIURANA, A. and VALDÉS, F., 2007. Catalytic cracking of low-density polyethylene over H-Beta and HZSM-5 zeolites: Influence of the external surface. Kinetic model. *Polymer Degradation and Stability,* **92**(2), pp. 197-204.

MARCILLA, A., GÓMEZ-SIURANA, A. and VALDÉS, F., 2007. Catalytic pyrolysis of LDPE over H-beta and HZSM-5 zeolites in dynamic conditions: Study of the evolution of the process. *Journal of Analytical and Applied Pyrolysis,* **79**(1–2), pp. 433-442.

MARCILLA, A., REYES-LABARTA, J.A. and SEMPERE, F.J., 2001. DSC kinetic study of the transitions involved in the thermal treatment of polymers. Methodological considerations. *Polymer,* **42**(12), pp. 5343-5350.

MASTRAL, F.J., ESPERANZA, E., GARCÍA, P. and JUSTE, M., 2002. Pyrolysis of high-density polyethylene in a fluidised bed reactor. Influence of the temperature and residence time. *Journal of Analytical and Applied Pyrolysis,* **63**(1), pp. 1-15.

NEVES, I.C., BOTELHO, G., MACHADO, A.V. and REBELO, P., 2007. Catalytic degradation of polyethylene: An evaluation of the effect of dealuminated Y zeolites using thermal analysis. *Materials Chemistry and Physics,* **104**(1), pp. 5-9.

OVEREND, R.P.,1986. Thermochemical conversion of biomass. *Renewable energy sources charged with energy from the sun and originated from earth-moon interaction.
.* Reidel Publishing Co., .

PANDIT, S.S., JUVEKAR, V.A. and TRIVEDI, M.K., 1993. Stochastic simulation of polymer reactions. *Chemical Engineering Science,* **48**, pp. 1237.

RAYCHAUDHURI, S., 2008. Introduction to Monte Carlo Simulation, S.J. MASON, R.R. HILL, L. MÖNCH, O. ROSE, T. JEFFERSON and J.W. FOWLER, eds. In: *Proceedings of the 2008 Winter Simulation Conference*, 2008 2008, pp. 91.

REBELO, A., 2009. *Degradação catalítica do polietileno*. Escola de Engenharia/ Universidade do Minho

SCOETHERS, J.G. and BUEKENS, A.G., 1979. Pyrolysis of plastics in a steam fluidised bed, in International Recycling Congress. *Freitag Verlag,* , pp. 674.

TRAIN, P.M. and KLEIN, M.T., 1987. Chemical and Stochastic Modeling of lignin hydrodeoxygenation, *Prepr. Pap., Am. Chem. Soc., Div. Fuel Chem.; (United States); Journal Volume: 32:2; Conference: 193. national meeting of the American Chemical Society, Denver, CO, USA.*, 5 April 1987 1987, pp. 240.

WELLS, C.R., 2009. *Comparison of approximation schemes in stochastic simulation methods for stiff chemical systems*, University of Waterloo, Ontario, Canada.

ZIFF, R.M. and MCGRADY, E.D., 1986. Kinetics of polymer degradation. *Macromolecules,* **19**, pp. 2513.

APPENDIX

Following, the aspect of the *Excel worksheet 2007*, which is the model's interface, is presented. The user has to insert the type of molecule and the number of molecules to perform the simulation, as well as other data like kinetic and thermodynamic parameters and the experimental conditions.

	A	B	C	D	E	F	G	H	I
1	Number of molecules per molecule	21500		Number of molecules	40		Cp	1,5	Cal/g/K
2	k reference	8,00E-05	1/min	Heating rate	10	C/min	DH(C-C)	20000	Cal/mol
3	Activation energy	30000	Cal/mol	Initial temperature	25	C	DHv	277,8759373	Cal/g
4	dt	0,025	min	Final temperature	700	C			
5	dt2	0,5	min	Reference temperature	300	C			
6	Resultados:								
7	time	67,5	min		Iniciar Cálculos				
8	temperature	700,00	C						
9									
10	Overall products distribution								
11	1	679							
12	2	714							
13	3	740							
14	4	650							
15	5	691							
16	6	676							
17	7	693							
18	8	702							
19	9	719							
20	10	680							
21	11	701							
22	12	692							
23	13	675							
24	14	723							
25	15	676							

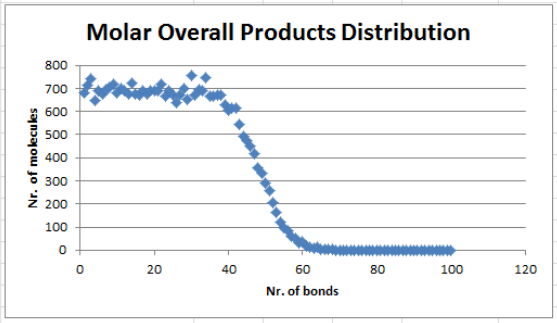

Resumo | Distribuicao de produtos | Distribuicao de Produtos gasoso | Fase Gasosa_Prods | DSC | Parametros